

Minor folds in coticule layers and their relationship to regional fold  
evolution, central Meguma Terrane, Nova Scotia

by

Michael Dylan Young

Submitted in partial fulfillment of the requirements  
for the degree of Bachelor of Science Honours  
in Earth Sciences

at

Dalhousie University  
Halifax, Nova Scotia  
May, 2000

© Copyright by Michael Dylan Young



Dalhousie University

Department of Earth Sciences

Halifax, Nova Scotia

Canada B3H 3J5

(902) 494-2358

FAX (902) 494-6889

DATE April 28, 2000

AUTHOR Michael Young

TITLE Minor folds in coticule layers and their relationship to  
regional fold evolution, central Meguma Terrane, Nova Scotia.

Degree B.Sc. Honours Convocation May Year 2000

Permission is herewith granted to Dalhousie University to circulate and to have copied for non-commercial purposes, at its discretion, the above title upon the request of individuals or institutions.

Signature of Author

THE AUTHOR RESERVES OTHER PUBLICATION RIGHTS, AND NEITHER THE THESIS NOR EXTENSIVE EXTRACTS FROM IT MAY BE PRINTED OR OTHERWISE REPRODUCED WITHOUT THE AUTHOR'S WRITTEN PERMISSION.

THE AUTHOR ATTESTS THAT PERMISSION HAS BEEN OBTAINED FOR THE USE OF ANY COPYRIGHTED MATERIAL APPEARING IN THIS THESIS (OTHER THAN BRIEF EXCERPTS REQUIRING ONLY PROPER ACKNOWLEDGEMENT IN SCHOLARLY WRITING) AND THAT ALL SUCH USE IS CLEARLY ACKNOWLEDGED.

## Distribution License

DalSpace requires agreement to this non-exclusive distribution license before your item can appear on DalSpace.

### NON-EXCLUSIVE DISTRIBUTION LICENSE

You (the author(s) or copyright owner) grant to Dalhousie University the non-exclusive right to reproduce and distribute your submission worldwide in any medium.

You agree that Dalhousie University may, without changing the content, reformat the submission for the purpose of preservation.

You also agree that Dalhousie University may keep more than one copy of this submission for purposes of security, back-up and preservation.

You agree that the submission is your original work, and that you have the right to grant the rights contained in this license. You also agree that your submission does not, to the best of your knowledge, infringe upon anyone's copyright.

If the submission contains material for which you do not hold copyright, you agree that you have obtained the unrestricted permission of the copyright owner to grant Dalhousie University the rights required by this license, and that such third-party owned material is clearly identified and acknowledged within the text or content of the submission.

If the submission is based upon work that has been sponsored or supported by an agency or organization other than Dalhousie University, you assert that you have fulfilled any right of review or other obligations required by such contract or agreement.

Dalhousie University will clearly identify your name(s) as the author(s) or owner(s) of the submission, and will not make any alteration to the content of the files that you have submitted.

If you have questions regarding this license please contact the repository manager at [dalspace@dal.ca](mailto:dalspace@dal.ca).

Grant the distribution license by signing and dating below.

---

Name of signatory

---

Date

## Abstract

The highly anisotropic turbidite sequences of the Meguma Group in southern Nova Scotia are folded into upright, noncylindrical, northeast-southwest trending box and chevron folds. Minor folds are well developed in spessartine-bearing carbonate quartzite layers, termed coticules, in the Beaverbank member, the basal unit of the Halifax Formation in central Nova Scotia. Classical interpretations for the development of minor folds involve layer-parallel shortening predating regional fold development, with minor folds becoming asymmetric as regional folds develop. This interpretation has been used for the origin of buckled bedding-parallel veins in the Meguma Group.

Minor fold geometry and related structures were documented in five outcrop locations in the central Meguma zone; two locations in a regional fold hinge, and three locations on regional fold limbs. Minor folds in coticule layers display ptygmatic, sinusoidal, box, and chevron fold geometries, and all folds are moderately noncylindrical. Fold geometry is mainly ptygmatic in regional fold hinges whereas minor folds are more open and commonly display box fold geometry on regional fold limbs. Some minor folds on regional fold limbs are asymmetric, consistent with flexural flow folding, whereas others are symmetric with axial planes and cleavage at high angles to bedding. Cleavage is axial planar to all minor folds on regional fold limbs and can locally diverge from the regional cleavage trend by up to  $90^{\circ}$ . Cleavage exhibits a divergent fan pattern around the outer arc of minor folds reflecting inverse tangential longitudinal strain. All coticule layers are folded in regional fold hinges, however, coticule layers are locally non-folded on regional fold limbs. Folding of coticule layers records significantly more shortening in regional fold hinges than on regional fold limbs. The average shortening recorded by minor folds in the regional fold hinge is 51% ( $N = 94$ ), whereas on regional fold limbs the average is 27% ( $N = 89$ ). The shortening values reported for regional fold limbs do not include the non-folded layers at one location on a regional fold limb.

In thin section, outer arc extension is common in folded coticule layers, recording tangential longitudinal strain. Extensional fractures occur along garnet grain boundaries indicating that fold initiation postdates garnet formation. Foliation-defining minerals wrap around spessartine grains and no inclusion trails are evident, indicating cleavage formed after spessartine formation. Coticule layers display boudinage parallel to regional cleavage which records significant vertical and hinge-parallel extension.

The observed minor fold geometries, in particular box folds, support development during layer-parallel shortening. However, the lack of minor folds in coticule layers on some regional fold limbs, and the contrast in the degree of shortening recorded by minor folds in regional fold hinges compared with limbs suggests that layer-parallel strain was not homogeneous across the terrane. The observed features of minor folds can be explained by layer-parallel shortening in the flat segments of early formed regional box folds followed by hinge migration, resulting in redistribution of minor folds from the hinge to limbs, and continued shortening in fold hinges during progressive fold development. This interpretation is consistent with the box and chevron fold character of regional folds; such folds typically initiate with little layer-parallel shortening and involve considerable hinge migration during development.

Keywords: minor folds, coticule, box fold, chevron fold, hinge migration, hinge propagation, fold symmetry, axial planar cleavage, layer-parallel shortening, shear strain.

# Table of Contents

<i>Abstract</i> .....	ii
<i>Table of Contents</i> .....	iii
<i>List of Figures</i> .....	vi
<i>List of Tables</i> .....	xi
<i>Acknowledgments</i> .....	xii
<i>Terminology</i> .....	xiii

## **Chapter 1: Introduction**

1.1 Introduction to the problem .....	1
1.2 Theory of minor fold development .....	2
1.2.1 Buckling and layer parallel shortening in single layers .....	2
1.2.2 Buckling in a multilayer sequence .....	6
1.2.3 Fold mechanics of box and chevron folds .....	8
1.2.4 Minor and regional fold relationships .....	13
1.3 Scope and objectives .....	18

## **Chapter 2: Regional Geology and Geologic Setting**

2.1 The Meguma Terrane .....	21
2.2 The Meguma Group .....	23
2.2.1 Stratigraphy .....	23
2.2.2 Structure .....	25
2.2.3 Previously proposed theories of minor fold development .....	28
2.2.3.1 General statement .....	28
2.2.3.2 Pre-regional fold buckle development model .....	29
2.2.3.3 Syn-regional fold buckle development model .....	29
2.3 Geology of the study area .....	31

### **Chapter 3: Analysis of Minor Folds**

3.1 Introduction	35
3.2 Outcrop locations	37
3.2.1 Location H <sub>1</sub> (Holland Road)	37
3.2.1.1 General geology	37
3.2.1.2 Minor folds	40
3.2.1.3 Extensional features	49
3.2.2 Location H <sub>2</sub> (Bennery Lake)	52
3.2.2.1 General geology	52
3.2.2.2 Minor folds	54
3.2.2.3 Extensional features	61
3.2.3 Location L <sub>1</sub> (South Uniacke Pit)	63
3.2.3.1 General geology	63
3.2.4 Location L <sub>2</sub> (Highway #1 Pit)	69
3.2.4.1 General geology	69
3.2.4.2 Minor folds	71
3.2.4.3 Extensional features	76
3.2.5 Location L <sub>3</sub> (Beaverbank Road)	80
3.2.5.1 General geology	80
3.2.5.2 Minor folds	84
3.2.5.3 Extensional features	94
3.3 Minor fold comparison and discussion	94
3.3.1 Fold styles	94
3.3.2 Bedding-cleavage relationships	97
3.3.3 Shortening recorded by minor folds	97

### **Chapter 4: Discussion and Conclusions**

4.1 Introduction	101
4.2 Evaluation of previous work on minor folds	101
4.2.1 Pre-regional fold buckling theory	102
4.2.2 Syn-regional fold buckling theory	102

4.3 Fold model for central the Meguma fold belt .....	102
4.3.1 Fold model (profile plane) .....	103
4.3.1 Fold evolution in plan view .....	106
4.4 Conclusions .....	108
4.5 Recommended further work .....	109
<b>Appendix 1: Photographs and sketches of slabs .....</b>	<b>111</b>
<b>Appendix 2: Table of shortening values .....</b>	<b>134</b>
<b>References .....</b>	<b>141</b>

## List of Figures

Figure 0.1	Schematic diagram showing the structural features of a fold. . . . .	xiii
Figure 1.1	Line drawings of fold shapes and their corresponding terminology used in this thesis. . . . .	3
Figure 1.2	Scheme showing the range of fold shapes produced by buckling in a less competent matrix material. . . . .	5
Figure 1.3	Schematic diagram showing the relationship between fold shape and layer spacing. . . . .	5
Figure 1.4	Schematic diagram of the relationship between competent layer spacing and thickness. . . . .	7
Figure 1.5	Models of fold development in regularly alternating competent and incompetent layers. . . . .	9 - 10
Figure 1.6	Three stage scheme illustrating the development of chevron type folds by the lateral migration of conjugate kink bands. . . . .	12
Figure 1.7	Plasticine models showing the progressive changes from box fold shape to chevron. . . . .	12
Figure 1.8	Scheme representing the various shape change histories for a single box fold during bulk shortening. . . . .	14
Figure 1.9	Scheme showing the relationship between parasitic fold symmetry and a larger order fold. . . . .	16
Figure 1.10	Diagram of a plot of limb dip versus shortening illustrating the gradual shortening of a tilted layer. . . . .	16
Figure 1.11	Scheme showing the sheared equivalent fold shapes of a ptygmatic and box fold. . . . .	17
Figure 1.12	Geometry of the superposition of an incremental strain ellipse on a finite strain ellipse. . . . .	19



Figure 2.1	Simplified map and cross-section of the Meguma Terrane showing the central Meguma study area. . . . .	22
Figure 2.2	Stratigraphic subdivision of the Meguma Group. . . . .	24
Figure 2.3	Simplified geology map and cross-section of the study area in the central Meguma zone. . . . .	26
Figure 2.4	Fold model of buckle development prior to regional folding. . . . .	30
Figure 2.5	Fold model of buckle development during regional folding. . . . .	32
Figure 3.1	Schematic diagram defining ordered relationship between multiple scales of folds. . . . .	38
Figure 3.2	Outcrop location map of H <sub>1</sub> (Holland Road) and H <sub>2</sub> (Bennery Lake) study locations. . . . .	39
Figure 3.3	Field photograph and sketch of ptygmatic folds (location H <sub>1</sub> ). . . . .	41
Figure 3.4	Field photograph and sketch of ptygmatic folds developed in layers of varying thicknesses (location H <sub>1</sub> ). . . . .	42
Figure 3.5	Field photograph and sketch of box-style folds with subsidiary folds developed in the median segments and parasitic folds on the box fold limbs (location H <sub>1</sub> ). . . . .	43
Figure 3.6	Field photographs of typical fold shapes at location H <sub>1</sub> . . . . .	44
Figure 3.7	Line drawings of a single folded coticule layer from four parallel slabs (location H <sub>1</sub> ). . . . .	46
Figure 3.8	Thin section map of cleavage on photomicrographs (location H <sub>1</sub> ). . . . .	47
Figure 3.9	Photomicrograph of a locally steepened folded coticule layer (location H <sub>1</sub> ). . . . .	48
Figure 3.10	Histogram of shortening values recorded by folded coticule layers (location H <sub>1</sub> ). . . . .	50

Figure 3.11	Field photographs of an exposed cleavage plane (SW facing) revealing coticule nodules that are locally boudinaged (location H <sub>1</sub> ). . . . .	51
Figure 3.12	Photograph of a locally steepened, folded, and boudinaged coticule layer (location H <sub>1</sub> ). . . . .	53
Figure 3.13	Field photograph and sketch of ptygmatic and modified box folds (location H <sub>2</sub> ). . . . .	55
Figure 3.14	Field photograph and sketch of subsidiary folds developed in the median segment of a box fold (location H <sub>2</sub> ). . . . .	56
Figure 3.15	Line drawings of a single folded coticule layer from four parallel, 4-cm thick slabs cut perpendicular to the hinge (location H <sub>2</sub> ). . . . .	58
Figure 3.16	Thin section map of cleavage on photomicrographs (location H <sub>2</sub> ). . . . .	59
Figure 3.17	Thin section map of cleavage on photomicrographs (location H <sub>2</sub> ). . . . .	60
Figure 3.18	Histogram of shortening values recorded by folded coticule layers (location H <sub>2</sub> ). . . . .	62
Figure 3.19	Slab cut parallel to the strike of cleavage and corresponding thin section showing a boudinaged coticule layer (SW facing) (location H <sub>2</sub> ). . . . .	64
Figure 3.20	Outcrop location map of L <sub>1</sub> (South Uniacke Pit) and L <sub>2</sub> (Highway #1 Pit) study locations. . . . .	65
Figure 3.21	Outcrop scale exposure of steeply dipping non-folded coticule layers (location L <sub>1</sub> ). . . . .	66
Figure 3.22	Close-up field photograph and sketch of the non-folded coticule layers (location L <sub>1</sub> ). . . . .	67
Figure 3.23	Photomicrograph of a spessartine-bearing slate adjacent to a coticule layer (location L <sub>1</sub> ). . . . .	68

Figure 3.24	Field photographs and sketches of a vertical face exposure (location L <sub>2</sub> ). . . . .	at back
Figure 3.25	Field and hand sample photographs of crenulation cleavage (location L <sub>2</sub> ). . . . .	70
Figure 3.26	Field photograph and sketch showing symmetric and asymmetric folds developed in the same layer (location L <sub>2</sub> ). . . . .	72
Figure 3.27	Field photographs of selected fold styles (location L <sub>2</sub> ). . . . .	73
Figure 3.28	Thin section map of cleavage on photomicrographs (location L <sub>2</sub> ). . . . .	75
Figure 3.29	Slab photograph and sketch of four folded coticule layers (location L <sub>2</sub> ). . . . .	77
Figure 3.30	Slab photograph and sketch of a moderately asymmetrically folded coticule layer (location L <sub>2</sub> ). . . . .	78
Figure 3.31	Histogram of shortening values recorded by folded coticule layers (location L <sub>2</sub> ). . . . .	79
Figure 3.32	Photomicrographs of well-developed outer-arc extension (location L <sub>2</sub> ). . . . .	81
Figure 3.33	Photomicrograph and sketch showing a thin boudinaged coticule layer (location L <sub>2</sub> ). . . . .	82
Figure 3.34	Outcrop location map of location L <sub>3</sub> (Beaverbank Road). . . . .	83
Figure 3.35	Field photograph and sketch of folded coticule from a profile section on the east side of the Beaverbank Road (location L <sub>3</sub> ). . . . .	85
Figure 3.36	Field photograph and sketch of two steeply dipping folded coticule layers (location L <sub>3</sub> ). . . . .	86
Figure 3.37	Field photograph and sketch of two folded coticule layers (location L <sub>3</sub> ). . . . .	87

Figure 3.38	Line drawings of two folded coticule layer from six parallel, 4-cm thick slabs cut perpendicular to the hinge (location $L_3$ ). . . . .	89
Figure 3.39	Plan view sketch of a doubly plunging folded coticule layer (location $L_3$ ). . . . .	90
Figure 3.40	Histograms of shortening values (location $L_3$ ). . . . .	92
Figure 3.41	Photomicrographs showing a folded coticule layer of varying thickness (location $L_3$ ). . . . .	93
Figure 3.42	Histogram comparing the range of values of shortening from the regional fold hinge and limb. . . . .	98
Figure 3.43	Illustrated chart comparing the various minor fold features between all locations. . . . .	at back
Figure 4.1	Scheme showing a possible sequence of fold development in the profile plane for the central Meguma Terrane. . . . .	at back
Figure 4.2	Plan view schematic diagram showing the possible methods of fold development involving hinge migration. . . . .	107
Figure A1.1	Slab photographs and sketches of folded coticule layers from location $H_1$ . . . . . (Appendix 1)	112 - 115
Figure A1.2	Slab Photographs and sketches of folded coticule layers from location $H_2$ . . . . . (Appendix 1)	116 - 119
Figure A1.3	Slab Photographs and sketches of folded coticule layers from location $H_2$ . . . . . (Appendix 1)	120 - 124
Figure A1.4	Slab Photographs and sketches of folded coticule layers from location $H_2$ . . . . . (Appendix 1)	125 - 127
Figure A1.5	Slab Photographs and sketches of folded coticule layers from location $L_3$ . . . . . (Appendix 1)	128 - 133

## List of Tables

Table 3.1	Table of competency contrast ratios from each location. ....	36
Table 3.2	Table of shortening values for each location. ....	99

## Acknowledgements

I am appreciative for the efforts of Rick Horne, my supervisor at the Nova Scotia Department of Natural Resources (NSDNR), for suggesting and supervising this project. I would also like to extend my gratitude to the NSDNR for permitting me the use of computers, printers, and plotters, and for paying for photograph developing. Slab photographs were done by Carol Murphy at the NSDNR. All figures in this thesis were drafted by the author, but slides for a talk and defence were produced by the drafting department at the NSDNR.

An important part of the process in completing this thesis was the feedback and communication with the other honours students this year. I would like to thank and congratulate the rest of the Honours 2000 class for an exceptional job well done. I am especially indebted to Ryan Campbell and Megan Surette for their friendship and light humour, making each step that much easier.

I appreciate the effort of Nicholas Culshaw, my supervisor in the department, for his suggestions and support. It was a challenge to convince Nick, but in the end I think we both learned a lot from each other. Finally, Rick Horne provided assistance and support well past what was expected. I am deeply grateful to Rick for treating me like a colleague throughout this project.

## Terminology

The terminology used in this thesis is primarily standard structural terms. These terms are defined below. Special terminology not adopted universally is introduced in the body of the thesis.

***General fold-related terms*** (See Figure 0.1 for an illustration of the features defined)

*Bedding-cleavage intersection lineation*: The line defined by the intersection of cleavage and bedding. The bedding-cleavage intersection is parallel to the fold hinge where cleavage is axial planar to the fold.

*Axial plane*: A plane which bisects the limbs of the fold.

*Fold hinge*: A line connecting the points of maximum curvature of the fold.

*Hinge zone*: The curved section of fold between planar limbs.

*Principal axis*: The principal axes of the fold are, by convention: a axis is normal to the axial plane, the b axis parallels the fold hinge and the c axis is perpendicular to the hinge and contained within the axial plane.

*Profile (ac) plane*: The plane which is perpendicular to the fold hinge.

*Plunge*: The angle between the fold hinge and the horizontal measured within a vertical plane containing the fold hinge.

### ***Orientation data***

*Strike*: Azimuth of structural contour, or intersection of a plane with the horizontal.

*Dip*: The inclination of a planar surface.

*Trend*: The azimuth, projected into the horizontal, and the dip, within a vertical plane, of a lineation.

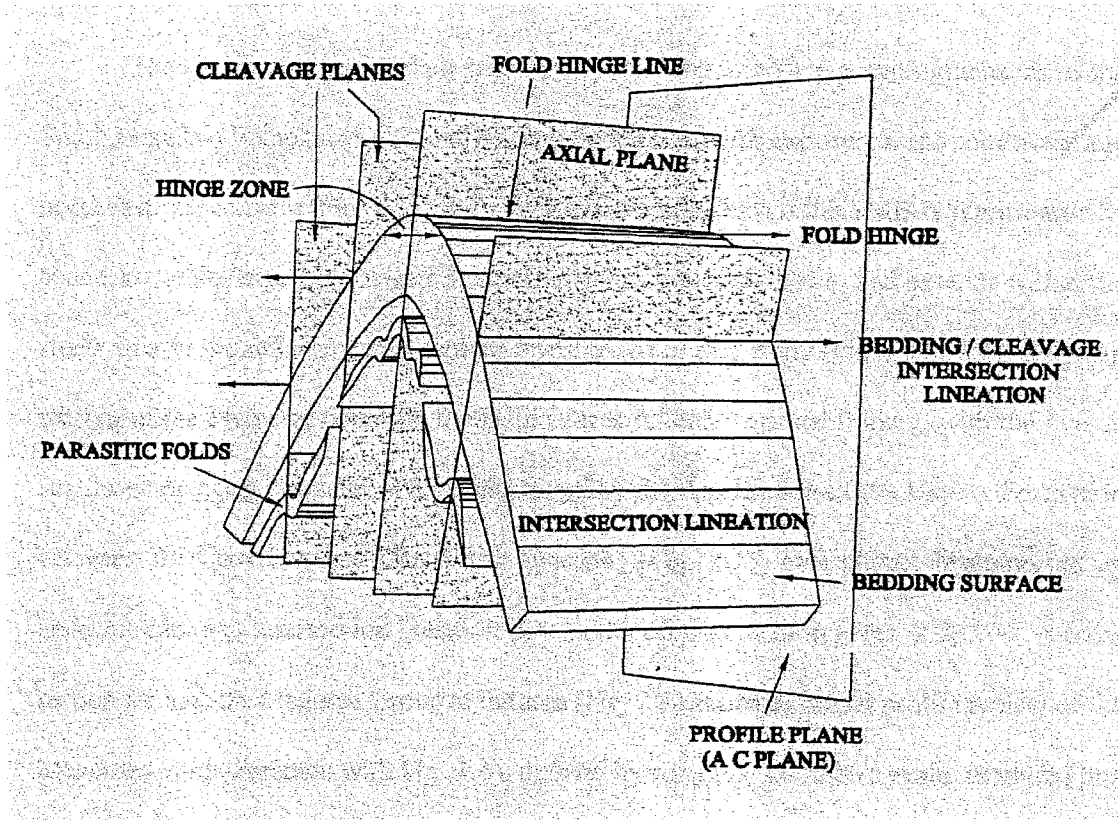


Figure 0.1. Schematic diagram showing the structural features of a fold. (From Boulter, 1989).



## **Chapter 1: Introduction**

### **1.1 Introduction to the problem**

The relationship between minor and regional folds can provide information on the history of fold belt development. The classical interpretations of parasitic folds describe a pre-regional fold origin for the development of minor folds (Ramsay and Huber, 1987; Price and Cosgrove, 1990; de Sitter, 1958). Regional fold style is traditionally modeled as simple, regularly sinusoidal upright folds. Minor folds have been termed parasitic because their shape typically follows that of the regional fold, sheared on the limbs and upright in the hinge (de Sitter, 1958). These observations of symmetry aid the field geologist in determining the geometry of regional folds.

Minor folds are known to occur in the Meguma Group of Nova Scotia and have been used to interpret the regional fold history (Graves and Zentilli, 1982; Henderson et al., 1986; Mawer, 1987; Williams and Hy, 1990; Horne, 1998). However, little systematic detailed documentation of minor folds has been done. It is generally accepted that the fold history of the Meguma Group is complex (e.g. Faribault, 1899, 1913; Henderson et al., 1986; Horne, 1998; Williams and Hy, 1990). However, minor folds have not been described in detail with respect to the complex fold history.

This thesis presents a systematic description of minor folds from some regional fold hinges and limbs. The minor folds are developed in spessartine-carbonate-quartz layers called coticles. The geometric styles of these minor folds are used to present a model of regional fold development for a particular area in the Meguma zone of Nova Scotia. A key

focus of this thesis is to consider the history of minor fold development within the context of regional box fold development, where hinge migration may be a significant folding mechanism. Terminology used in this thesis relating to box folds is shown in Figure 1.1.

Chapter 1 provides a theoretical background to fold development; chapter 2 presents a geological setting of the Meguma Terrane and an overview of previous theories of fold development; chapter 3 describes the results of the minor fold analyses; and chapter 4 is a discussion of the previous theories in light of this study and presents a model of fold development for the study area.

## **1.2 Theory of fold development**

### **1.2.1 Buckling and flattening during layer parallel shortening in single layers**

Making a clear distinction between buckling and flattening during layer parallel shortening is necessary in a discussion of fold mechanics. Ramsay and Huber (1987, pg. 309) define buckling as the process of fold development by the "...growth ... of mechanical instabilities setting up sideways deflections during the shortening along a planar feature...". The buckle type of strain is characteristic where there is a high competence contrast between layers. Ramsay and Huber (1987, pg. 403) define flattening as "[t]he homogenous or nearly homogenous strain that can develop when a layered rock is shortened parallel to the lithological layering.... This type of strain is characteristic of deformation of layers where the competence contrast between the materials is small". In summary, buckling occurs when layers of high competence contrast are shortened, whereas flattening occurs in layers of similar competence where shortening is accommodated by changing the thickness of the layers.

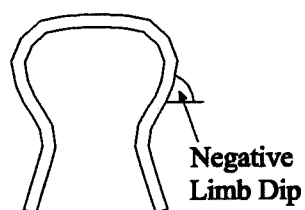
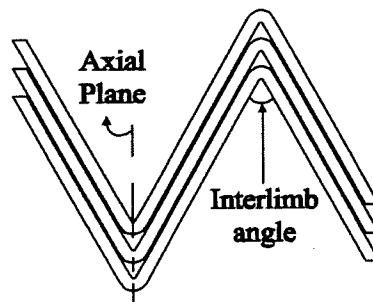
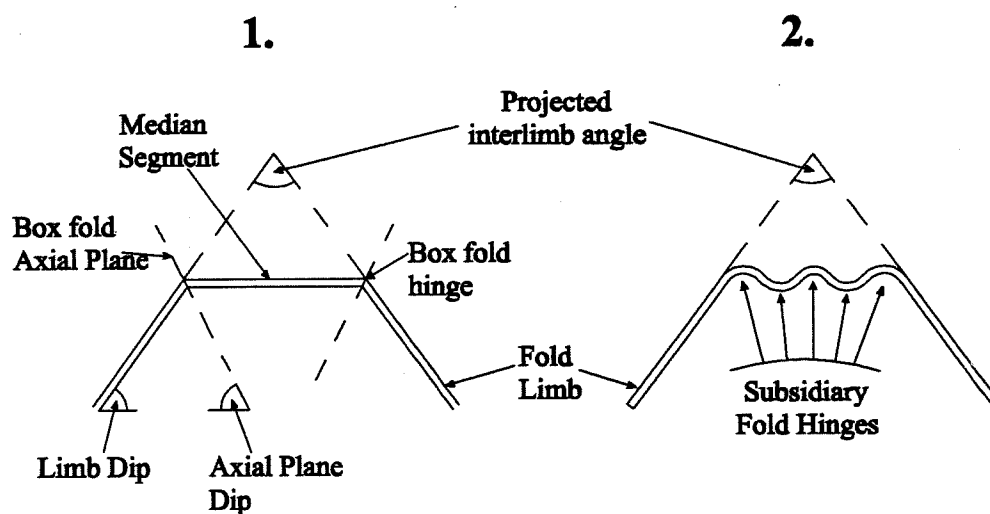
**(a) Ptygmatic****(b) Chevron****(c) Box fold and box fold with subsidiary fold hinges**

Figure 1.1. Line drawings of fold shapes and their corresponding terminology used in this thesis. Fold styles include (a) ptygmatic, (b) sinusoidal, (c 1) box fold, and (c 2) box fold with subsidiary folds developed in the median segment. (Modified from Fowler and Winsor, 1996).

The physical properties of the layers being folded affect the style of folding. Such physical properties in single layer folding include layer thickness, and competency contrast (Ramsay and Huber, 1987; Price and Cosgrove, 1990).

Layer competence contrast, or viscosity contrast, is controlled by the mineralogy of the respective layers and usually is represented as a ratio. Using simple field measurements of the fold arc length and the layer thickness the *Biot-Ramberg equation* can be applied to obtain the layer competence contrast ratio:

$$\mu_1/\mu_2 = 0.024 (L/t)^3 \quad (\text{Eq. 1.1})$$

where  $\mu_1$  and  $\mu_2$  are the viscosities of the competent and incompetent layers, respectively, and  $L/t$  is the ratio of fold arc length to layer thickness (from Ramsay and Huber, 1987). A practical example of a high competency contrast is an interlayered sequence of quartzite and slate. Competence contrast is an important property when considering the overall shortening a multilayer sequence has experienced. Variations in competency contrast can affect whether a layer accommodates shortening entirely by buckling, flattening, or some combination of the two end members (Fig. 1.2). Ramsay and Huber (1987) determined that layers with viscosity contrasts ( $\mu_1/\mu_2$ ) greater than 50 will buckle perfectly, layers with viscosity contrasts less than 10 will primarily be flattened and amplify sluggishly, and layers in the range  $10 < \mu_1/\mu_2 < 50$  will produce some combination of buckling and flattening (i.e. Fig. 1.2).

Layer thickness influences the fold wavelength. A particular layer thickness will control the wavelength of the fold. In a practical geologic case, a folded sedimentary layer that originally was tapered will display relatively large fold wavelengths in the thicker

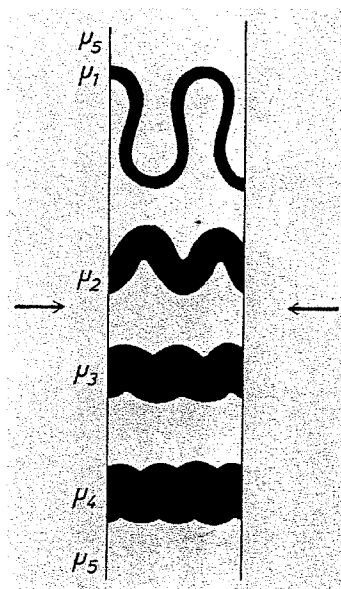


Figure 1.2. Scheme showing the range of fold shapes produced by buckling in a less competent matrix material. The upper pyriform fold represents pure buckling with the maximum viscosity contrast  $\mu_1/\mu_5$ . The lowest fold (cusate-lobate) represents the minimum contrast, of  $\mu_4/\mu_5$ , where the majority of shortening is accommodated by flattening. The two middle folds represent a combination of buckling and flattening. (From Ramsay and Huber, 1987).

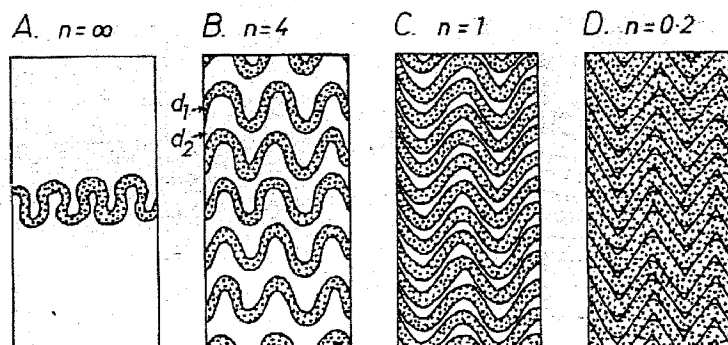


Figure 1.3. Schematic showing the relationship between fold shape and layer spacing. As the incompetent layers progressively decrease in thickness,  $d_2$ , the fold shapes become less curved until, in the case of chevron folds, only the fold crests are curved. The proportion of incompetent to competent layer thickness is given by  $n = d_2/d_1$ . (From Ramsay and Huber, 1987).

segments while displaying smaller fold wavelengths and amplitudes in the tapered thinner segments

### **1.2.2 Buckling in a multilayer sequence**

The physical properties of layers spaced closely to one another affect the fold style in a multilayer sequence. The zone of influence of a particular layer on adjacent layers is determined by half the fold wavelength and is called the zone of contact strain (Ramsay and Huber, 1987). As the spacing between competent layers decreases, the fold styles change from a ptygmatic style with negative interlimb angles to a chevron style where curvature becomes increasingly restricted to the hinge zones (Figs 1.1 and 1.3). Figure 1.4 illustrates the relationship between competent layer spacing and thickness, termed harmony. In disharmonic folding (Fig. 1.4B) the sideways deflections of widely spaced adjacent folded layers are not great enough to influence the other layer so that the layers essentially act as single layers. If however, the zone of contact strain overlapped each layer then there would be some geometric influence in the competent layers. If the competent and incompetent layers were of similar thickness, spacing, and competency contrasts throughout the sequence then harmonic folds would form (Fig. 1.4C). On the other hand, if the competent layers display variable thickness or have different competency contrasts, the wavelengths in each folded layer may differ resulting in polyharmonic folding (Fig. 1.4D). The thinner layer commonly displays sympathy to the thicker layer. That is, the enveloping surface of the thinner buckled layer harmonizes to the wavelength and amplitude of the thicker layer.

Ramsay and Huber (1987) have identified six fold models for multilayer sequences (Fig 1.5A-F) of varying competency contrast and layer spacing. The first three models (A-C)

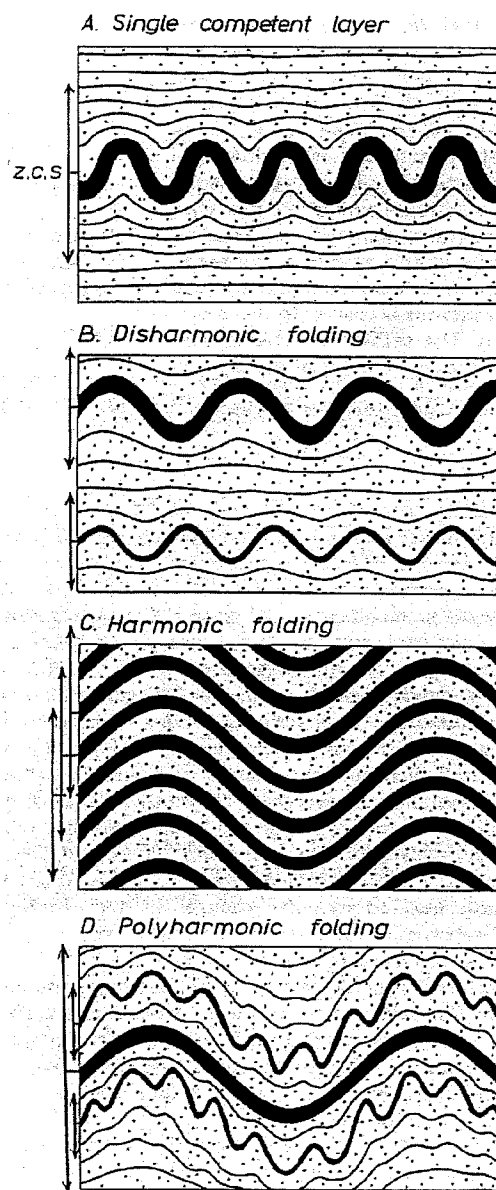


Figure 1.4. Schematic representation of the relationship between competent layer spacing and thickness. The relationship is based on the interactions of the zones of contact strain (Z.C.S.) around each competent layer. (From Ramsay and Huber, 1987).

vary in layer spacing and have low competency contrasts. Because the conditions in these models do not represent the general conditions in the Meguma Group or the study locations these three models will not be considered further. The last three models (D-F) display fold styles represented in the Meguma Group and the study locations. As evident by the models, as layer spacing between the competent layers decrease so does the curvature of the folds. At moderate and low competent layer spacing the fold styles are characterized by regular chevron folds, and box- and irregular chevron folds, respectively.

### **1.2.3 Fold mechanics of box and chevron folds**

Because box folds are the dominant regional fold style in the Meguma Group (see section 2.2 and Fig. 2.1) their mechanics of development and evolution through fold development must be considered. Experimental studies indicate that box- and chevron-style folds initiate by development of conjugate instabilities reflecting the high anisotropies in multilayered sequences (Fig. 1.6, Biot, 1965; Cobbold et al., 1971; Dubey and Cobbold, 1977; Fowler and Winsor, 1996; Price and Cosgrove, 1990; Weiss, 1980). Folds of this style inherently show no systematic vergence when shortening is perpendicular to layering (Figs. 1.6 and 2.1).

Box folds, or conjugate kink folds, differ from other folds in some important ways. The most evident feature of a box fold is its median segment (Fig 1.1c). In upright box folds the median segment is the horizontal to subhorizontal segment of the fold connecting the fold limbs. Fowler and Winsor (1996) constructed plasticine multilayer models which produced box folds and chevron folds. Their main objective in building these models was to document the fold profile shape changes through the evolution of fold development. Their study shows



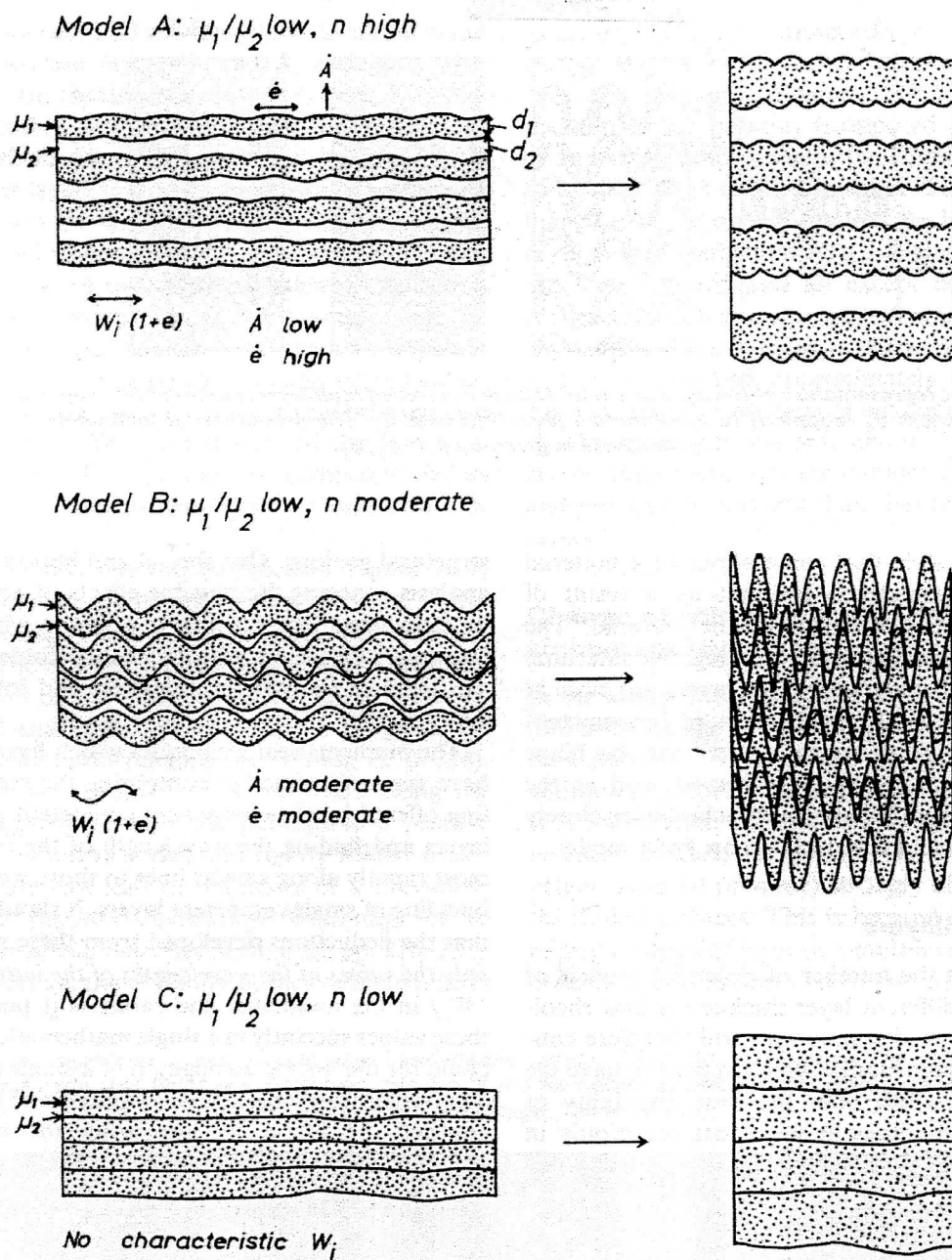


Figure 1.5. Models of fold development in regularly alternating competent and incompetent layers. Variables built into the models are competency contrast ( $\mu_1/\mu_2$ ) and layer spacing ( $n=d_2/d_1$ ). The models A-C (this page) represent low competency contrasts with variable layer spacing and the models D-F (next page) represent high competency contrasts with variable layer spacing. (From Ramsay and Huber, 1987).

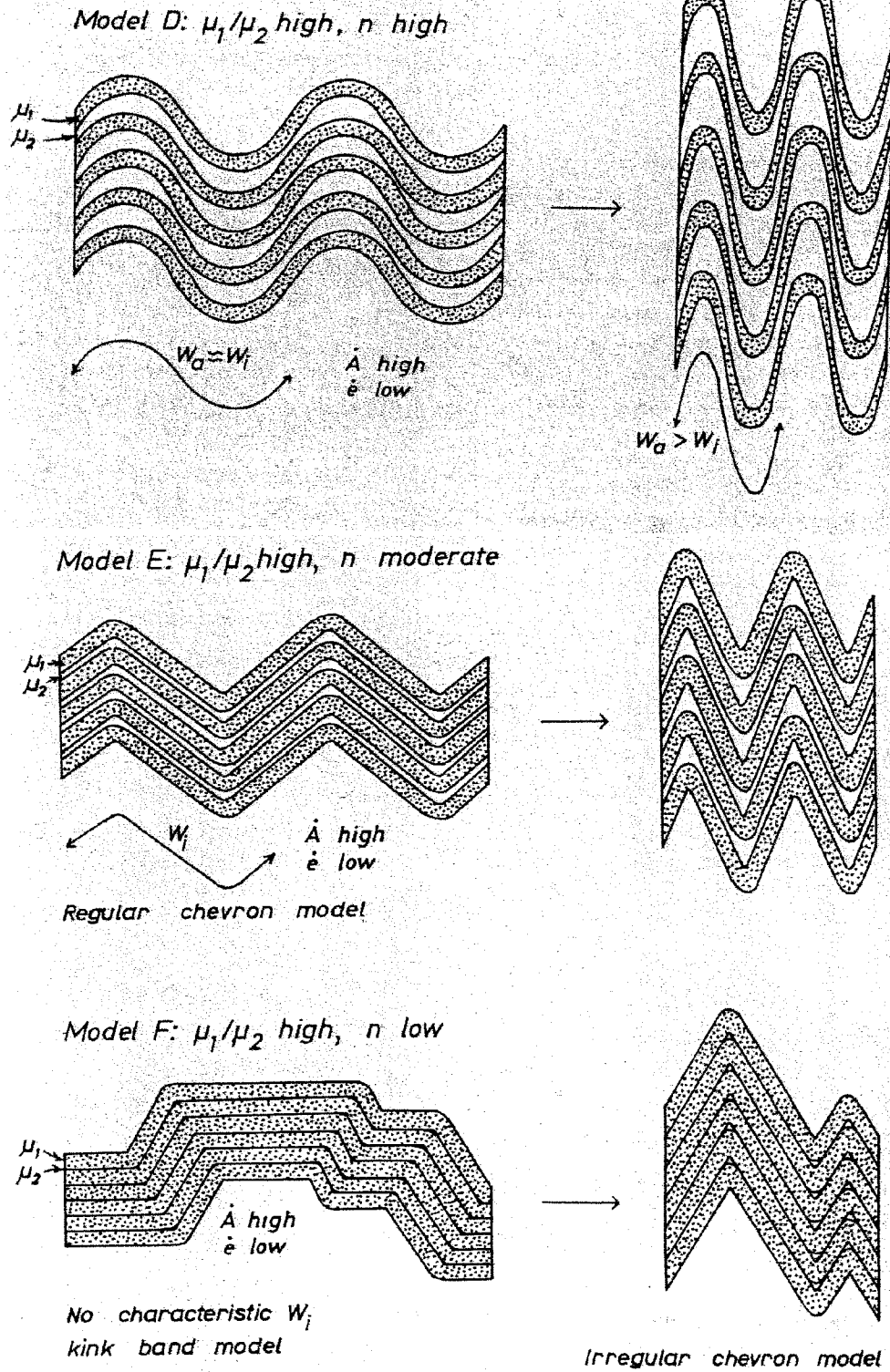


Figure 1.5 continued.

that profile shape changes included hinge migration and limb rotation during monophasic deformation. In some instances of their plasticine models, they documented that when the median segment was oriented parallel to the shortening direction, subsidiary folds in the median segment were formed (Figs 1.7 and 1.1c).

Another important element to box folds is the orientation of the axial planes. As in kink folds, axial planes in box folds develop at an oblique angle to the maximum principal stress direction whereas in sinusoidal or chevron folds axial planes are oriented perpendicular to the principal shortening direction (Fig 1.1). The significance of the orientation of the axial planes is in how they react to progressive deformation. Fowler and Winsor (1996) found that, in the fold profile, the axial planes of box folds fuse together to form chevron folds (Fig. 1.7). Weiss (1980) determined that conjugate kink bands developed by the sideways migration of axial surfaces where chevron folds form at the limit of sideways migration (Fig. 1.6).

The median segments and axial planes of box folds described above are important physical properties in controlling how box folds change shape during folding. Three major processes can occur in shape changes of box folds: hinge migration, hinge fusion, and limb rotation (Fig. 1.7). Hinge migration is a process that, mathematically, must take place in many models (Ghosh et al., 1996; Treagus and Treagus, 1981), but field evidence for hinge migration can be difficult to establish.

As implied, hinge migration refers to the movement of a hinge, with respect to a fixed point on the layer, during progressive fold development. Hinge fusion is the migration of two adjacent hinges together and results in the formation of chevron folds (Figs. 1.7 and

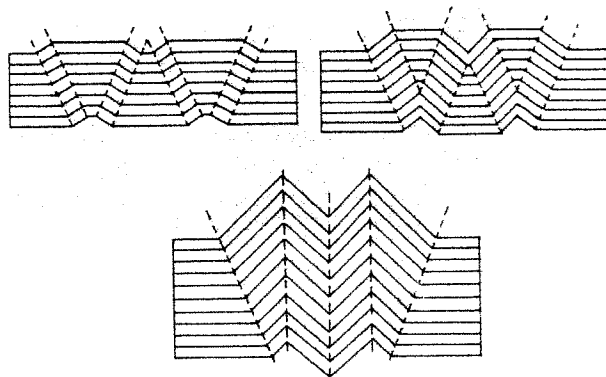


Figure 1.6. Three stage scheme illustrating the development of chevron type folds by the lateral migration of conjugate kink bands. Hinge migration is intrinsically necessary in this type of chevron fold formation. This necessity suggests that second order structures sometimes found in the hinge areas should not be localized around the final positions of the hinges, but should also exist along the parts of the layers through which the hinge has migrated. (From Price and Cosgrove, 1990).

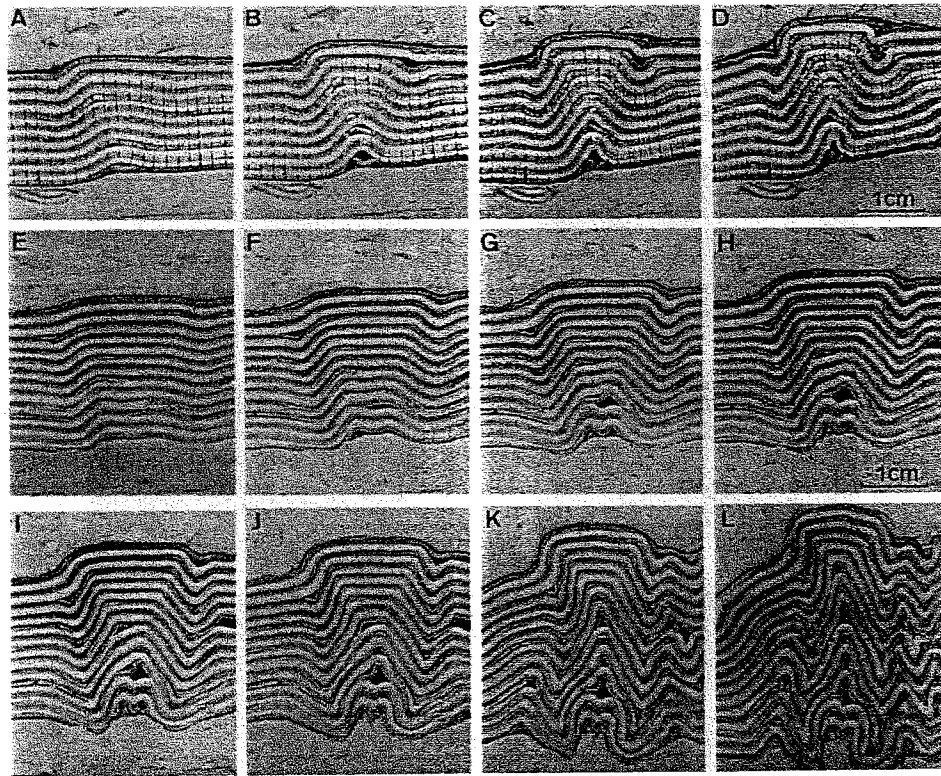


Figure 1.7. Plasticine models showing the progressive changes from box fold shape to chevron. Note that in the transition from box folds to chevrons (specifically, E-L) there is lateral migration of axial planes progressively decreasing the length of the median segment and increasing the length of the limbs. Note that the initially flat lying layers at the right edge is buckled into tight chevrons late in the folding of this sequence. Hinge migration is inherent in this type of fold development. Layer interfaces were very lightly brushed with oil, leading to ease of interlayer slip. Note that the sequences A-D and E-L are different model experiments (From Fowler and Winsor, 1996).

1.8a). Hinge "jamming" was documented by Fowler and Winsor (1996) and is described as an interruption or a slowed rate in hinge migration. That is, during progressive folding a migrating hinge may be intermittently fixed or the rate in which the migration occurs is slowed. Two important points come out of hinge "jamming": (1) the evolution to chevron shape can be aborted and the box fold shape persist possibly permitting the formation of subsidiary folds in the median segment (Fig. 1.8b and c), and (2) one hinge can be "jammed" while the other remains mobile so that the median segment fuses with the limb resulting in an irregular chevron (Fig. 1.8d). Limb rotation (Fig. 1.8e) refers to the process of limb steepening during fold development.

#### **1.2.4 Minor and regional fold relationships**

Folding within a complex multilayer may occur on several different scales during a single phase of compression. Classical interpretations of minor folds suggest a buckling of competent layers prior to the initiation of regional folds (de Sitter, 1958; Price and Cosgrove, 1990; Ramsay and Huber, 1987). During regional folding these minor folds are incorporated onto limbs and into hinges and occur as folds parasitic to the regional fold (de Sitter, 1958). Parasitic folds display an asymmetry on regional fold limbs (Z or S form) and symmetry in regional fold hinges (M or W form) (Fig. 1.9). The asymmetry of minor folds is a result of flexural shear strain as the regional fold limbs steepen through continued compression. Folds of different scales are also considered in terms of orders. That is, the larger scale fold can be considered the first order and each successively smaller fold is one order higher. For the purposes of this thesis, specific identification of the particular orders of folds have been made and are explained in Figure 3.1. For reference, regional folds are considered first order;

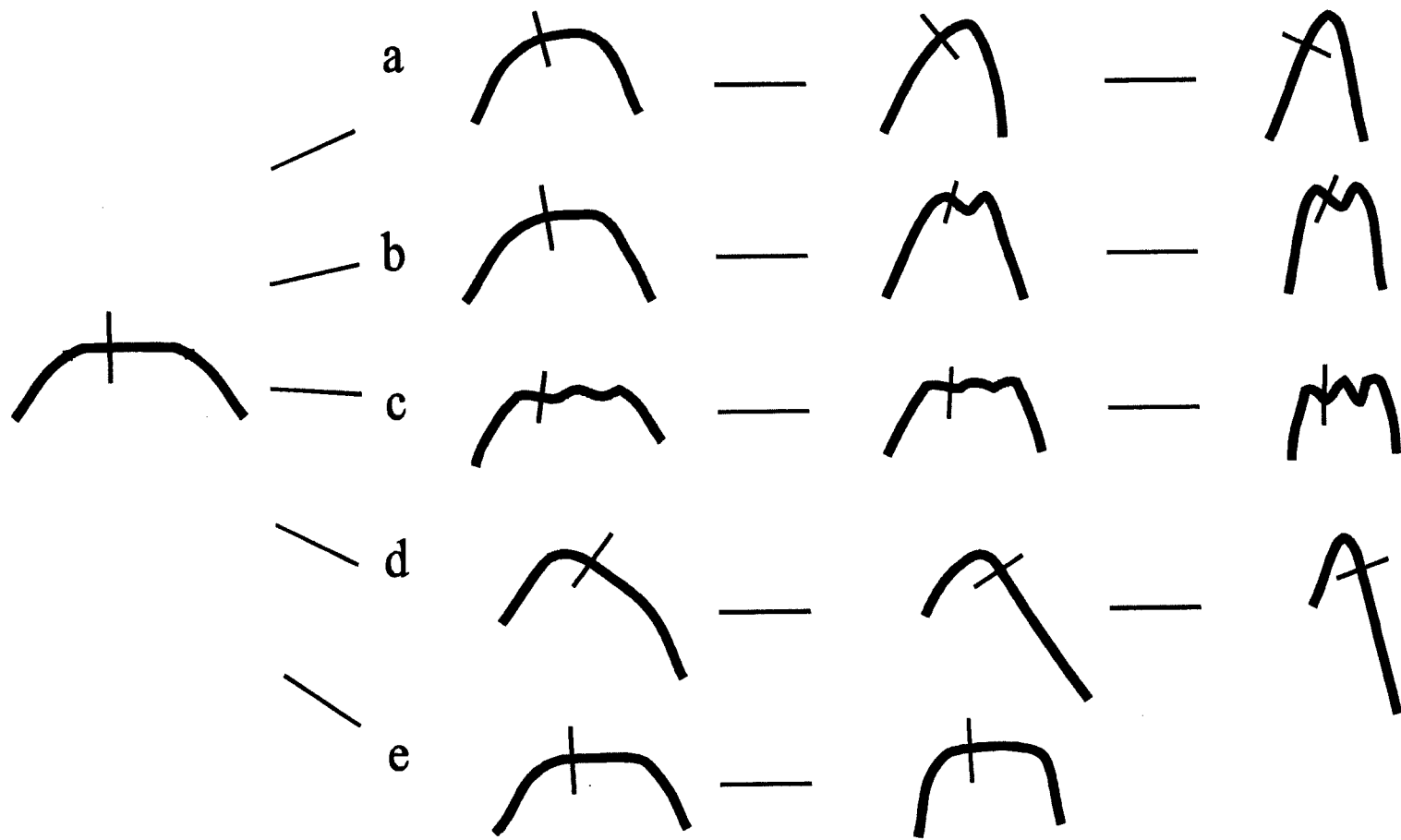


Figure 1.8. Scheme representing the various shape change histories for a single box fold during bulk shortening. (a) Hinge migration and fusion to form a chevron. (b) Buckling of the median segment forming subsidiary folds. (c) Buckling of the median segment initially forming gentle subsidiary folds, which are subsequently tightened during further bulk shortening. (d) Fusion of the median segment with one fold limb by the jamming (fixing) of one hinge and migration of the other forming an asymmetric chevron. (e) Fixed hinges and rigid median segment with shortening accommodated by limb steepening. The passive marker traces the approximate path in each shape change history. (Modified from Fowler and Winsor, 1996).

mesoscale folds (~10 m wavelength) are considered second order; minor folds (the majority of folds described in this study, 2-20cm) are considered third order; and subsidiary folds developed in the median segment of a third order box fold are considered fourth order folds.

Figure 1.10 shows how a layer originally at a low angle to the principal compression develops a fold that becomes increasingly tight and asymmetric with continued steepening of the regional limb (de Sitter, 1958). de Sitter (1958) also observes that the axial plane of the minor fold must remain parallel to the regional fold axial plane throughout limb steepening.

Descriptions of parasitic folds typically specify originally ptygmatic or sinusoidal shape and not of box fold shapes. Minor folds with box fold shapes do not fit into the parasitic model well. They display two axial planes not originally parallel to the regional axial plane and therefore, when sheared on a regional fold limb the minor box fold axial planes will not be co-axial-planar with the regional fold (Fig. 1.11).

#### *A Note on Unfolding*

The concept of unfolding of parasitic-type folds may be relevant to this study. Ramsay and Huber (1983) suggest that as regional fold limbs rotate to steep limb dips they enter a theoretical zone of extension. This zone of extension is defined by negative finite longitudinal strain ( $e_f$  -ve) and positive incremental longitudinal strain ( $e_i$  +ve) in the superposed incremental strain ellipse on the finite strain ellipse (Fig. 1.12a). Geologically, this strain condition can be related to a competent layer, initially folded ( $e_f$  -ve) then rotated into an extensional strain state ( $e_i$  +ve) where unfolding and boudins form (Ramsay and Huber, 1983). de Sitter (1958) also shows that as a layer rotates to limb dips greater than  $45^\circ$

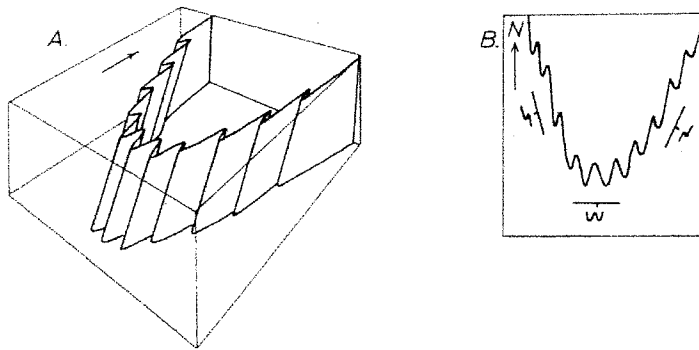


Figure 1.9. Scheme showing the relationships between parasitic fold symmetry and a larger order fold. B shows the map pattern and symbols used to communicate the type of parasitic fold symmetry. (From Ramsay and Huber, 1987).

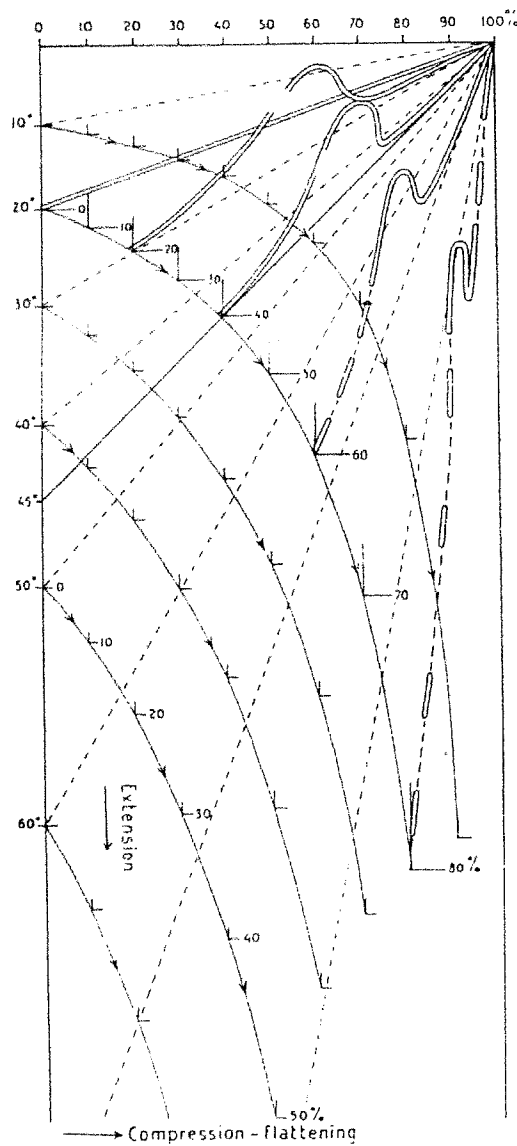
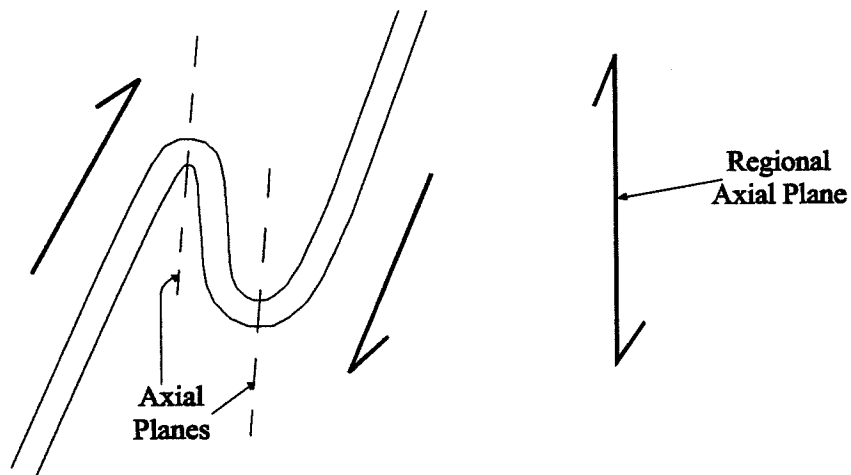


Figure 1.10. Plot of limb dip versus shortening (percentage) illustrating the gradual shortening of a tilted layer with increasing shortening until a dip of  $45^\circ$  is reached, afterwards extension occurs. Note that the buckle fold is not unfolded by the extension, and that the buckle fold is axial planar through the fold history. (From de Sitter, 1958).



**(a) Sheared ptygmatic or tight chevron fold**



**(b) Sheared box fold**

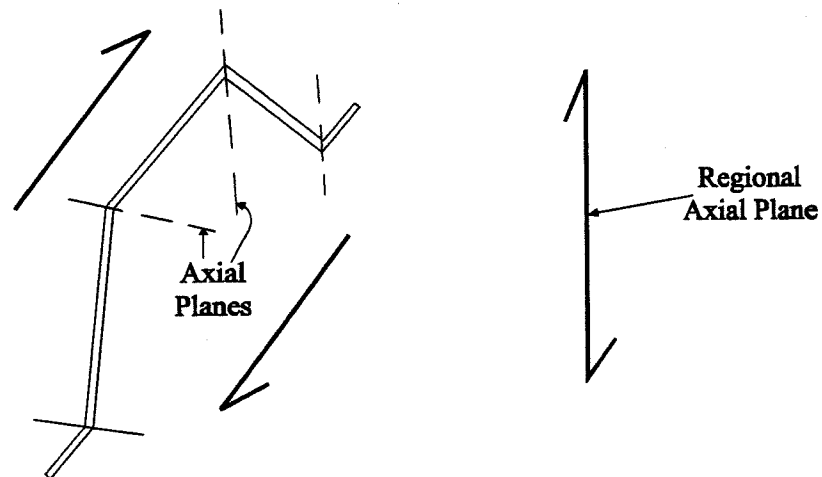


Figure 1.11. Scheme showing the sheared equivalent fold shapes of (a) a ptygmatic and (b) box fold. Shearing is caused by flexural flow as the folded layers are rotated from flat lying to steeply dipping. Important to note, the sheared ptygmatic fold is regionally axial planar, but the sheared box fold displays variable orientation with respect to the regional axial plane.

that layer experiences extension (Fig. 1.10). In contrast to the interpretation of Ramsay and Huber (1983), de Sitter (1958) suggests that although layer-parallel boudinage occurs in this strain state, unfolding of minor folds does not.

### **1.3 Scope and Objectives**

This study examines minor folds in coticule layers and their regional setting in the central Meguma zone in the Mt Uniacke and Kinsac Synclinoriums (Fig. 2.1). The coticule layers occur in the upper Beaverbank member, the lowermost unit of the Halifax Formation (Figs. 2.1 and 2.2). The coticule layers have a very high viscosity with respect to their host rock and minor folds are well developed in these layers. The study location outcrops are representative of regional structure and occur on regional fold limbs and hinges. Previous studies of minor folds in the Meguma Group have primarily focused on folds developed in bedding-parallel quartz veins. However, quartz veins are not primary layering and therefore may not reflect the entire strain history of the fold belt. The coticule layers are primary layers and do reflect the entire strain history.

The objectives of this thesis are to document minor folds at various regional structural settings, including fold shape, bedding-cleavage relations, and shortening, and to document extensional features displayed by the coticule layers. In light of the documentation of minor folds, previous fold development models are evaluated. Finally, a model for the minor and regional fold history in the study area is developed.

Field observations, structural data, and hand samples for slab and thin section analyses were collected at each of the study locations. Field observations include photography of key exposures, documenting lithology changes in the host rock and coticule,

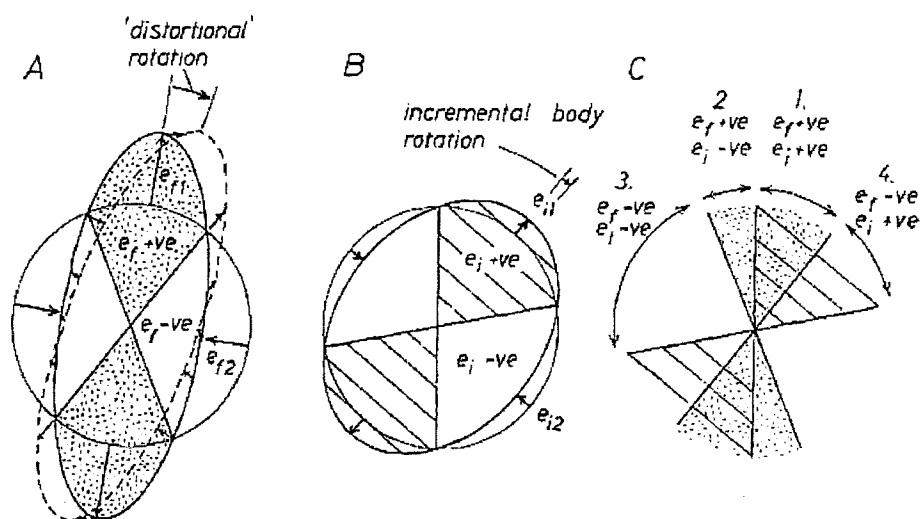


Figure 1.12. Geometry of the superposition of an incremental strain ellipse  $i$  (B) on a finite strain ellipse  $f$  (A). C shows the quadrants of possible combinations of positive and negative finite longitudinal strain,  $e_r$ , with positive and negative incremental strain,  $e_i$ . Quadrant 4 is the theoretical sector in which unfolding may occur where finite strain is shortening and incremental strain is extension. (From Ramsay and Huber, 1983).

and thickness and spacing variations of the coticule layers. Structural data include measurements of bedding, cleavage, bedding-cleavage intersection lineation, direction of vergence, trace of axial surface of minor folds, and the hinge of minor folds. Slab and petrographic observations include mineralogy, fold shape changes along the hinge trace, extensional textures, and cleavage relationships.

## Chapter 2: Regional Geology and Geologic Setting

### 2.1 The Meguma Terrane

Nova Scotia is divided into north and south domains, the Avalon Terrane and the Meguma Terrane, respectively (Fig 2.1). These terranes are separated by the steeply-dipping, dextral Cobequid-Chedabucto Fault System extending more than 300 km (Mawer and White, 1986). The Meguma Terrane represents a suspect terrane accreted to the Avalon Platform (Schenk, 1991; Keppie, 1983). The Meguma Terrane is named for the extensive Meguma Group, a thick succession of Cambrian-Ordovician, deep-water, clastic metasediments. Ordovician-Early Devonian metasedimentary and metavolcanic rocks conformably to paraconformably overly the Meguma Group. Voluminous, Late Devonian granitic and lesser mafic plutons generally truncate regional fold patterns and related cleavage within the metamorphic rocks. Schenk (1995) upgraded the Meguma Group to the Meguma Supergroup; however, regional mapping done in the study area has not adopted the new terminology and therefore, the Meguma Group terminology will be used in this thesis.

The Cambrian to Early Devonian rocks were deformed and metamorphosed to sub-greenschist to lower amphibolite facies during the Mid-Devonian Acadian Orogeny.  $^{40}\text{Ar}/^{39}\text{Ar}$  dating constrains the orogeny to 415-385 Ma (Muecke et al., 1988; Keppie and Dalmeyer, 1987; Hicks et al., 1999; Kontak et al., 1998), likely reflecting accretion of the Meguma Terrane to Avalon (Keppie, 1983; Muecke et al., 1988). The range in metamorphic ages possibly reflects long-lived deformation and development of related cleavage across the terrane (Keppie and Dalmeyer, 1987; Keppie, 1993; Kontak et al., 1998).

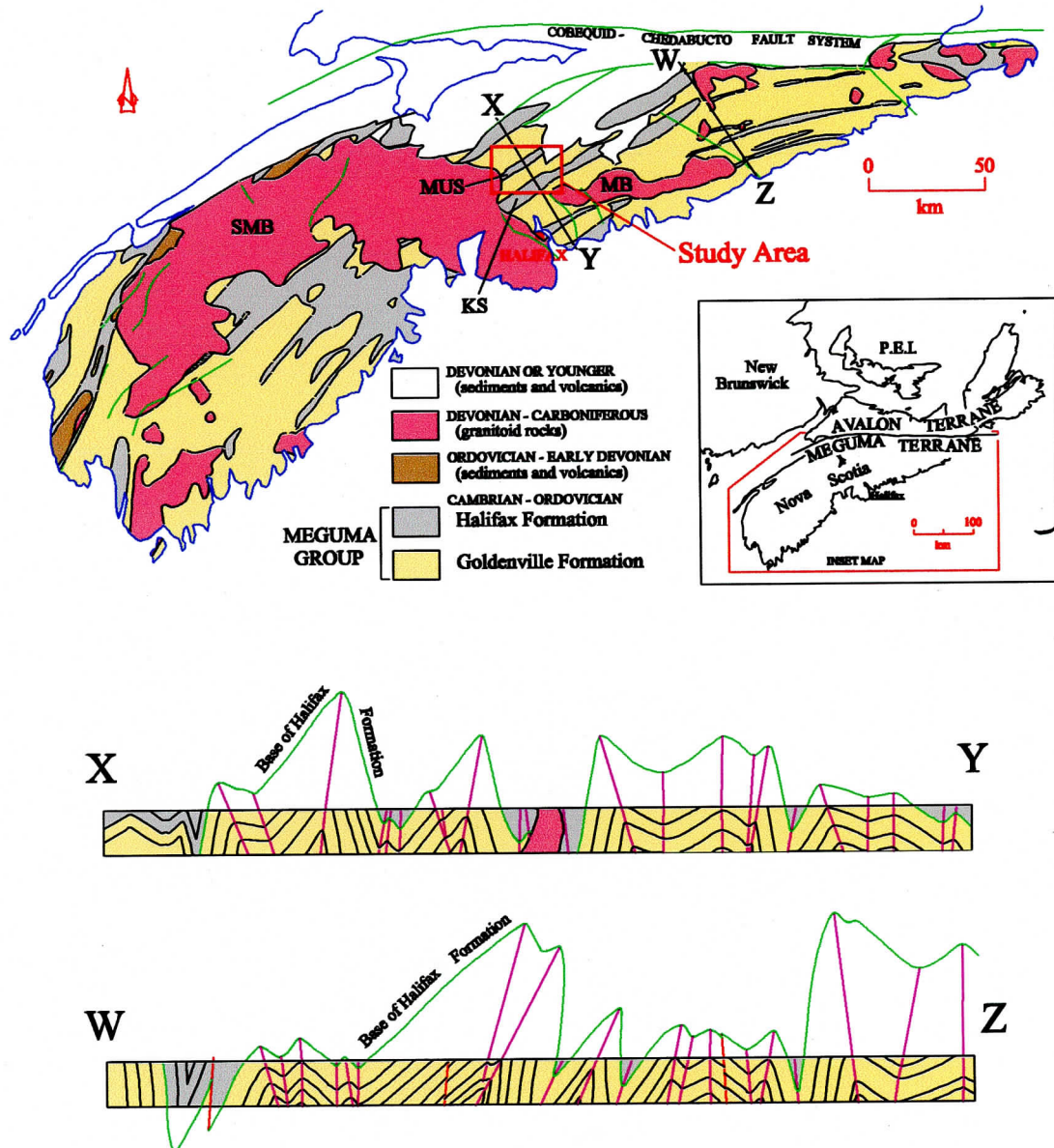


Figure 2.1. Simplified map and cross-section of the Meguma Terrane showing the location of the central Meguma study area. Cross sections modified from Fletcher and Faribault, 1911. MUS - Mount Uniacke Synclinorium; KS - Kinsac Synclinorium; SMB - South Mountain Batholith; MB - Musquodobit Batholith.

## 2.2 The Meguma Group

### 2.2.1 Stratigraphy

The Meguma Group consists of deep-sea to near-shelf gradational fan-complexes (Schenk, 1995). It has traditionally been divided into two formations, the lower metasandstone-rich Goldenville Formation and the upper slate/phyllite-rich Halifax Formation (Fig. 2.2). The Goldenville Formation is composed of grey to greenish grey metaquartzarenite, metagreywacke, quartzite, and subordinate grey, black, and green metasilstone and slate (Schenk, 1995). The Halifax Formation conformably overlies the Goldenville Formation and consists of greyish green to black slate and metasilstone. The Goldenville and Halifax formations have locally been subdivided (Fig. 2.2, O'Brien, 1988; Waldron, 1992; Schenk, 1991, 1995; Ryan et al., 1996).

The boundary between the Goldenville and Halifax formations is locally characterized by units enriched in manganese and carbonate (Waldron, 1992; Schenk, 1995; Graves and Zentilli, 1988; Feetham et al., 1997). The upper Beaverbank unit in the central Meguma Terrane is especially enriched in manganese and carbonate. The enrichment results from the precipitation of manganese-rich carbonate near the sediment-water interface (Graves and Zentilli, 1988). The enrichment represents the transition between oxidation (lower sandy units) and reduction (overlying sulphitic black shales) (Waldron, 1992; Schenk, 1995). During metamorphism spessartine garnet developed at the expense of the carbonate (Graves and Zentilli, 1988). As a result, spessartine-bearing quartzite and carbonate layers are locally abundant and are termed coticles (Keenan and Kennedy, 1983; Feetham et al., 1997). Coticule layers range in thickness, from microscopic to 20 cm (typically 2-4 cm), and

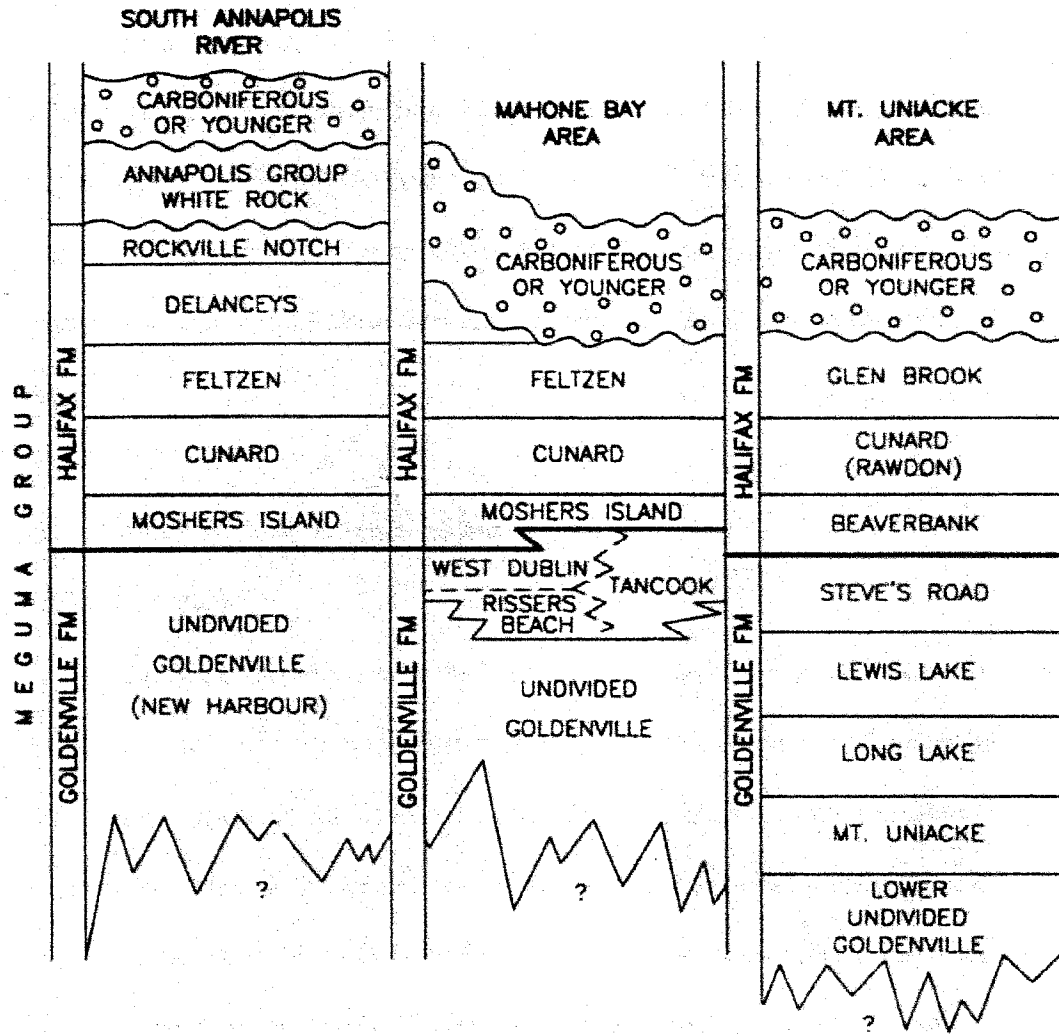


Figure 2.2. Stratigraphic subdivision of the Meguma Group in the South Annapolis River and Mahone Bay areas (Schenk, 1995) and Mount Uniacke area (Ryan et al., 1996). (Modified from Schenk, 1995).



occur in multilayer packages typically 4-6 m, and up to 20 m thick, with variable layer spacing. The host material to the coticles consists of variable calcareous slate and/or metasilstone with minor spessartine (Feetham, 1997). Figure 2.3 shows the distribution in plan and cross-section of the coticule outcrops studied in this thesis.

### **2.2.2 Structure**

Northwest directed-transpression during the Acadian deformation resulted in northeast- to north-trending folds in the Meguma Group (Fig. 2.1). Folds are typically doubly-plunging, with terminations plunging moderately, to locally steeply, in both northeast and southwest directions, locally defining domal structures in anticlines (Faribault, 1899; Malcolm, 1929). Bedding-parallel quartz veins in gold deposits commonly outline elliptical patterns in plan view reflecting these domal structures (Mawer, 1987; Malcolm, 1929). Cross-sections of the Meguma Terrane (Fig. 2.1) illustrate that folds consist of tight- to open-chevrons and modified box folds (i.e. box folds with subsidiary folds in flat segments), with no systematic vergence in the orientation of the axial planes. As mentioned earlier, these fold styles are indicative of buckled, anisotropic, multilayered sequences such as the turbidite package of the Meguma Group. The modified box folds define a series of regional-scale anticlinoria and synclinoria, which, at the current level of exposure, generally correlate with the distribution of the Goldenville and Halifax formations, respectively (Fig. 2.1).

Minor folds are common in the Meguma Group and have been described as displaying a parasitic relationship to regional folds (Henderson et al., 1986; Horne, 1995; Horne et al., 1997, 1998; Williams and Hy, 1990). Descriptions of minor folds are mainly of buckled quartz veins and rare buckled metasandstone layers. Mawer and Williams (1990)

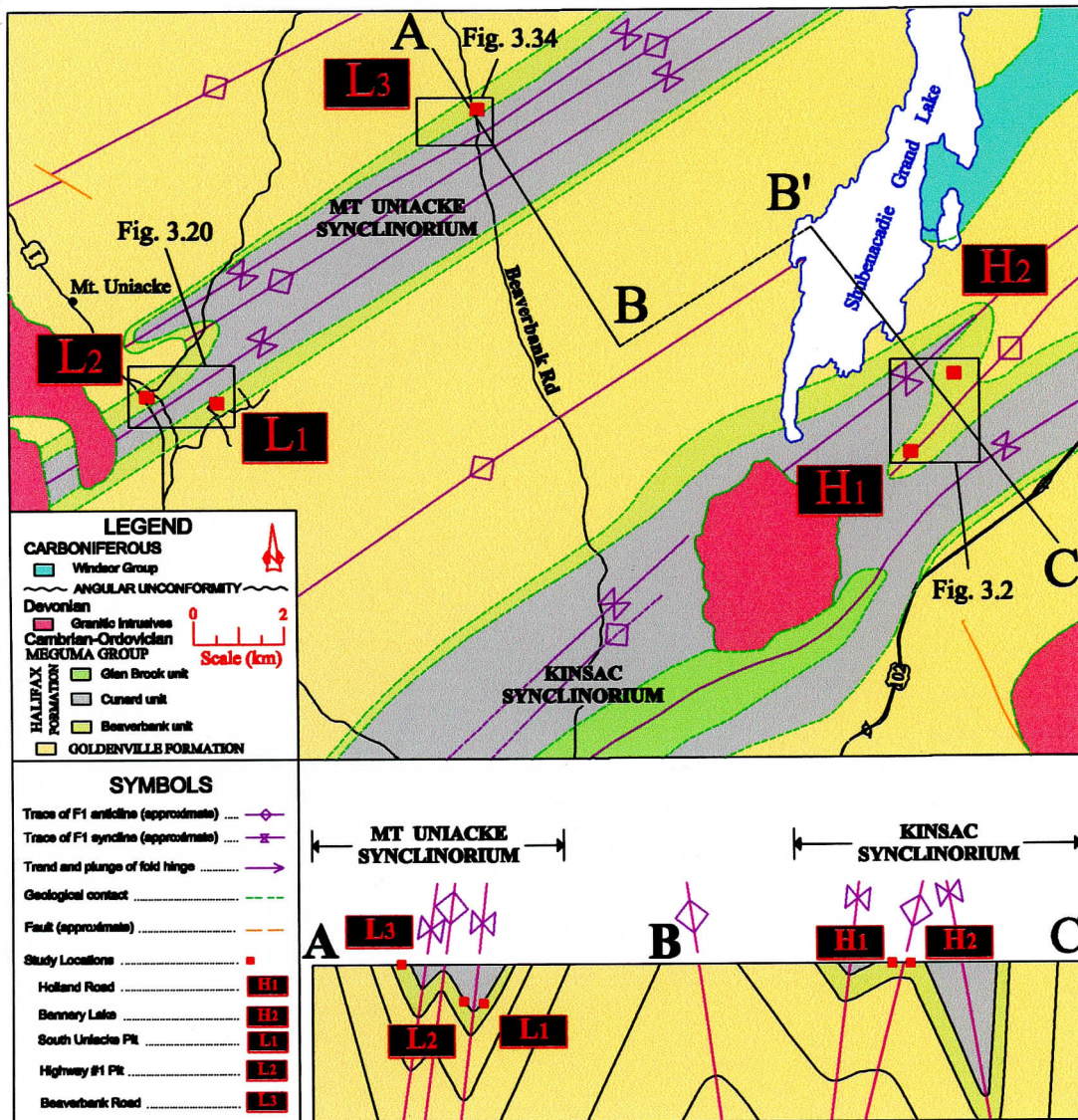


Figure 2.3. Simplified geology map and cross-section of the study area in the central Meguma zone. (Geologic data compiled from NSDNR open file maps and NSDNR unpublished data from 11 D/13, and from regional maps by Faribault, 1909).

have described minor folds in sedimentary layering (coticules) adjacent to the Cobequid-Chedabucto Fault System. They concentrated on describing the minor fold characters that result from high shear strains associated with the Cobequid-Chedabucto Fault System. Specific minor fold geometries in non-sheared sedimentary layering have yet to be documented in detail.

Cleavage ( $S_1$ ) is well developed as continuous cleavage in the slates and a variably developed spaced cleavage in the metasandstone (Henderson et al., 1986; Horne et al., 1997; Horne, 1998). Cleavage is axial planar in upright chevron folds (Henderson et al., 1986; Horne et al., 1997). In box folded sequences, Horne et al. (1998) describe bedding-cleavage angles that are similar for each limb, regardless of dip. The significance of this relationship is that cleavage may not be parallel across a regional box fold. Based on observations that worm tubes and sand volcano pipes coincide with cleavage regardless of bedding-cleavage angle Henderson et al. (1986) suggest that cleavage developed prior to regional folding. Horne (1998) documented a cleavage fan in a slate bed in the hinge zone of a tight regional chevron fold interpreted as reflecting inverse tangential longitudinal strain. Ramsay and Huber (1987) suggest that such cleavage patterns indicate little shortening prior to folding. This early formation of regional folds would be consistent with the chevron and box style of folding in the Meguma Group. Such folds initiate and amplify with little to no flattening associated with layer parallel shortening (Price and Cosgrove, 1990; Ramsay and Huber, 1987).

Wright and Henderson (1992) attribute the lack of evidence for fold-related extension (down-dip and hinge-parallel) to significant volume loss, up to 60%, during cleavage

formation. Chemical mass balance analyses (Fueten, 1984) were interpreted as supporting significant volume loss. However, Erslev and Ward (1994) used macroprobe analyses to map element distributions which indicated that redistribution of elements did occur, but there was no associated large non-volatile volume loss during cleavage formation. It should be noted that hinge-parallel and down-dip extension, defined by pressure shadows on metamorphic porphyroblasts and stretched detrital grains, have been documented throughout the Meguma Group (Haysom et al., 1997; Horne et al., 1997, in press; Horne, 1998; Graves and Zentilli, 1982; Williams and Hy, 1990; Nicholas Culshaw, personal communication).

### **2.2.3 Previous theories of minor fold development in the Meguma Group**

#### **2.2.3.1 General statement**

Considerable debate has focused on the origin and structural relationships of bedding-parallel gold-bearing quartz veins in the Meguma Group. In their work on gold-bearing veins workers have proposed various fold models for the Meguma Group based on structural analysis of these veins (Graves and Zentilli, 1982; Henderson et al., 1986; Henderson and Henderson, 1986; Mawer, 1987; Williams and Hy, 1990; Horne, 1998). Two particular and contrary theories on the timing of the quartz veins have come out of these models. One theory suggests that the bedding-parallel veins formed everywhere and buckled prior to regional folding, whereas the other theory suggests that the veins were emplaced during synfold shortening and buckled only in the hinge zones of regional folds.

The relevance of these theories to this study is in the relative timing of parasitic fold (or minor fold) development with respect to regional folding. The following are brief

summaries of the theories of fold development in the Meguma Group presented by various workers.

#### **2.2.3.2 Pre-regional fold buckle development model (Fig. 2.4)**

Graves (1976) and Graves and Zentilli (1982) first proposed a model in which minor folds were interpreted to pre-date regional folds. They proposed a sequence of  $D_1$  events indicated by their field observations which included: (1) hydraulic fracturing and vein crystallization, followed by (2) folding, ending with (3) the fixing of axial-plane cleavage defined by greenschist metamorphic minerals (Fig. 2.4, Graves and Zentilli, 1982). In this model, minor folds and cleavage are developed prior to regional folding (stage (2)) predicting that minor folds would reflect the same bedding-plane strain everywhere, regardless of structural location. Their strain study supported similar strain across a fold (i.e. bedding-plane strain is the same on regional fold limbs as in hinges).

Henderson et al. (1986) proposed a history of cleavage development and folding which includes: (1) formation of bedding-parallel quartz veins by hydraulic fracturing; (2) homogenous, layer parallel shortening resulting in cleavage development and buckling of bedding-parallel veins, and; (3) development of regional folds with limb amplification by flexural flow, where cleavage acted as a passive marker. Through flexural flow the buckled veins are sheared such that they are congruent with regional fold axes.

#### **2.2.3.3 Syn-regional fold buckle development model (Fig. 2.5)**

In contrast to the models advocated by Graves and Zentilli (1982) and Henderson et al. (1986) several studies propose that quartz veins were emplaced synfolding and therefore the buckling of these veins would also be synfolding (Faribault, 1899, 1913; Keppie, 1976;

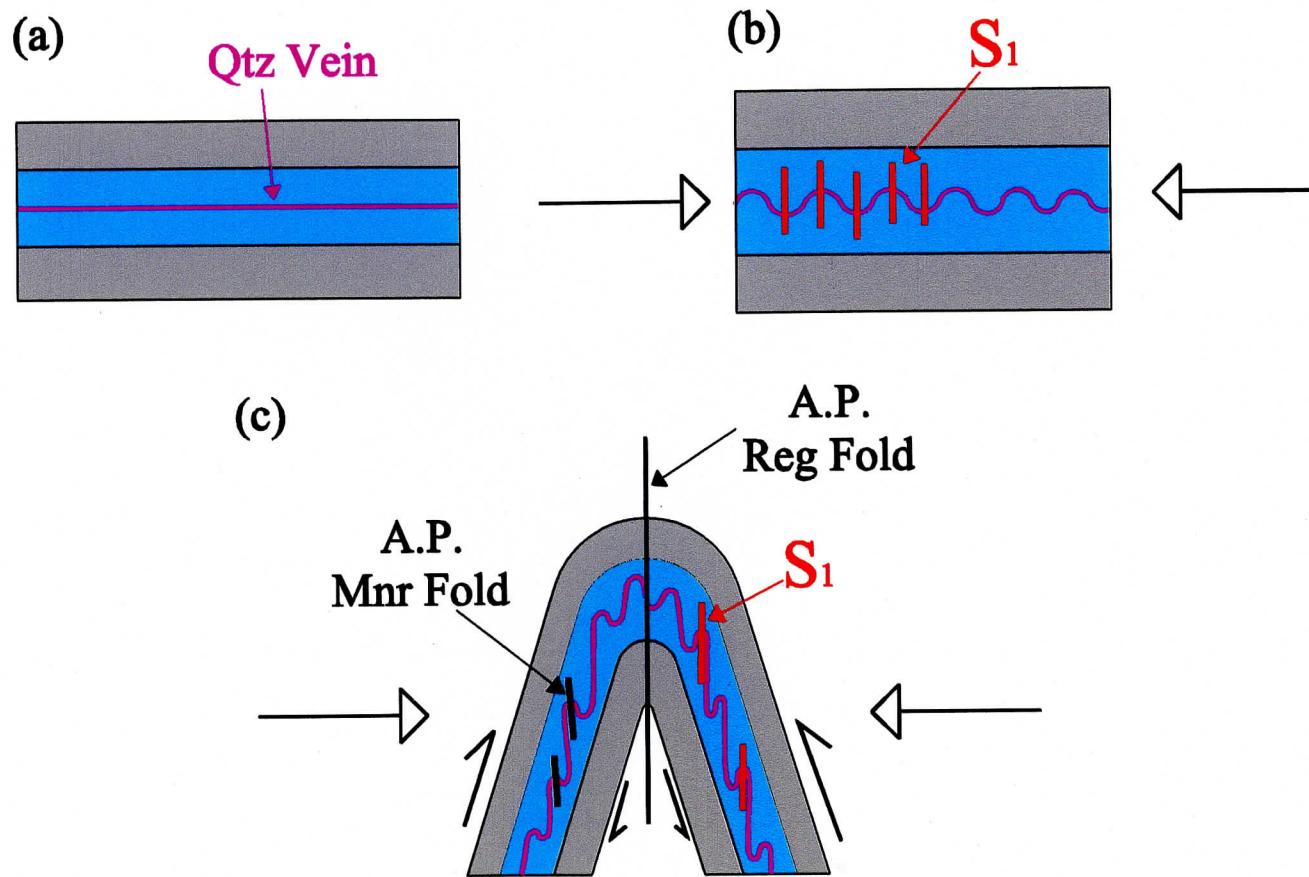


Figure 2.4. Fold model of buckle development prior to regional folding. Key features are competent layers (quartz veins) are buckled during cleavage development and prior to regional folding. The model predicts that the axial planes of parasitic folds will be parallel to the regional axial plane.

Mawer, 1987; Williams and Hy, 1990; Horne, 1998). Faribault (1899) and Horne (1998) document that some bedding-parallel quartz veins occur along planes of flexural slip, which occurred late in the fold history. Horne (1998) documents in detail features indicative of late fold reactivation by flexural slip at the Ovens and Halifax areas. Many of the bedding-parallel quartz veins at these locations occur along the slip planes, where they are planar on the fold limbs and buckled in the fold hinges. He also documents thrust sheets, with buckled metasandstone layers, interpreted to originate from an adjacent flat segment of a regional synformal box fold. These observations of buckled metasandstone layers from a hinge and planar metasandstone layers on fold limbs support the model of active layer parallel shortening during regional folding and not before (Horne, 1998).

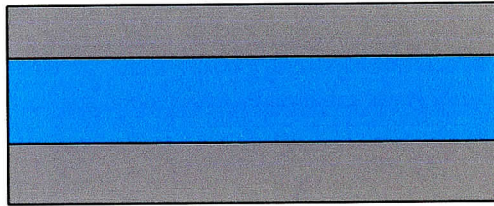
Williams and Hy (1990) suggest that quartz veins are buckled in regional fold hinges but planar on regional fold limbs. They also note that those bedding-parallel quartz veins, which are traceable across a fold, exhibit recrystallized polygonal aggregates in the hinge area and only moderate undulose extinction when planar on the limbs. Based on this data they attribute the buckling of quartz veins to be contemporary with regional folding.

The models described above are similar in that they indicate that layer-parallel shortening results in buckle folds and they both predict minor folds and cleavage to be axial planar to regional folds. Where the models differs is whether buckles are developed only in fold hinges or in both hinges and limbs.

### **2.3 Geology of the study area**

The study area is in the central Meguma Terrane and covers approximately 25 km east-west and 20 km north-south (Fig. 2.3). The study area is underlain primarily by the

(a)



(b)

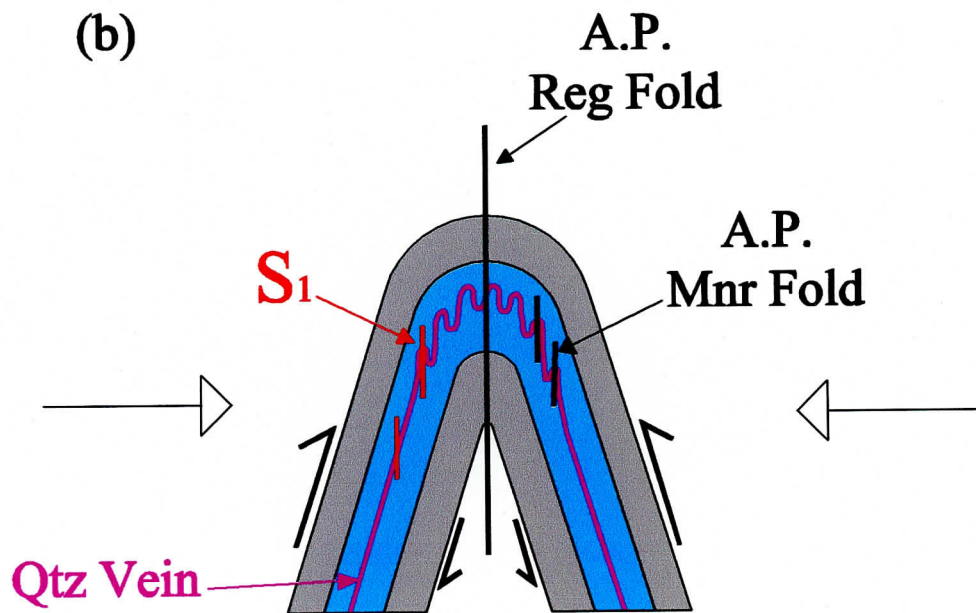


Figure 2.5. Fold model of buckle development during regional folding. Key features are competent layers (quartz veins) are buckled only in the hinge zone of the regional folds. The model predicts planar competent layers on the limbs of regional folds and buckled competent layers in the hinge of regional folds.



Meguma Group, with granitoids of the South Mountain Batholith (SMB), Kinsac Pluton, and Musquodobit Batholith exposed in the west, centre, and southeast, respectively. Contact aureoles are characterized by abundant cordierite porphyroblasts and partial annealing of cleavage, and extend only weakly into one of the five outcrop study locations. The Halifax Formation occurs in two synclineriums, Mt. Uniacke to the north and Kinsac to the south. The Goldenville Formation occurs in tight anticlines bounding the synclineriums. The regional folds are characteristic of the modified box and chevron fold styles of the Meguma Group (compare with Fig. 2.1). Regional metamorphism in the area is within the low- to mid-greenschist facies.

As discussed earlier, this study has focused on the minor folds developed in coticule layers of the Beaverbank member, the lowermost unit of the Halifax Formation. The upper Beaverbank unit is locally abundant in coticule layers and nodules. Five outcrop locations in the study area were chosen in order to represent both the regional fold hinge zone and fold limbs. The outcrop locations are numbered H<sub>1</sub>, H<sub>2</sub>, L<sub>1</sub>, L<sub>2</sub>, and L<sub>3</sub>, where H and L refer to the regional fold hinge and limb, respectively (Fig.2.3).

Other studies conducted on the coticule layers have mainly focused on metal-enrichment potential in the coticule and related rocks (Graves and Zentilli, 1988; MacInnis, 1986; Binney et al., 1986). Feetham et al. (1997) conducted a lithochemical characterization of the Beaverbank member in the central Meguma zone and concentrated on delimiting potential acid-rock drainage sources from the Beaverbank unit. O'Beirne-Ryan (in press) conducted a petrographic study of the coticule layers in the area. She concluded that the metamorphic garnet predated well-developed foliation and extension in the coticule layers,

where fractures occur along garnet grain boundaries. Horne et al. (1997) report buckled coticule layers in a regional fold hinge in the eastern portion of the study area. Henderson et al. (1992) used a photograph of a folded coticule layer from a regional fold hinge in the study area for a field trip guidebook.

No structural studies concentrating on the coticule layers have been done in the area and no structural studies on the buckled coticule layers with a focus on regional folding have been done in the Meguma Group.

## Chapter 3: Features of the Minor Folds

### 3.1 Introduction

This chapter presents the descriptions of the minor folds and extensional structures documented in the study area. Features of each of the five locations are described separately and a summary provides comparison of minor folds from regional fold hinges and limbs. Because features of the minor folds are compared it is necessary to establish that the coticule layers from the various locations behave the same when folded. As folding is dependent on layer competence contrasts changes, in lithology of either the competent layer (coticule) or the host layers (matrix material) may result in impure buckling. That is, if the competence contrast is sufficiently low then shortening may be accommodated by some combination of flattening and buckling. It is important to know whether there was a component of flattening during shortening of the coticule layers because, if this is the case, shortening recorded by the minor folds would not be fully representative of the finite strain. The following is a discussion of how the competence contrast of layers at each location has been determined and that buckling occurred without a component of flattening regardless of lithology variations in the coticule layers and matrix material.

The outcrops vary slightly in lithology, both in the matrix and coticule layers. However, overall there is considerable consistency in layer behavior as a result of folding; the coticule layers are highly buckled. Ramsay and Huber (1987) have identified three ranges of competency contrast ratios, (1)  $\mu_1/\mu_2 > 50$ , (2)  $10 < \mu_1/\mu_2 < 50$ , (3)  $\mu_1/\mu_2 < 10$ , which correspond with pure buckling, some combination of buckling and flattening, and

primarily flattening, respectively (refer to Fig. 1.2 for graphical representation). Table 3.1 shows how, regardless of lithology, based on the fold arc length and layer thickness of the coticule layers a representative selection of coticule layers have competency contrast ratios well above the minimum for assumed pure buckling.

Location	$\mu_1/\mu_2$ Ratio
H1 (Holland Road)	114
	140
	110
H2 (Bennery Lake)	225
	192
	190
L1 (South Uniacke Pit)	N/A, non-folded layers
L2 (Highway#1 Pit)	89
	112
	78
L3 (Beaverbank Rd)	166
	98
	110

Table 3.1. Selected representative competence contrast ratios based on the *Biot-Ramberg equation*  $\mu_1/\mu_2 = 0.024(L/t)^3$  where L is the arc length and t is the layer thickness. See text for discussion. At L<sub>1</sub> coticule layers are non-folded, however, the layers have similar lithologies and therefore similar rheologies as L<sub>2</sub>.

Therefore, regardless of lithology differences, which might otherwise affect the rheological properties of the rock, it is assumed that all individual coticule layers studied have undergone pure buckling with limited flattening.

### ***Organization and Methods***

Minor folds were documented in the field and, from hand samples and thin sections. For comparison, all photographs, images and sketches of folds are shown in the fold profile

view and facing northeast unless specified otherwise. As described earlier, multiple scales of folds can be described in terms of orders. For the purposes of this thesis, regional folds are considered first order, 1 - 10 m scale folds are considered second order, folds referred to as minor folds are considered third order (2-20 cm fold wavelength), and folds parasitic to minor folds are considered fourth order (Fig. 3.1). The description of minor folds is divided into three sections: fold style, bedding-cleavage relationships, and shortening recorded by minor folds. Descriptions of fold style consist of identifying the shape (e.g. ptygmatic, box, tight, open etc....), the extent of noncylindricity, and the degree of symmetry of the folds. Bedding-cleavage relationships are expressed in thin section maps.

Measurements of shortening provide strain values for a particular rock and are important when comparing structural domains (i.e. regional fold hinge and limb). Photographs of outcrops and slabs cut from hand samples were scanned and each coticule layer was digitized using AutoCAD R14<sup>®</sup>. The bounding edges of each layer were digitized generating two lines for each layer. Using the equation  $e = (l - l_0)/l_0$ , where  $l$  is the current length between endpoints of a layer and  $l_0$  is the original or traced length of the folded layer, 183 values of shortening were generated for 94 coticule layers from four locations. Values for extension were generated using the same techniques as in shortening.

## **3.2 Outcrop locations**

### **3.2.1 Location H<sub>1</sub> (Holland Road)**

#### **3.2.1.1 General geology**

The H<sub>1</sub> outcrop is located on a woods road extension of Holland Road northeast of the Kinsac Pluton (Fig. 2.3 and 3.2). The outcrop is approximately 20 m by 10 m and 2 m

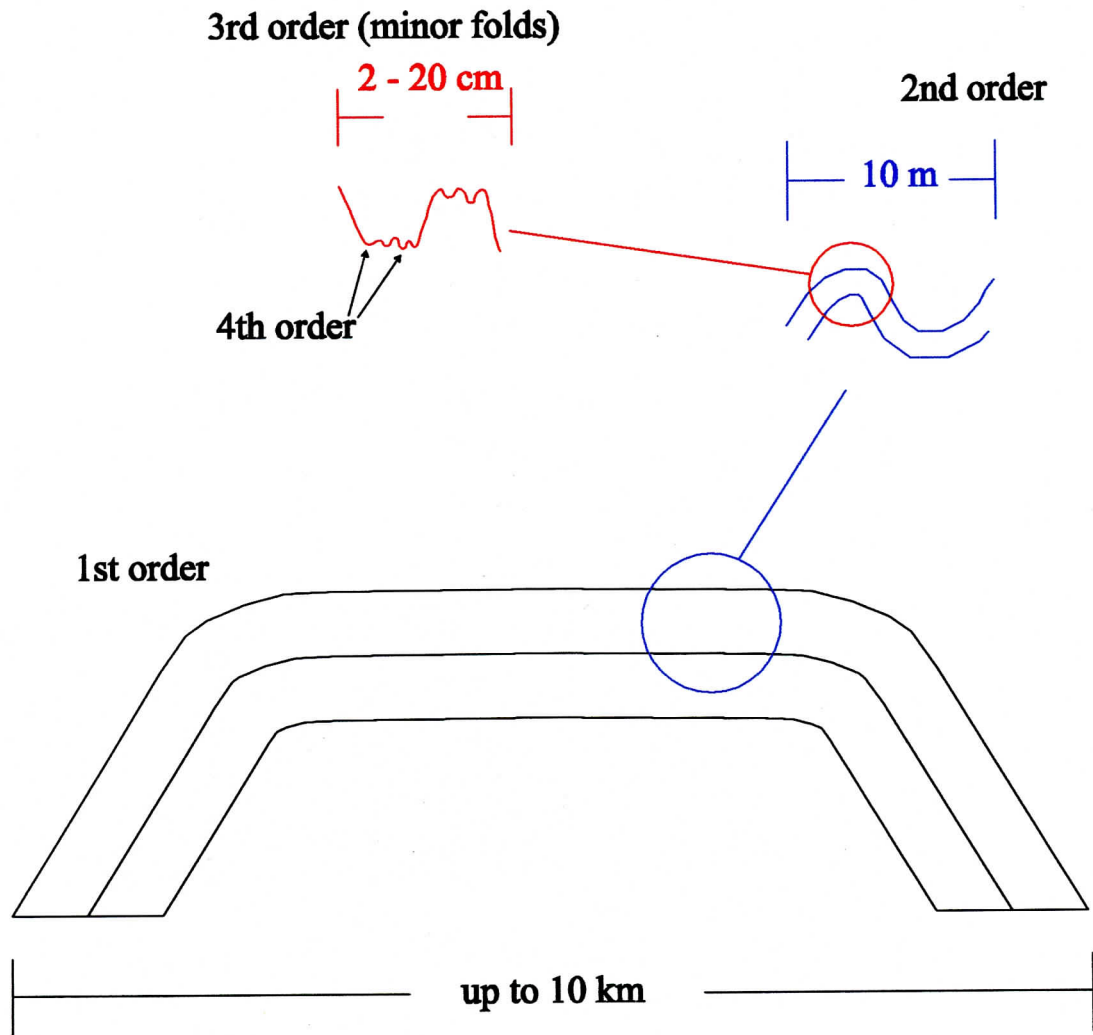


Figure 3.1. Schematic diagram defining ordered relationship between multiple scales of folds. 1st order represent regional scale folds; 2nd order represents mesoscale folds; 3rd order represents the minor fold scale; and 4th order represents subsidiary folds developed in the median segment of a 3rd order box fold.



high and covered almost entirely by moss. Bedding ranges from 220/10 to 230/35 with locally developed mesoscale folds on which bedding dips as much as 70°. These mesoscale (second order) folds have wavelengths typically of 3 m and display asymmetry consistent with southeast vergence. Coticule layers are very well exposed as they protrude from the surrounding matrix as a result of differential weathering. Coticule layers are abundant in the outcrop and are typically just over 1 cm thick and all coticule layers are folded. Thin section evaluation indicates that coticule layers are uniform in lithology, consisting of approximately 50-60% spessartine garnet, 25% carbonate, 20% quartz, and minor ferromagnesian minerals. In outcrop the coticule layers appear coarsely crystalline. In thin section, spessartine is the coarsest mineral and is uniform in size, generally less than 0.5 mm in diameter. The matrix material is fine-grained slate with a well-developed fine, continuous cleavage. Minor spessartine is evident in the matrix material. The slate matrix horizons change thickness between closely spaced folded coticule layers (e.g. Figs. 3.4 and 3.6).

### **3.2.1.2 Minor folds**

#### ***Fold style:***

The shape of minor folds at H<sub>1</sub> is very consistent throughout the outcrop, and symmetric, ptygmatic shapes dominate (Figs. 3.3 and 3.4). However, those ptygmatic shapes tend to occur as modified box-style folds, host to fourth order subsidiary folds in the median (Figs. 3.4 and 3.5). Figure 3.6a also shows fourth order subsidiary folds developed in the median segment of a box fold, whereas fourth order folds are absent on the box fold limbs. Layer 'c' in Figure A1.1 in Appendix 1 is characterized by interlaminations of slate matrix material and coticule layers in the horizontal segments whereas the layer is not



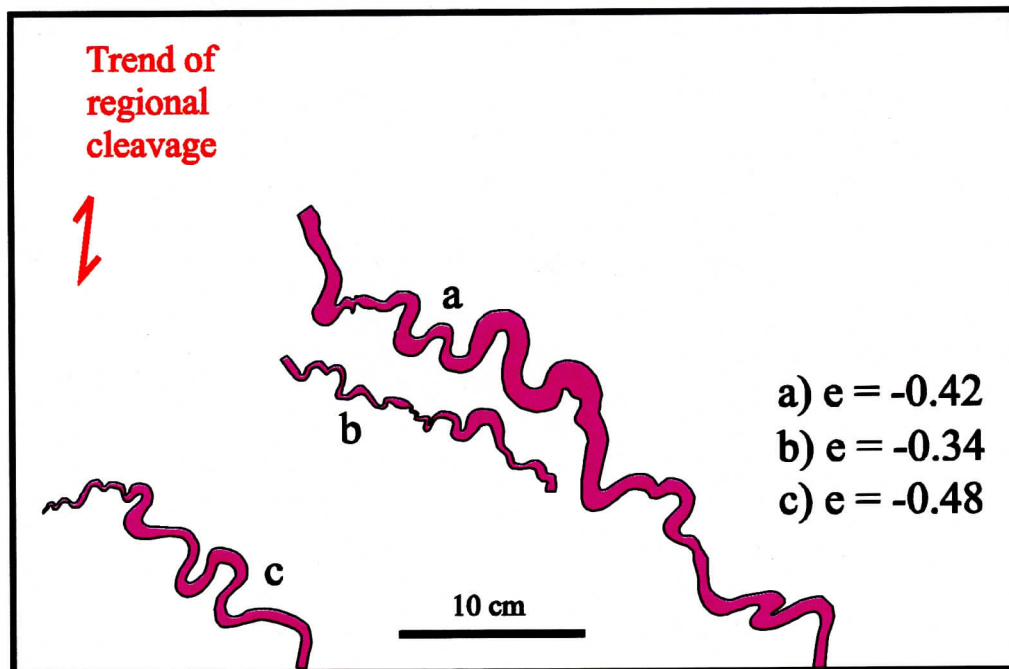


Figure 3.3. Field photograph and sketch of ptygmatic folds. Note that the folds are primarily symmetric and their axial planes are roughly parallel to the axial plane of the regional fold.

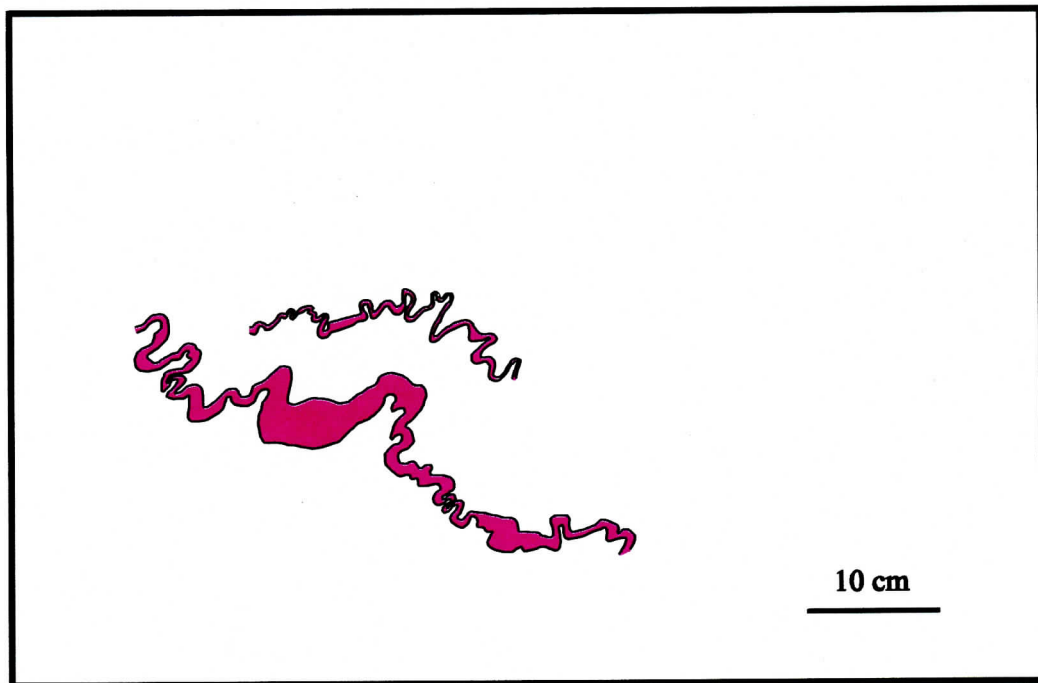
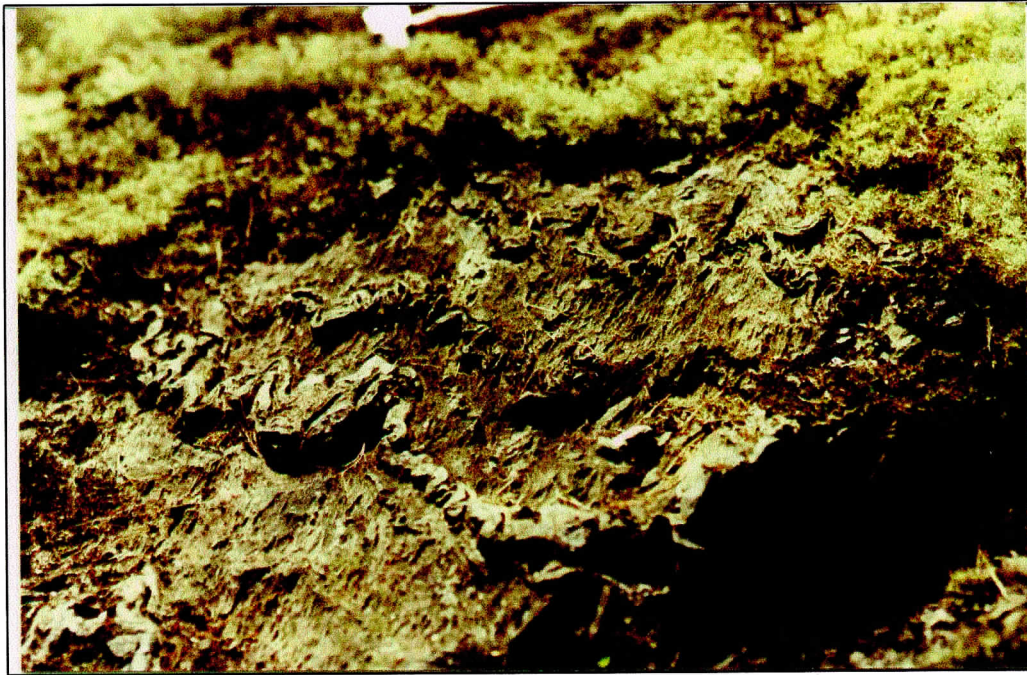


Figure 3.4. Field photograph and sketch of ptygmatic folds developed in layers of varying thicknesses. Note that in the thicker segments of the layer the fold wavelength and amplitude increase.

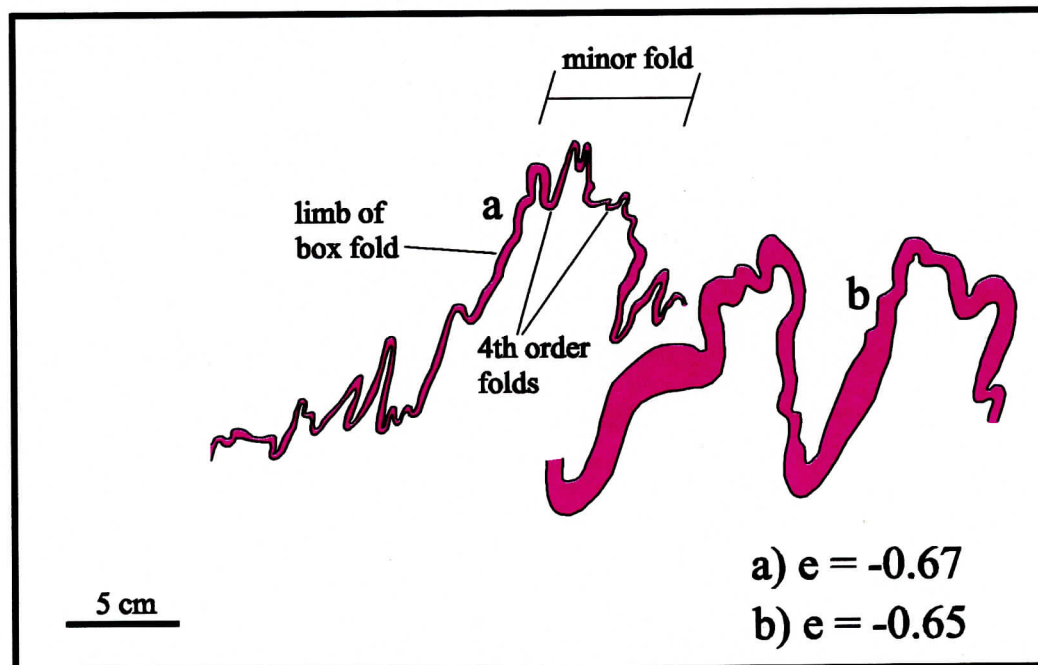


Figure 3.5. Field photograph and sketch of box-style folds with subsidiary folds developed in the median segments and parasitically on the box fold limbs. The axial planes of these minor folds parallel the axial plane of the regional fold.



Figure 3.6. Field photographs of typical fold shapes at  $H_1$ . The fold in (a) shows subsidiary ptygmatic folds developed in the median segment of a box-style fold. (b) shows a ptygmatic fold with a flat median segment typical of modified box folds. The folded layer in (c) shows how the thicker segments of the layer display greater fold wavelengths than the thinner segments.

interlaminated on the steep limbs directly adjacent to the horizontal segment. Overall, the third order fold shapes are characterized by box folds with low projected interlimb angles, typically less than  $15^{\circ}$  and as low as  $-10^{\circ}$ , and fourth order ptygmatic and isoclinal subsidiary folds developed in the median segment.

The minor folds exhibit moderate noncylindricity defined by fold shape change along the hinge. Figure 3.7 are line drawings of one coticule layer from successive slabs 4 cm thick cut from one hand sample. These line drawings are taken from the slab sketches shown in Figure A1.1 in Appendix 1. The most apparent feature in Figure 3.7 is how much the fold shape changes in such a short distance along the hinge. The indicated segments on each sketch display fourth order, small amplitude folds developed in a median segment of a box fold. By the fourth slab it is apparent that the median segment in slab 1 is rotated counterclockwise with respect to the vertical and now is parallel with the limb of the adjacent fold. This rotation indicates migration of hinges in fold profile can occur differentially along the hinge.

The minor folds display consistent symmetry in the ptygmatic, isoclinal and modified box folds. Asymmetric fourth order folds occur parasitically on the steep limbs of the minor folds (e.g. Fig 3.5 layer 'a'). Figure 3.9 shows a thin coticule layer on a steep limb with considerable asymmetry (Z form). The axial planes of these folds parallel the regional axial plane (vertical in this case).

#### ***Bedding-cleavage relationships:***

Figure 3.8 is a map of cleavage from photomicrographs and shows cleavage is generally axial planar to minor folds, with local variances. Cleavage diverges around the

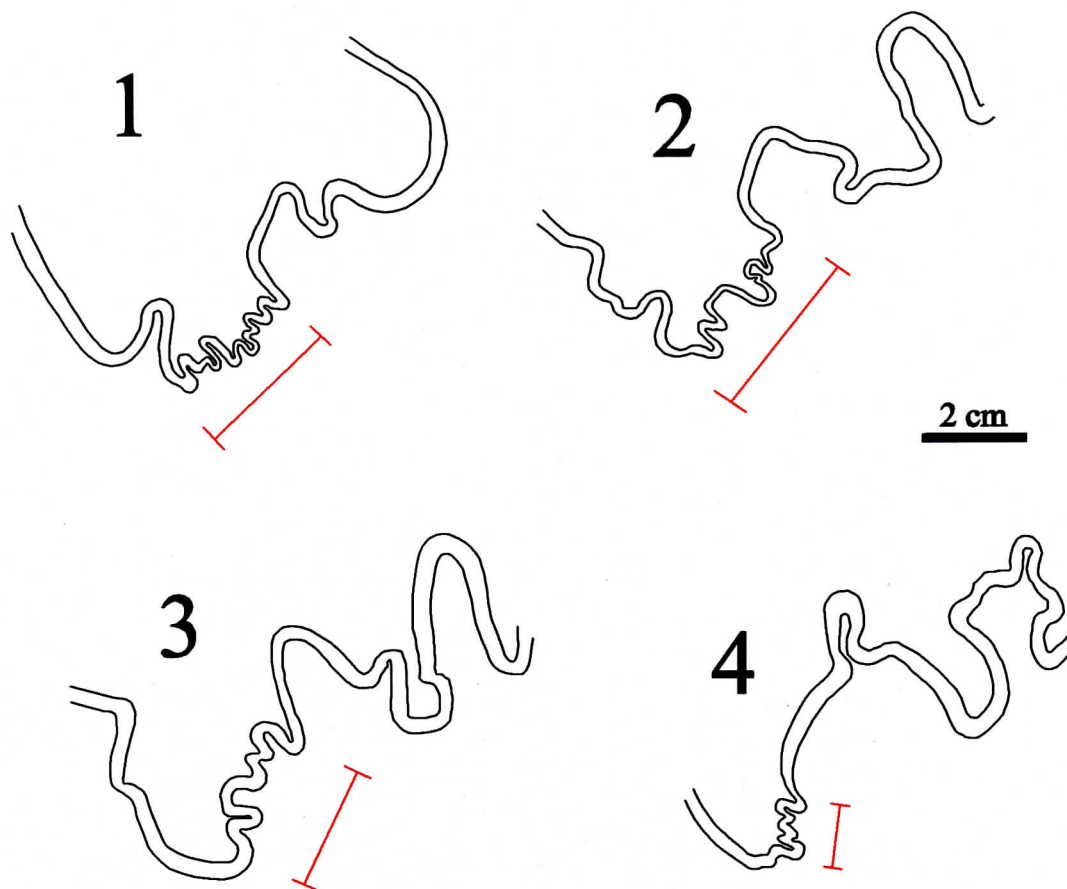


Figure 3.7. Line drawings of a single folded coticule layer from four parallel, 4-cm thick slabs cut perpendicular to the hinge. Note the dramatic changes in fold shape along the hinge. The indicated segment in slab 1 displays subsidiary folds in a median segment of a box fold, and by slab 4 this segment is rotated counterclockwise so that it parallels the former box fold limb. Sketches taken from Figure A1.1 in Appendix 1.

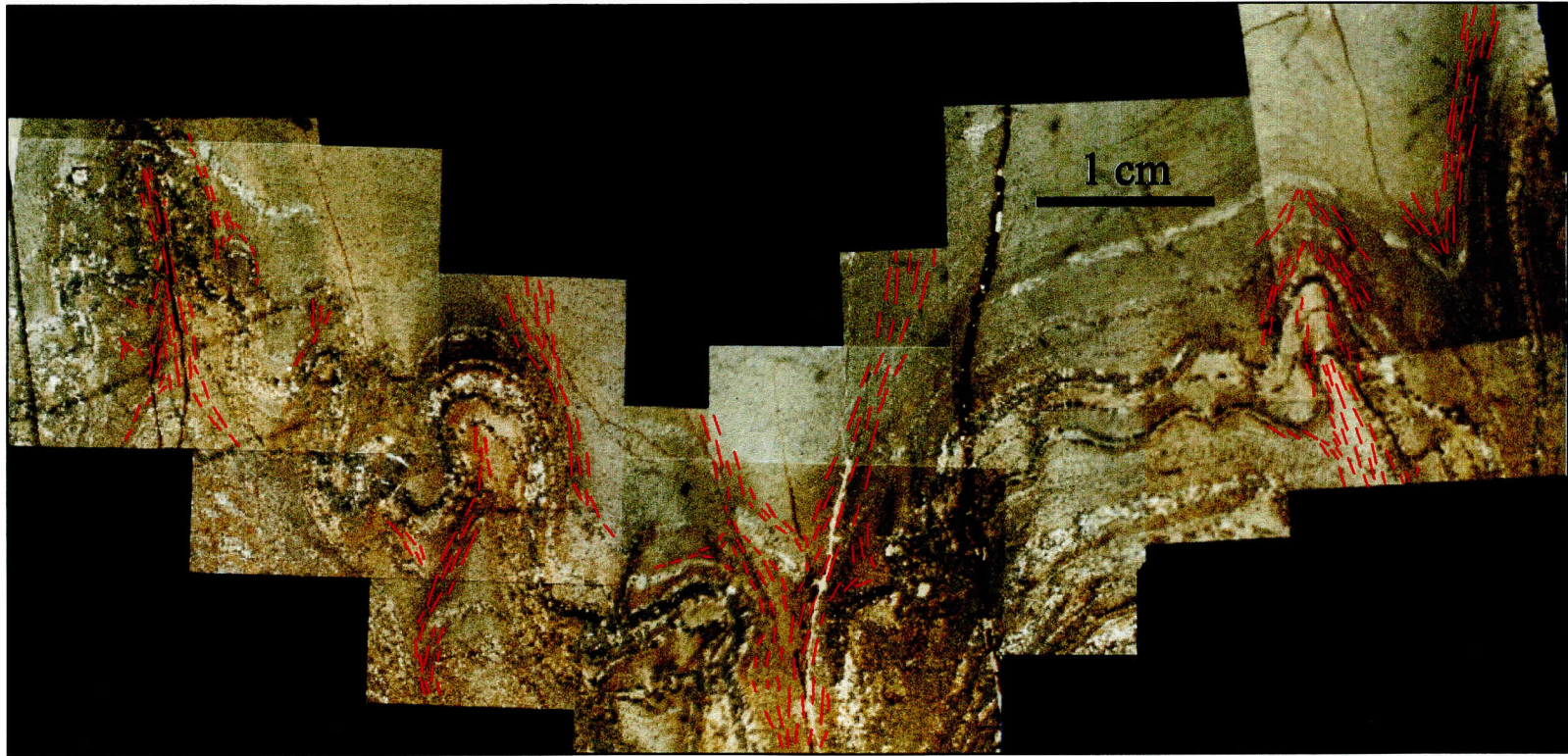


Figure 3.8. Thin section map of cleavage on photomicrographs. Foliation defining minerals are axial planar to minor and regional folds. Local variations are a result of deflections around coticles.



Figure 3.9. Photomicrographs of a locally steepened folded coticule layer. Cleavage bands commonly wrap around folded segments of the coticule layer. Divergent fans of cleavage occur around horizontal to shallowly dipping layer segments. Minerals inside the fans have no preferential lineation indicating low strain in these divergent fans.



outer-arc of minor fold hinges forming a divergent fan pattern and is more intensely developed in inner-arcs of the folds. Cleavage bands are common where they occur along and are deflected by steeply dipping coticule layers (Figs. 3.8 and 3.9). The fold crest in the centre of Figure 3.9 shows an example of how cleavage behaves around the outer-arc of folds. Cleavage is deflected by the folds in the coticule layers and is not developed in the shadows of fold crests.

***Shortening recorded by minor folds:***

Values of shortening consist of measurements from four successive slabs cut from one hand sample and three field photographs. A total of 34 values representing 19 coticule layers were generated and are listed in Appendix 2 and illustrated in Figure 3.10. Shortening values range from 34 - 68% and average 56%, with a standard deviation of 9.70% (Fig. 3.10). Values generated from slab photographs yield similar values to field photographs. In the successive slabs (Fig. A1.1 in Appendix 1) the shortening values are generally consistent for layers 'a' and 'b' ('a': 0.63-0.66; 'b': 0.58-0.61). Layer 'c' however, gives a range of 59 - 44% continuously decreasing in the northeast direction. Where layer 'c' appears more interlaminated (slabs 3 and 4) the shortening values are reduced. Shortening recorded in thick versus thin layers is similar. In Figure A1.1 in Appendix 1 the thin layer 'b' is sympathetic to the thicker layer 'c', however, both show the same amount of shortening.

**3.2.1.3 Extensional features**

Extensional features are defined by boudinage of coticule layers, where quartz infills the boudin necks. At  $H_1$  extensional features are observed in outcrop and thin section.

# H<sub>1</sub> (Holland Road)

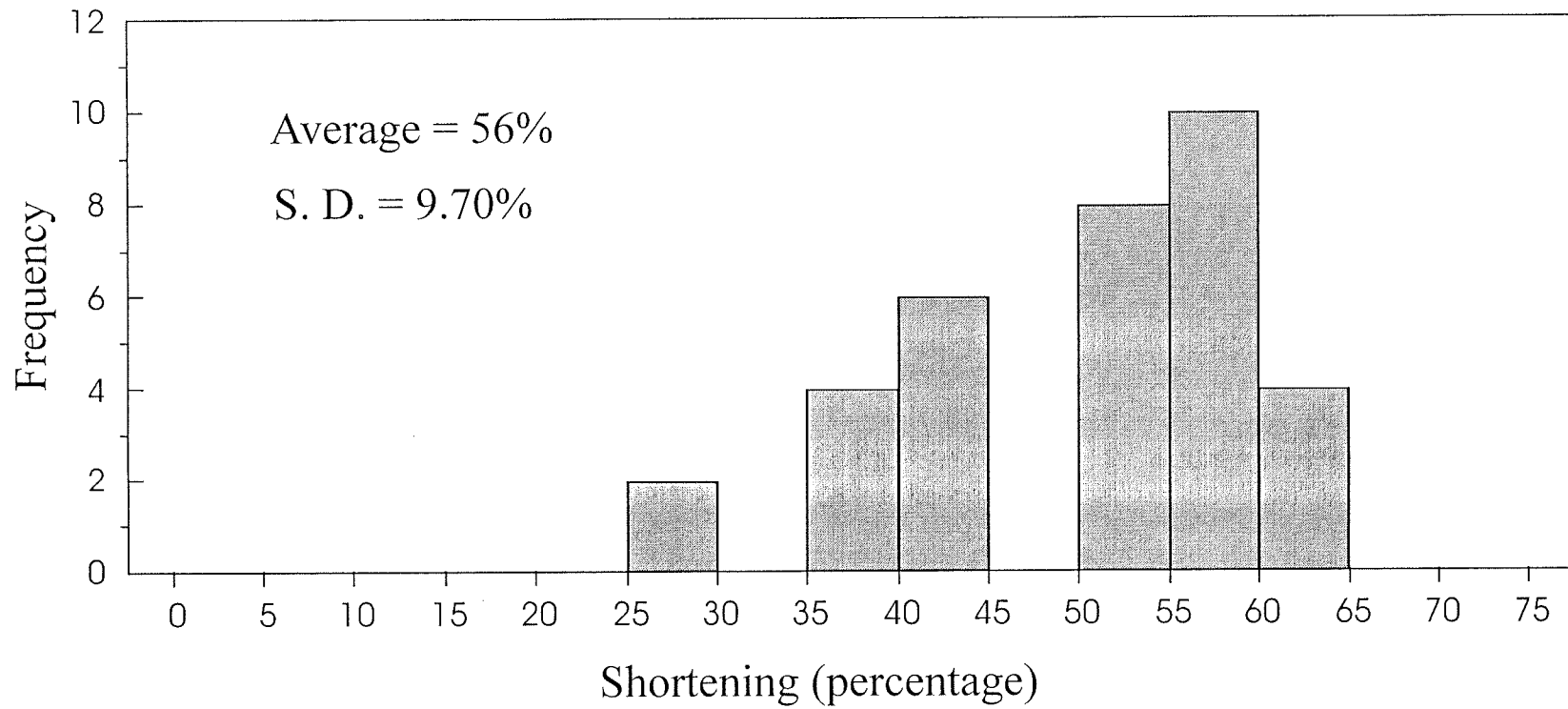


Figure 3.10. Histogram of shortening values. The average shortening value is 56% based on 34 data points (see Appendix 2).

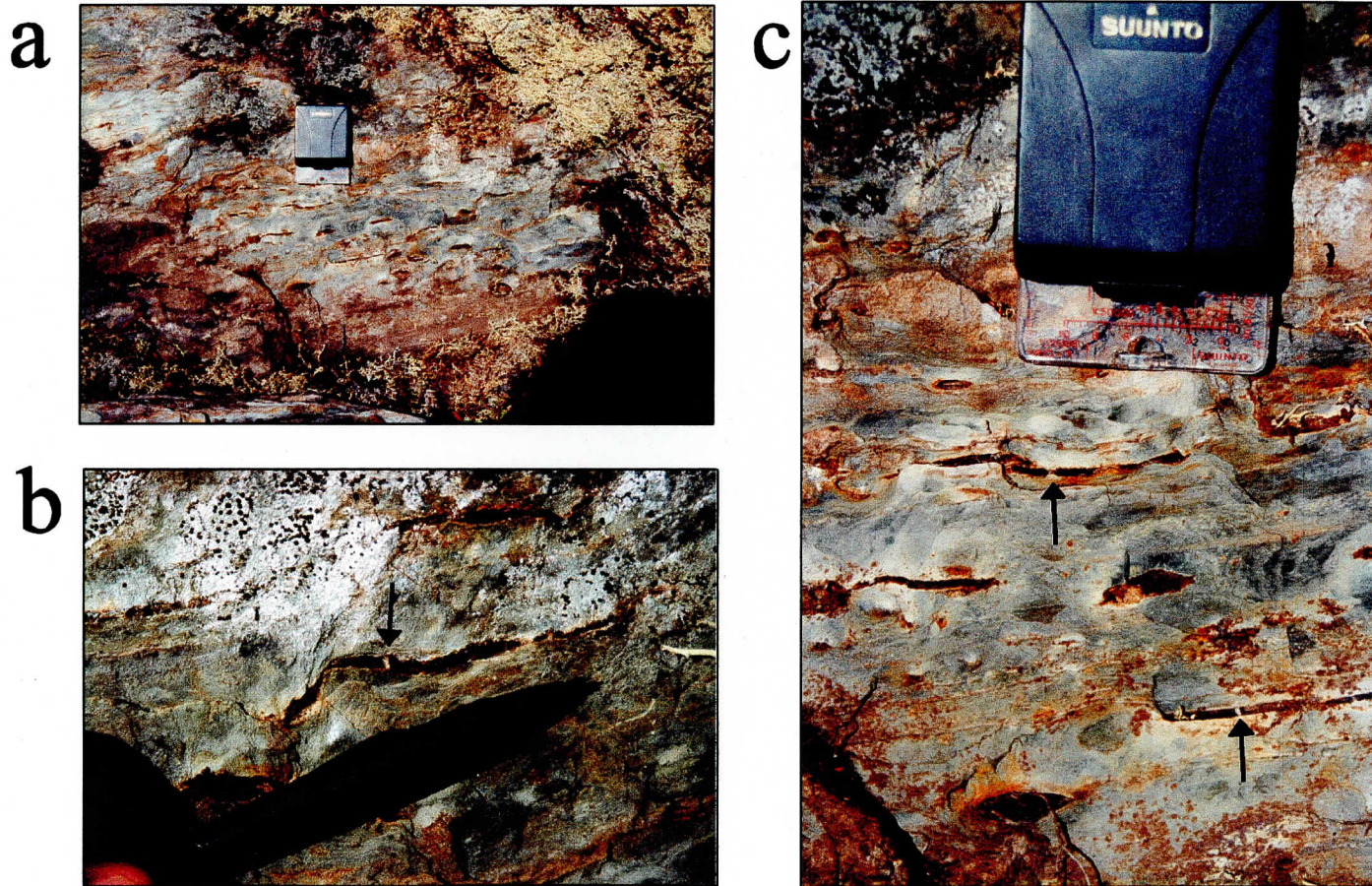


Figure 3.11. Field photographs of an exposed cleavage plane (SW facing) revealing coticule nodules that are locally boudinaged. Arrows in photographs (b) and (c) point to boudin necks that are filled with quartz.

Figure 3.11 shows various views of an exposed cleavage plane where bedding is flat dipping. Elongate coticule nodules that are parallel to the intersection lineation, and therefore hinge line, are boudinaged and the neck between the boudins is infilled with quartz. The boudinage of these coticule nodules represents 8% extension.

Coticule layers that are steeply dipping locally show down-dip boudinage (Fig. 3.12). The quartz that infills the necks between the boudins is primarily euhedral with slightly undulose extinction and locally, quartz crystals are elongate down-dip (Fig. 3.12). Down-dip extension defined by boudin necks measured in one thin section ranges from 9 - 20% and averages 13%. Extension, both down-dip and hinge-parallel, is characterized by sharp fractures that occur along the garnet grain boundaries.

### **3.2.2 Location H<sub>2</sub> (Bennery Lake)**

#### **3.2.2.2 General geology**

The H<sub>2</sub> outcrop is located in a new subdivision off of Highway #2, 1.5 km northeast of location H<sub>1</sub>, and occurs within the Kinsac Synclinorium (Figs. 2.3 and 3.2). The outcrop is relatively small, 5 m by 3 m, and is glacially striated on the top and exposed vertically (1 m) by a road cut. Enveloping surfaces of third order folds range from 038/30 to 225/10. This variation defines the alternating limbs of second order folds that have approximately 1 m wavelengths. Cleavage is apparently rotated 90° from regional cleavage and is 140/60, whereas regional cleavage elsewhere in the area is ~050/70. Intersection lineation is steep, at 165-34. To the north of this study location, outcrops in the Goldenville Formation are extremely fractured. In addition to this information, digital elevation data overlain by total field magnetic anomaly data show a northeast trending lineament in the area interpreted as

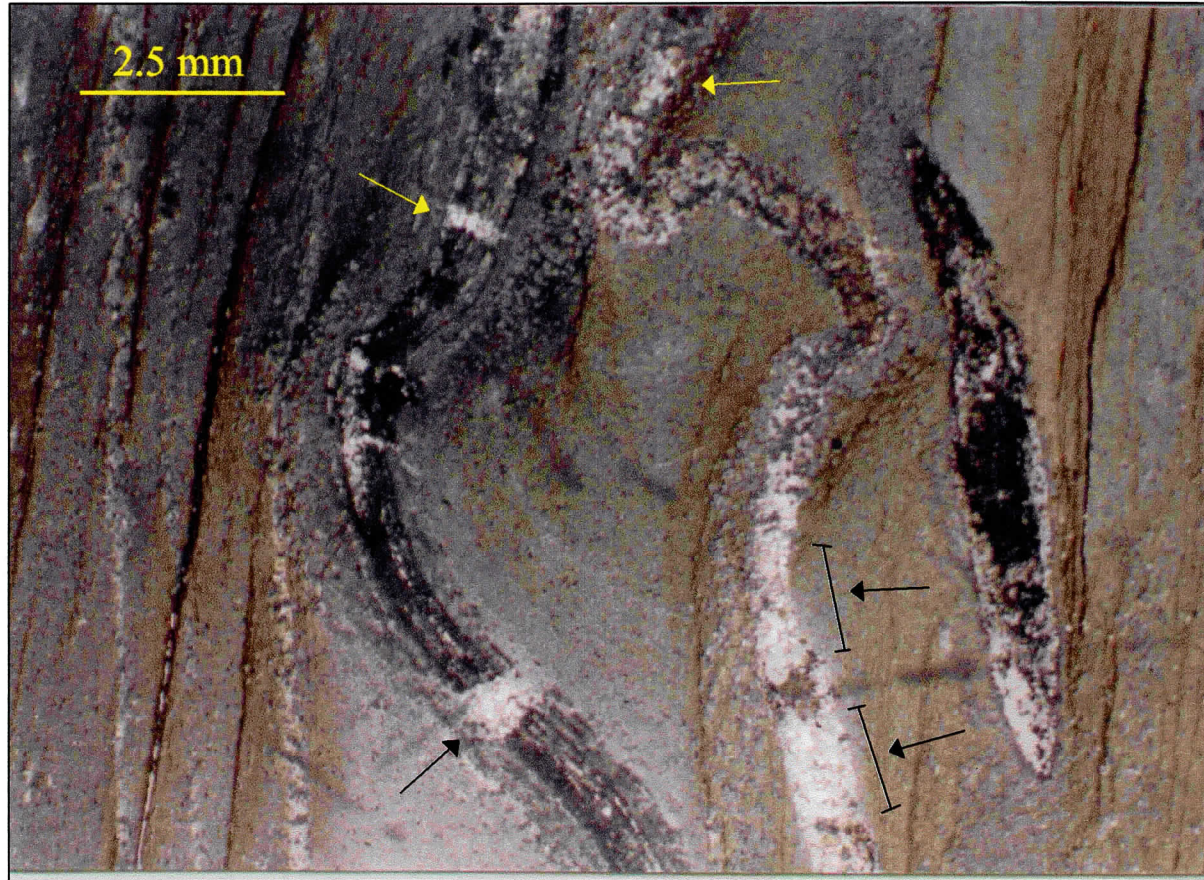


Figure 3.12. Photograph of a locally steepened folded and boudinaged coticle layer. Boudin necks are filled with quartz and indicated by arrows. Boudinage in the layer on the left represents 9% extension and boudinage in the layer on the right represents 22%.

being contemporaneous with known regional-scale northwest trending faults (King and Home, 2000). These fault systems are late brittle structures and did not affect the fold style of the coticule layers.

Coticules are well exposed, appearing as dark purple layers in a grey slate matrix. Coticule layers are relatively abundant and all are folded. The layers are consistent in thickness, around 1 cm, and layer spacing is around 5 cm. Lithologically, the coticule layers are similar to those at H<sub>1</sub> and consist of 40-55% spessartine garnet, 25-30% carbonate, 20% quartz, and minor ferromagnesian minerals. The matrix material is generally uniform fine-grained slate with well-developed cleavage. Minor spessartine is evident in the matrix material, especially adjacent to the coticule layers.

#### **3.2.2.2 Minor folds**

##### ***Fold style:***

Minor folds at location H<sub>2</sub> range between uniformly ptygmatic and modified box folds. Figure 3.13 illustrates the ptygmatic fold style which occurs both as the minor fold shape and as subsidiary folds in the median segments of modified box folds. Figure 3.14 displays a distinct fold shape of a box fold with fourth order subsidiary folds in the median segment (refer also to Fig. A1.2 in Appendix 1). In the median segment of some minor box folds distinct interlaminations of slate matrix rock and coticule are evident (Fig. 3.16). These interlaminations are not present on the limbs of those box folds. Overall, the fold shapes are characterized by ptygmatic and box folds with low projected interlimb angles, typically less than 20° and as low as -10°, and ptygmatic subsidiary folds developed in the median segment.

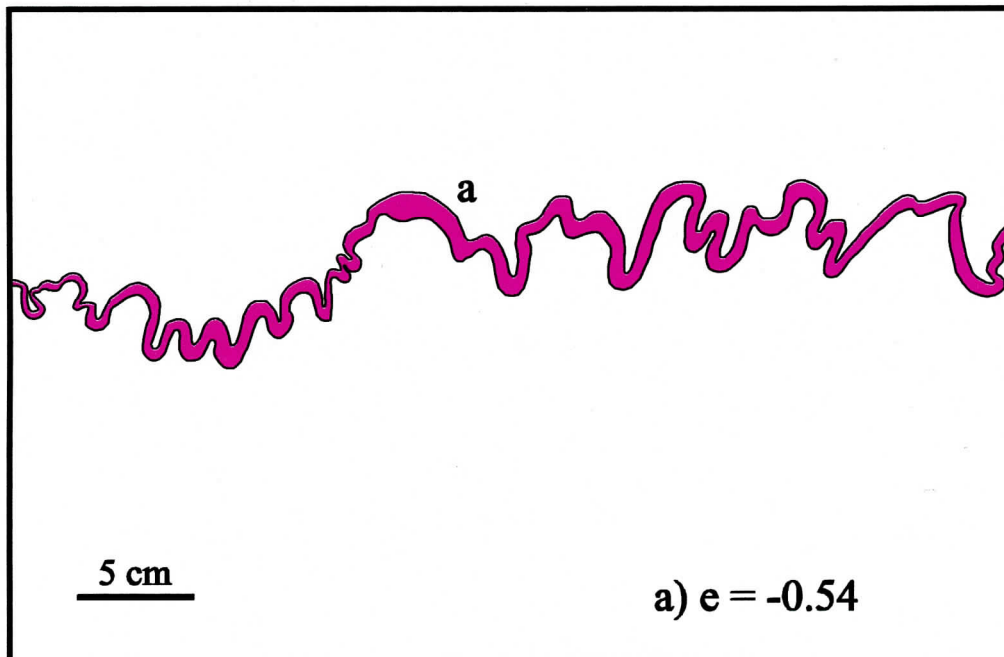
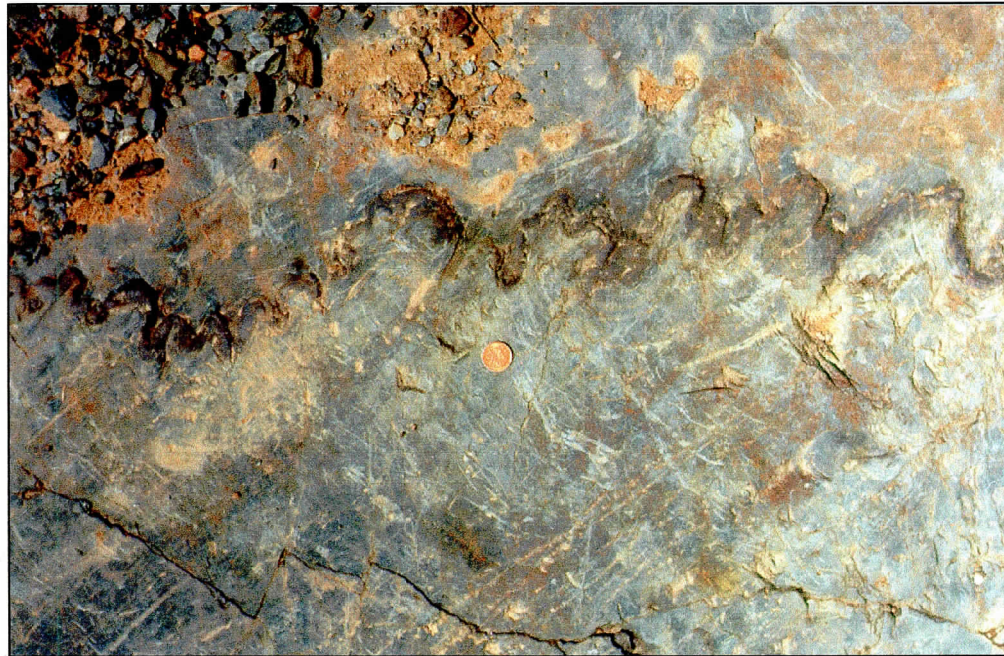


Figure 3.13. Field photograph and sketch of ptygmatic and modified box folds. Note that the folds are primarily symmetric and their axial planes are roughly parallel to the axial plane of the regional fold.

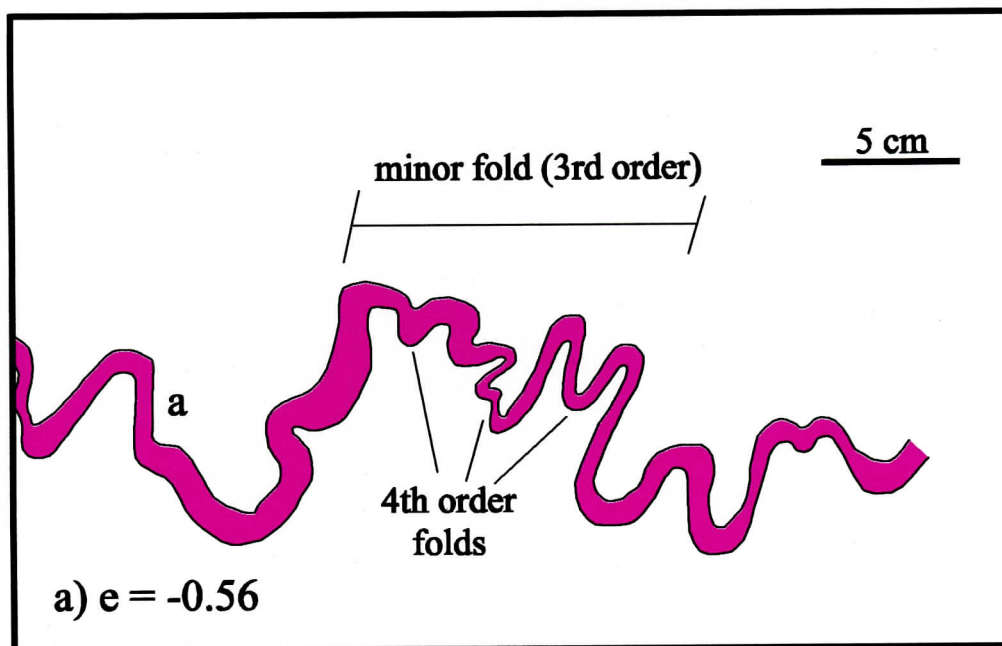


Figure 3.14. Field photograph and sketch of subsidiary folds developed in the median segment of a box fold.



The minor folds exhibit moderate noncylindricity defined by fold shape change along the hinge. Figure 3.15 shows line drawings taken from parallel slab sections cut in the fold profile shown in Figure A1.3 in Appendix 1. In Figure 3.15 the slabs are cut every 4 cm and clearly display fold shape change along the hinge. Also evident is the lateral variation in layer thickness, which affects the fold shape in terms of the wavelength and amplitude (see section 1.2.2.1). The circled segments of the fold shows how an initially regular box fold in slab 2 has subsidiary folds developed in the median segment by slabs 4 and 5.

The folds at this location exhibit slight asymmetry, consistent with southeast vergence and shear strain. Important to note is that the asymmetry displayed at this location and  $H_1$  is minor, and therefore consistent with these folds being formed during layer-parallel shortening.

***Bedding-cleavage relationships:***

Bedding-cleavage relationships are similar to those at  $H_1$ . Figures 3.16 and 3.17 are maps of cleavage from photomicrographs. Cleavage in slate intervals is regionally axial planar with variations resulting from local deflections. Cleavage bands tend to characterize cleavage development. Cleavage is best developed adjacent to steep, long limbs of minor folds of cotucle layers (Fig. 3.16) and other bands tend to trace fold crests and troughs. In Figure 3.17 cleavage consistently occurs adjacent to steeply dipping limbs and traces fold crests and troughs. Divergent cleavage fans are common around the outer-arc of folded cotucle layers.

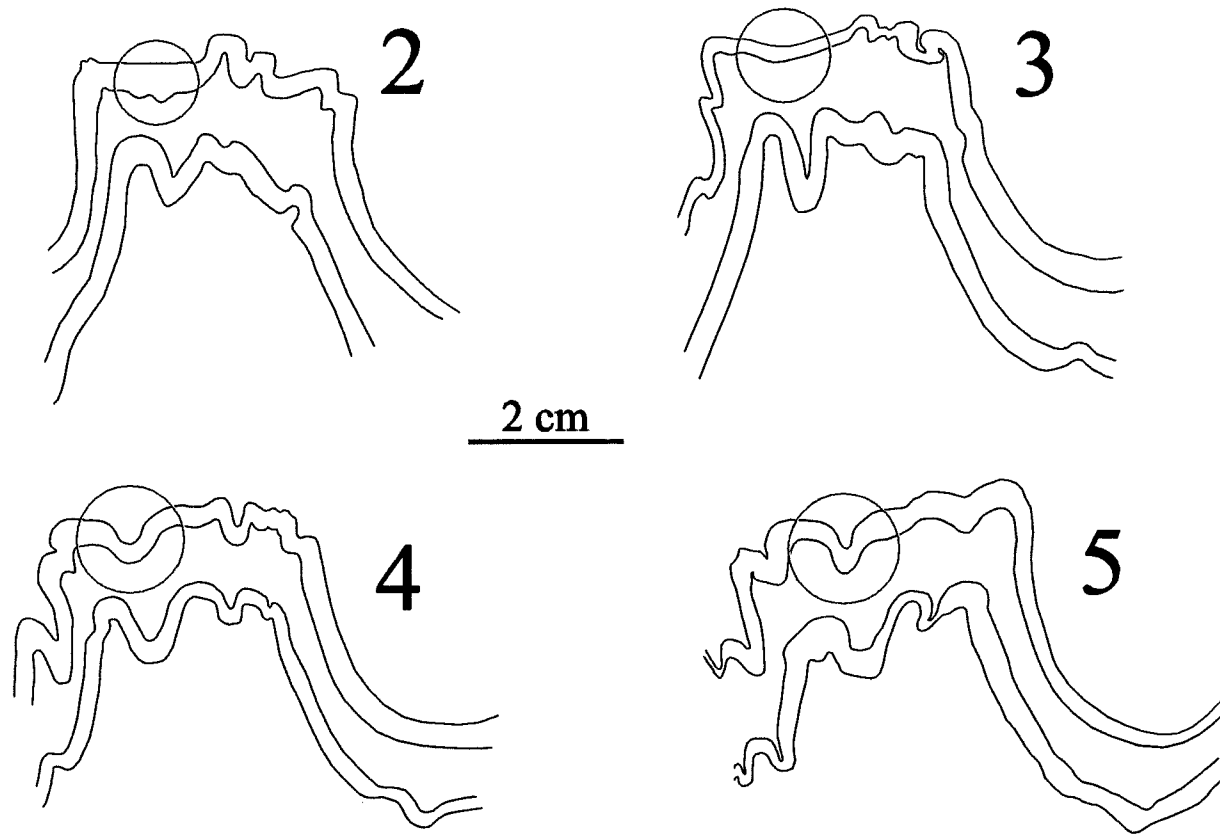


Figure 3.15. Line drawings of a single folded coticle layer from four parallel, 4-cm thick slabs cut perpendicular to the hinge. Note the dramatic changes in fold shape along the hinge. In slabs 2 and 5 the shape of the folds in the middle layer is controlled in part by the thicker, overlying layer. Note that there is lateral layer thickness variation that affects the style of folding. Sketches taken from Figure A1.2 in Appendix 1.

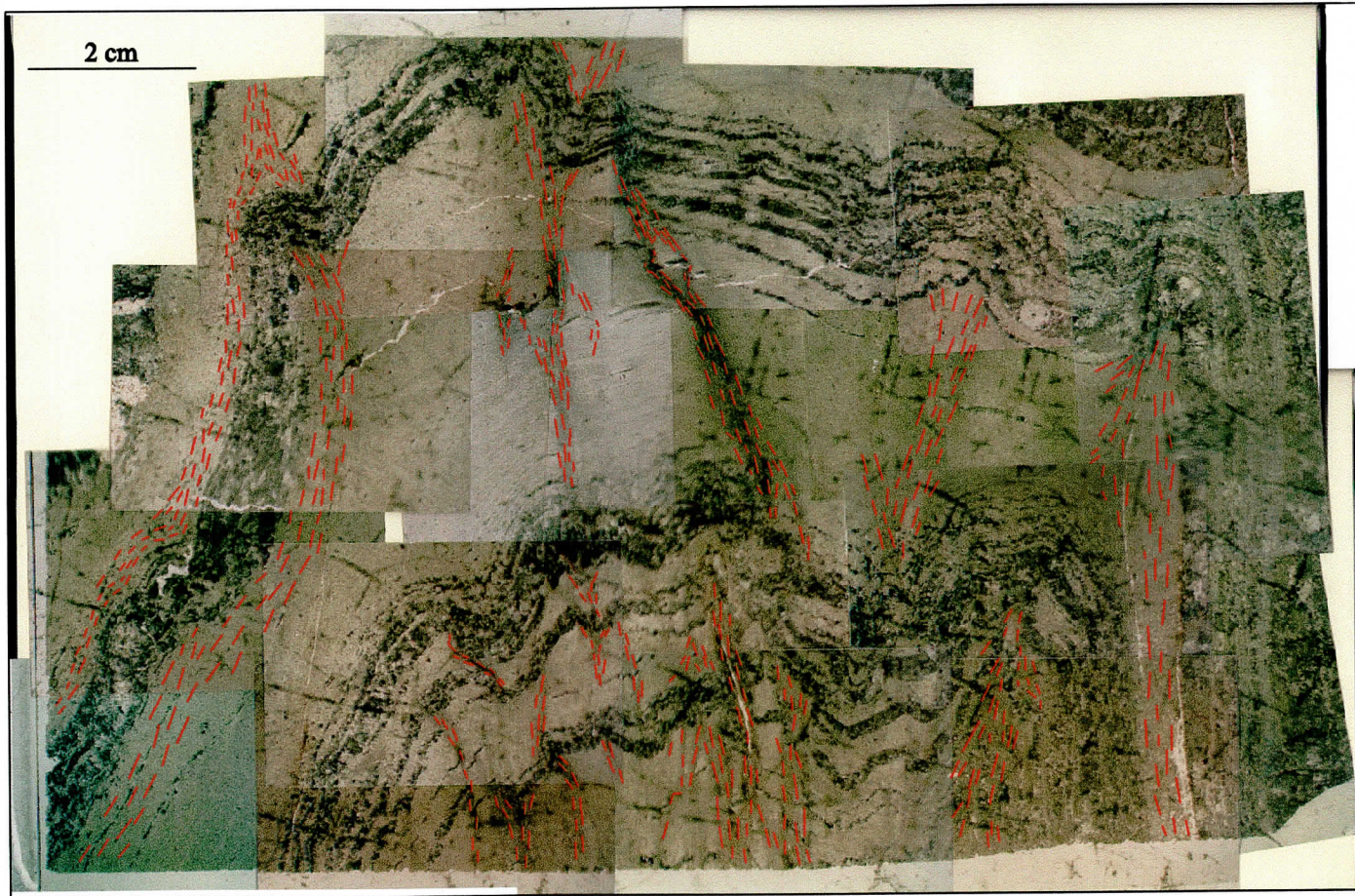


Figure 3.16. Thin section map of cleavage on photomicrographs. Foliation defining minerals are axial planar to minor and regional folds. Local variations are a result of deflections around cotichules. Note that the cleavage bands track the steep layers and are focused in the inner arcs of folds.

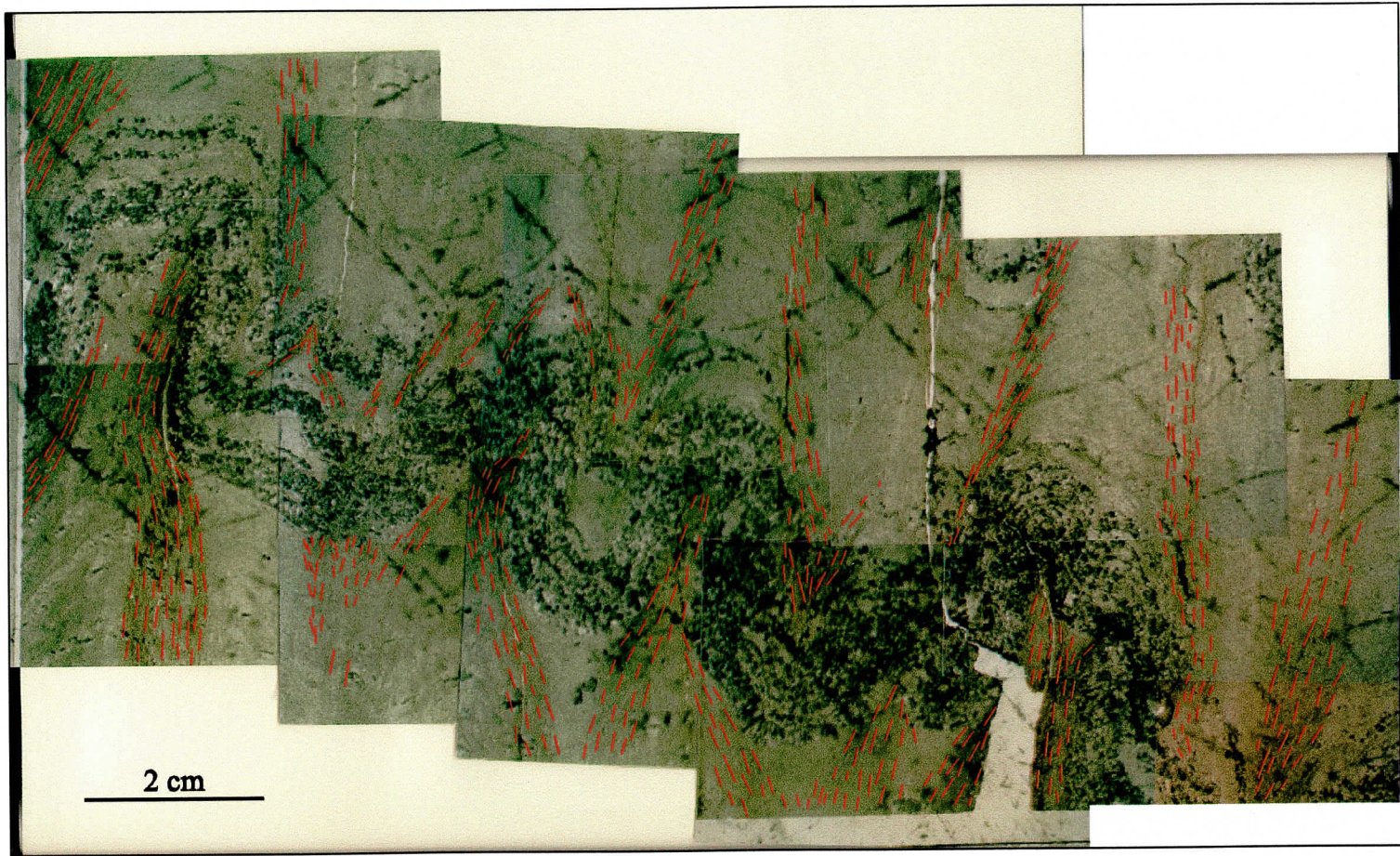


Figure 3.17. Thin section map of cleavage on photomicrographs. Cleavage tends to be focused in bands that are axial planar to the minor and regional folds. Local variations are a result of deflections around cotichules. Note that the cleavage bands initiate only in the inner arcs of folds and trace the fold limbs out of the inner arcs.

***Shortening recorded by minor folds:***

Values of shortening were obtained from measurements from three sets of slabs, 12 slabs in total, and two field photographs. A total of 64 values representing 32 coticule layers were generated and are listed in Appendix 2 and illustrated in Figure 3.18. Shortening values range from 40 - 57% and average 48% with a standard deviation of 4.10%. The four values generated from the field photographs (53%, 54%, 56%, 57%) are markedly elevated compared with the values for the slabs. In general though, fold styles displayed in the slabs are representative of the folds observed in the field and therefore the values of shortening are considered representative of the location.

In some layers, significant variation in shortening is recorded between parallel slabs (Fig. A1.4 in Appendix 1). Layer 'a' varies from 41% to 50% to 43% between slabs 1-3. Layer 'c' in the same slabs records a progressive increase in shortening from 45% to 50% and finally to 53%. Layer 'b', on the other hand, remains relatively constant in all three slabs. The other slab series (Figs. A1.2 and A1.3 in Appendix 1) consist of layers that record similar differentiated changes in shortening along the hinge.

Thin layers are generally sympathetic to thicker layers when closely spaced, and record similar amounts of shortening. For example, in slabs 2 and 5 of Figure A1.2 in Appendix 1 the thinner layer 'b' displays well developed harmony with the overlying thicker layer 'a' and both record similar values of shortening.

**3.2.2.3 Extensional features**

A photomicrograph of a thin section taken from the lower section of slab cut along the strike of the cleavage plane and facing northwest is shown in Figure 3.19. Two boudin

## H<sub>2</sub> (Bennery Lake)

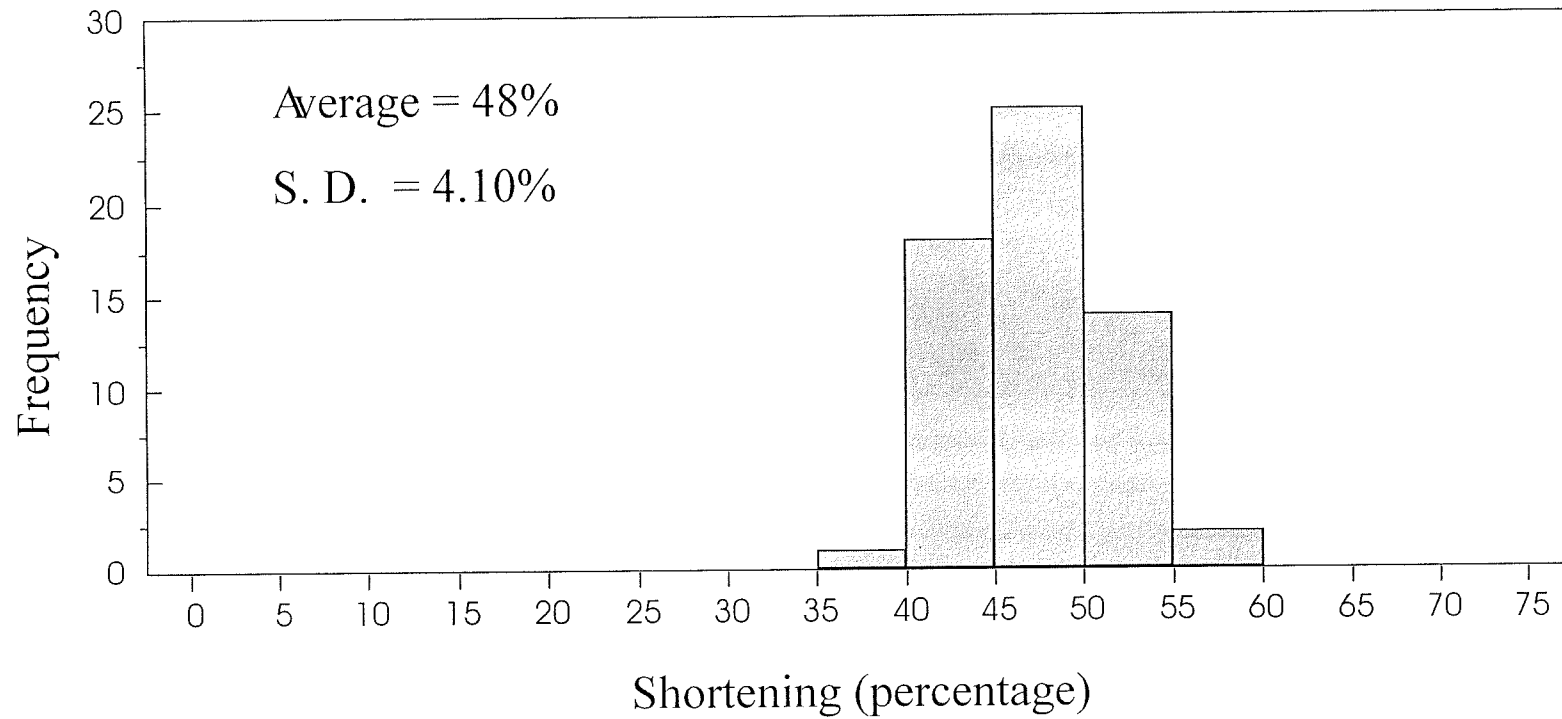


Figure 3.18. Histogram of shortening values. The average shortening value is 48% based on 60 data points (see Appendix 2).

necks are developed in a coticule layer. The fracturing of the coticule layer occurs along garnet grain boundaries. The coticule layer tapers toward the boudin necks. The quartz grain in both necks are highly elongate in the direction of the hinge, which is oriented roughly parallel to the coticule layer. Boudinage in this sample represents 25% extension.

### **3.2.3 Location L<sub>1</sub> (South Uniacke Pit)**

#### **3.2.3.1 General geology**

The L<sub>1</sub> outcrop is located in an inactive gravel pit near the community of Mt. Uniacke (Figs. 2.3 and 3.20). A small outcrop of the Beaverbank member is exposed in the east end of the pit. The outcrop is about 8 m along strike and 3 m wide and 1.5 m in height (Fig. 3.21). Bedding is 232/88 and cleavage is 045/78, consistent with southwest vergence (Fig. 3.22). Bedding and cleavage are uniform throughout the entire pit.

Exposure of coticule layers is very good and they are a bright mauve colour. Coticule layers are relatively abundant. Layer thickness is around 1.5 cm. The coticule layers are uniform in lithology and thin section evaluation indicates they consist of 60-70% spessartine garnet, 15-20% quartz, 15% carbonate, and minor ferromagnesian minerals. In thin section, the coticule layers at this locality differ from those at locations H<sub>1</sub> and H<sub>2</sub>, having a higher spessartine abundance and lower carbonate concentration. The matrix material is fine-grained slate with well-developed cleavage. It is important to note that the coticule layers are not folded at this location (Figs. 3.21 and 3.22) and there is no remnant evidence that any layer was ever folded. All coticule layers record 0% shortening at this location.

Figures 3.22 and 3.23 shows the relationship between bedding and cleavage typical at all locations in the study area. Cleavage is very well developed in the slate adjacent to the

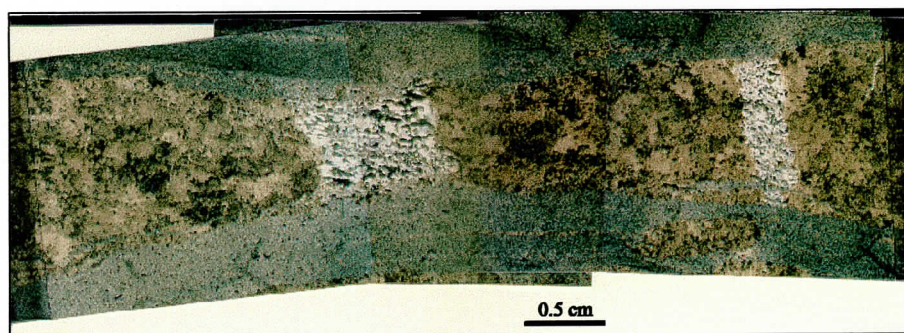
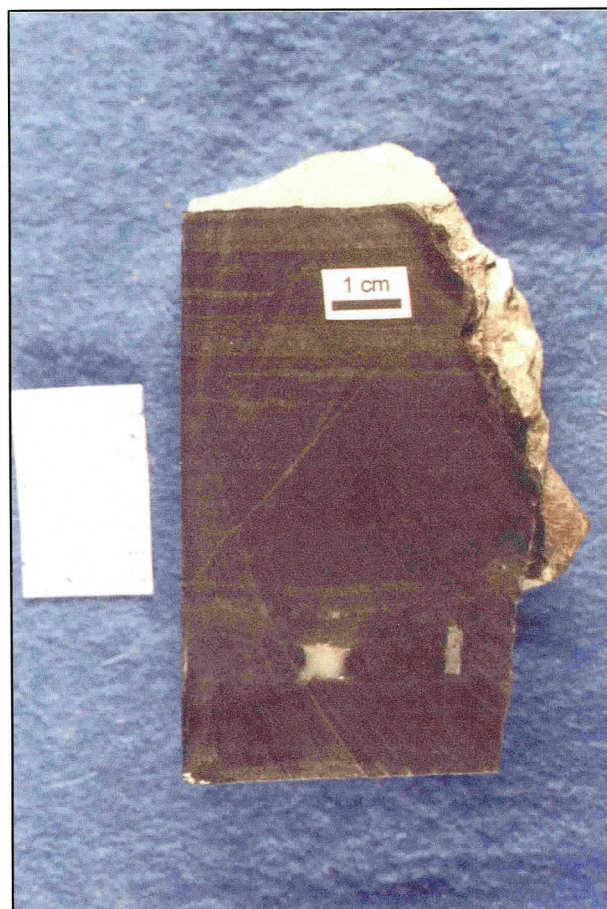


Figure 3.19. Slab and corresponding thin section cut parallel to the strike of cleavage (SW facing) showing a boudinaged cotecule layer. The boudinage is parallel to the hinge of the regional fold. In thin section, mineral lineations also parallel to the hinge are evident. The boudinage represents 25% extension.



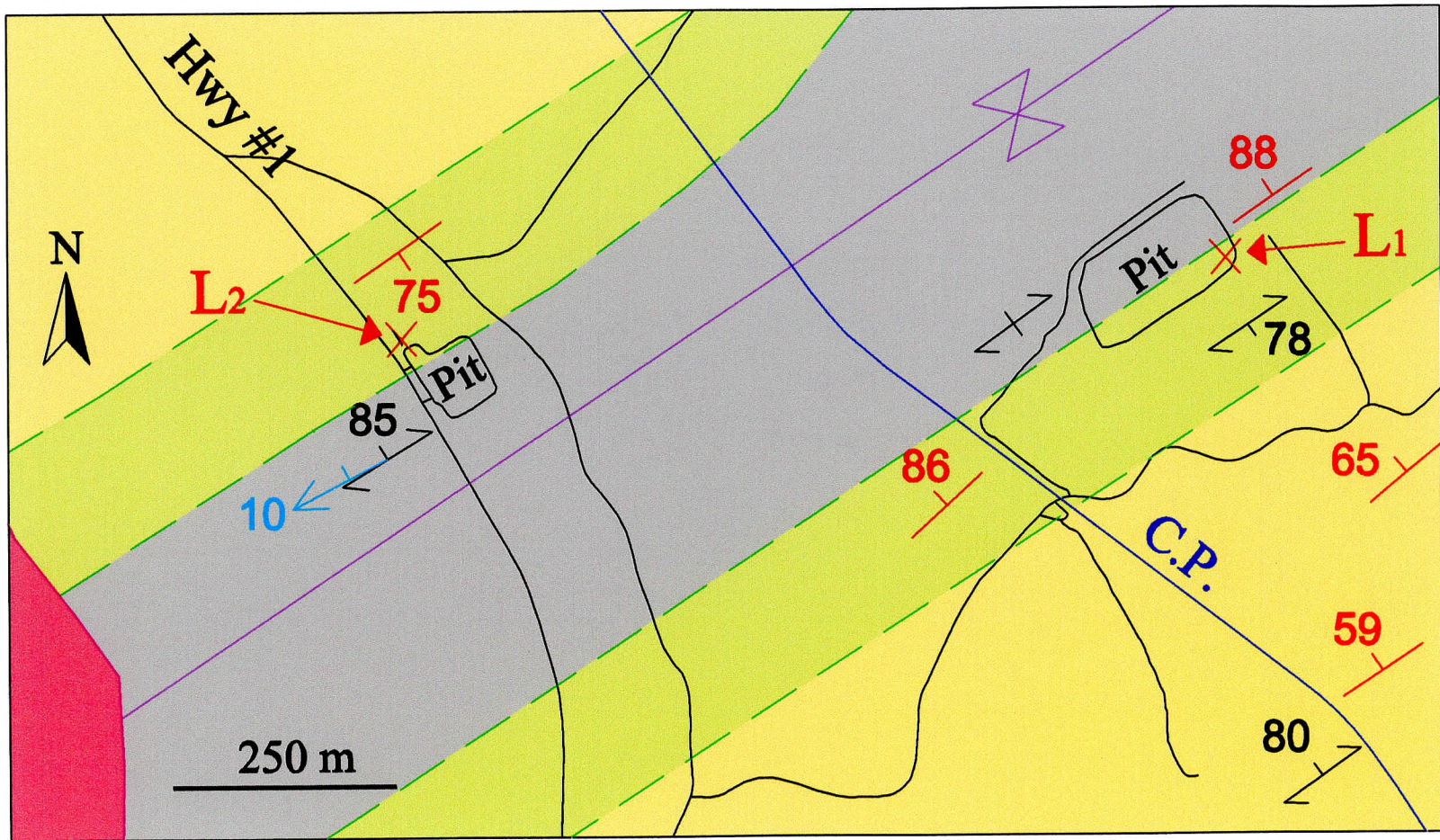


Figure 3.20. Outcrop location map of L<sub>1</sub> (South Uniacke Pit) and L<sub>2</sub> (Highway #1 Pit). Refer to Figure 2.3 for symbol definitions.



Figure 3.21. Outcrop scale exposure of steeply dipping non-folded coticule layers. Coticule layers are planar and no remnants of unfolded folds are observed.

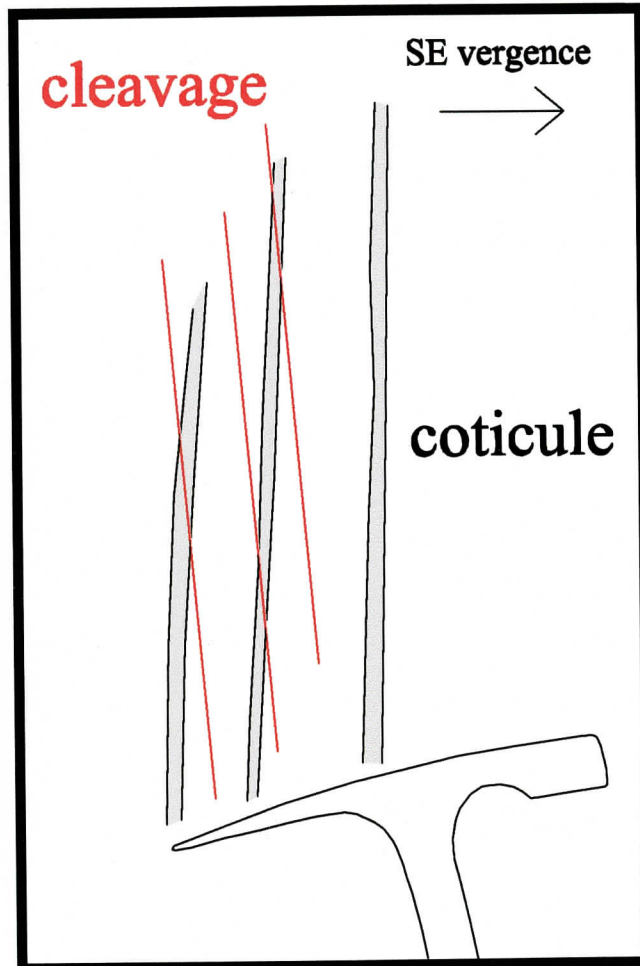
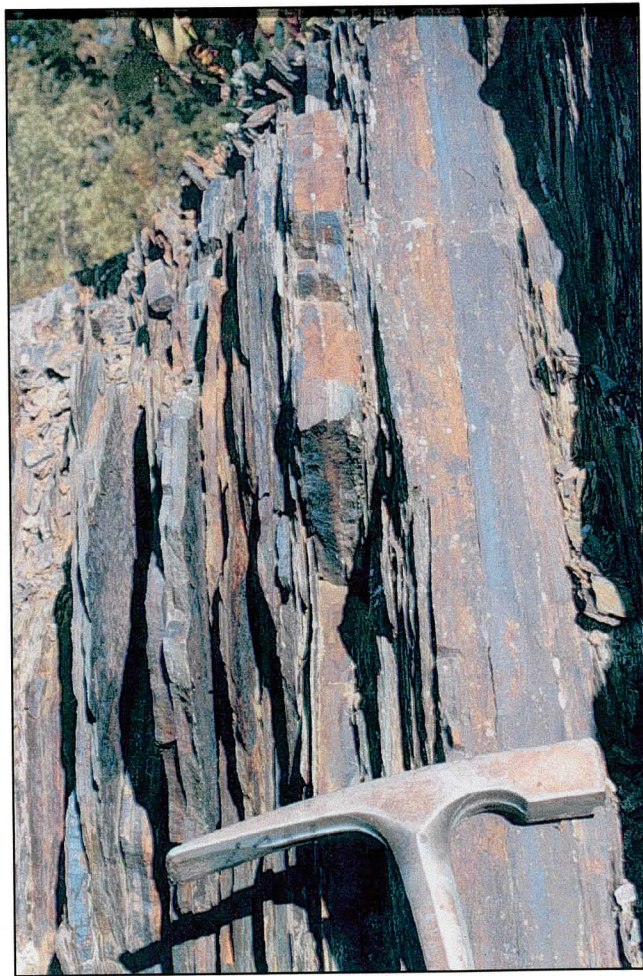


Figure 3.22. Close-up field photograph and sketch of the non-folded coticule layers. The bedding-cleavage angle is small and indicates southeast vergence.



Figure 3.23. Photomicrograph of a spessartine-bearing slate adjacent to a coticule layer. Foliation is deflected by the spessartine grains indicating spessartine grew prior to cleavage development. No inclusion trails in the spessartine are evident.

coticule layers and is defined by parallel oriented mica grains. Cleavage is axial planar to the regional fold and is slightly oblique to bedding. Cleavage tends to wrap around euhedral to subhedral spessartine garnets and pressure shadows parallel to the cleavage plane are common around the garnets (Fig. 2.23).

### **3.2.4 Location L<sub>2</sub> (Highway #1 Pit)**

#### **3.2.4.1 General geology**

The L<sub>2</sub> outcrop is located at the northwest end of an inactive gravel pit off of Highway #1, 7 km south of Mt. Uniacke (Fig. 2.3 and 3.20). The South Mountain Batholith is exposed 450 m to the west-southwest and minor cordierite is present. Slaty cleavage is well developed in the slates of the Cunard member and slate sections of the Beaverbank member suggesting only a small influence by contact metamorphism. Minor cordierite present overprints slaty cleavage. The upper Beaverbank member is exposed on a small hill at the northwest corner of the pit. A vertical face exposes an 8 m wide by 3 m high surface parallel to the fold profile plane where numerous cotucle layers are exposed (Fig. 3.24 in back). The exposure reveals cotucle layers protruding from the matrix by as much as 5 cm, making it easy to recognize the fold shapes displayed by the layers.

The L<sub>2</sub> outcrop is located on the north limb of a syncline whereas L<sub>1</sub> occurs on the south limb of the same syncline. Bedding is consistent through the pit, at 052/75. Cleavage is well developed and is 238/85, and the intersection lineation trends 242-10 (i.e. toward the batholith). In the fine-grained slates of the Cunard member, isolated crenulation cleavage occur along bedding planes (Fig. 3.25, Horne et al., 1997). The crenulation lineation, hinge of microfolds, vary systematically, defining scallop-like patterns on bedding-parallel surfaces



Figure 3.25. Field and hand sample photographs of scallop-shaped crenulation. The crenulation occurs along the bedding plane of slate layers. The crenulation is made up of stacked recumbent folds with highly curved hinge lines. Sulphitic minerals occur between the limbs of the stacked folds. It is interpreted to have formed by flexural slip where an inconsistency in the overlying layer dragged the crenulation at one point to form the scallop shape.

(Fig. 3.25). Sulfide mineralization is common in the interstices between limbs of individual micro folds. No crenulation folds of this nature are evident in the Beaverbank member. These crenulation folds may be a result of late fold tightening accommodated by flexural slip (Horne et al., 1997).

Coticule layers are abundant, occurring on average every 4 to 7 cm. Average layer thickness is around 1.5 cm, but some are up to 5 cm. Lithologically, the coticule layers are very similar to those at  $L_1$  where there is an abundance in spessartine garnet. The matrix material is fine-grained slate with minor metasiltstone and cleavage is well developed.

#### **3.2.4.2 Minor folds**

##### ***Fold style***

The shape of minor folds at  $L_2$  is variable, including box, pygmatic, open sinusoidal, and modified box folds. Figure 3.24 shows the entire spectrum of fold styles. In panel 2 layer 'b' of Figures 3.24 and 3.27d a direct relationship between layer thickness and fold wavelength and amplitude is evident, where the thicker segments of the layer have greater fold wavelengths and amplitudes. In Figure 3.26 symmetric folds in the centre and top of the image are juxtaposed with moderately asymmetric folds at the bottom of the image. The symmetric folds consist of a box fold with a  $-55^\circ$  projected interlimb angle and a tight fold with a horizontal axial plane (Fig. 3.26). The axial planes of the sheared and symmetric box folds in Figure 3.26 shows the divergence of axial planes in the same fold. This divergence is a result of the originally divergent pattern of the axial planes of a box fold prior to shearing (refer to Fig. 1.1).

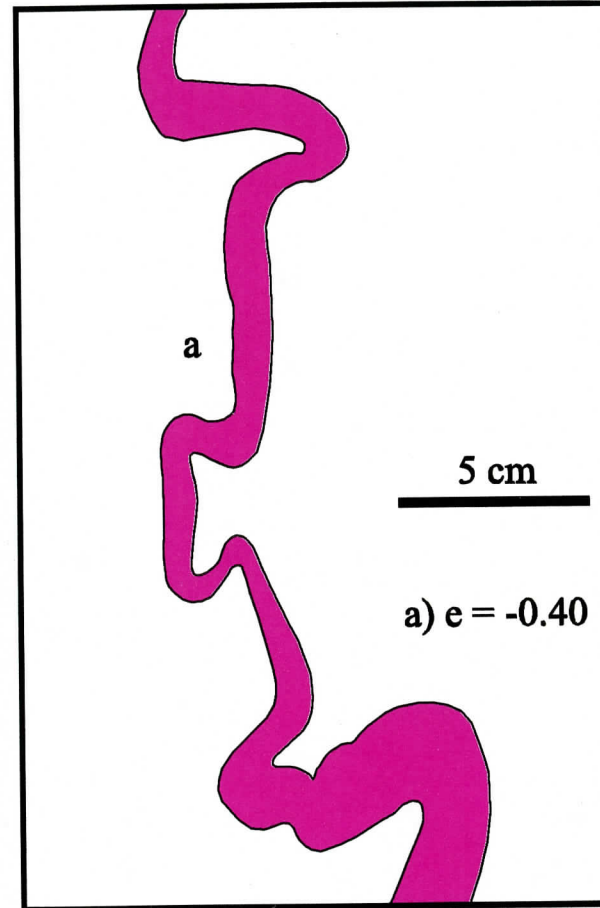


Figure 3.26. Field photograph and sketch showing symmetric and asymmetric folds developed in the same layer. The tight box fold in the middle of the sketch is symmetric whereas the fold at the bottom of the sketch is moderately asymmetric. Distinct zones throughout this outcrop display folds with highly variable symmetry.



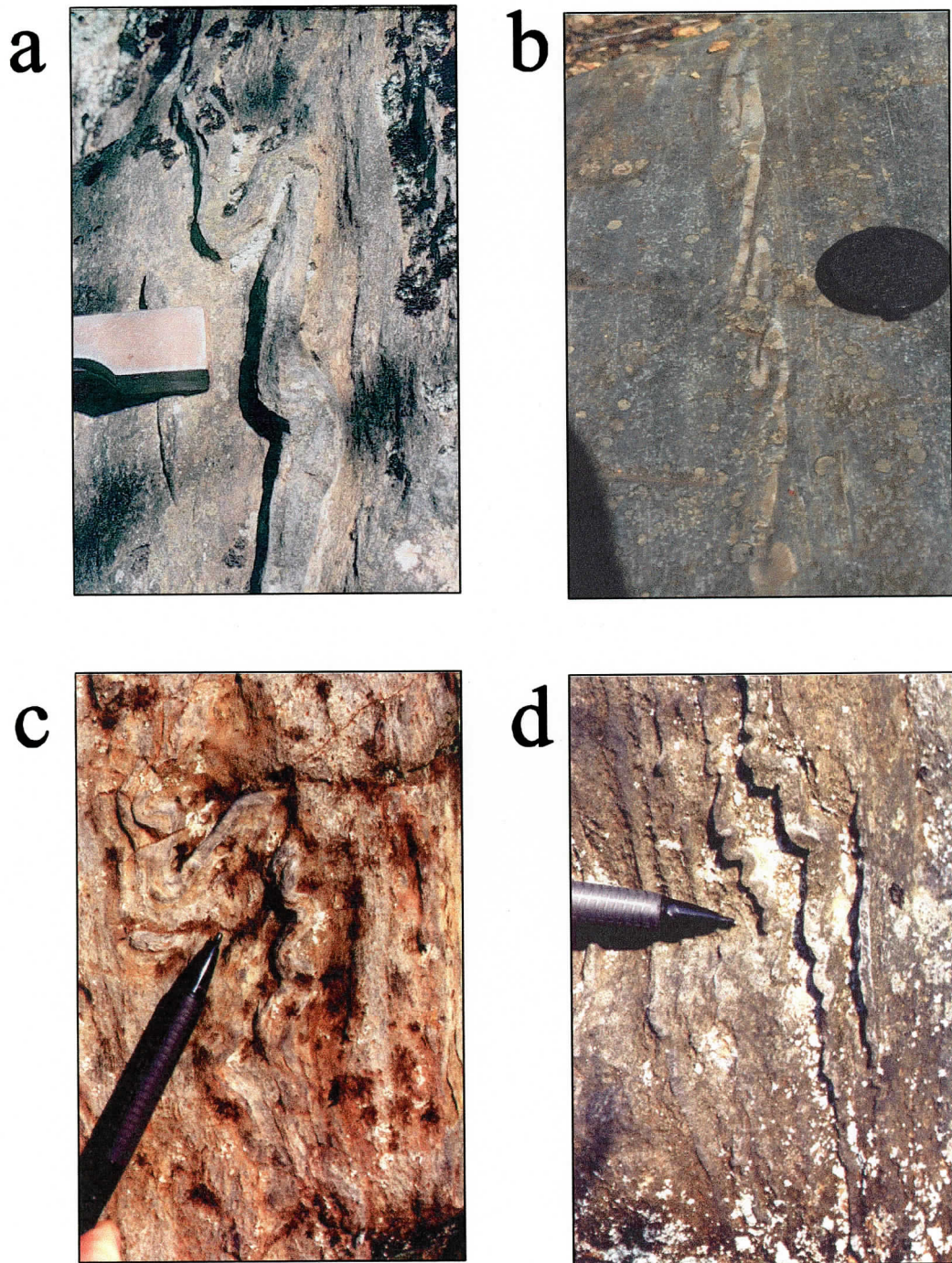


Figure 3.27. Field photographs of selected fold styles. Photographs (a) and (b) show highly asymmetric folds (axial planes are parallel to the regional fold axial plane) whereas photograph (c) shows a moderately asymmetric box fold with subsidiary folds developed in the median segment. The folds in photograph (d) nicely displays the relationship between layer thickness and fold wavelength and amplitude. As the layer thickens the fold wavelength and amplitude increase accordingly.

Symmetry of the minor folds at this location is quite variable. As described above some folds exhibit horizontal axial planes, and in Figure 3.24 selected axial plane traces have been drawn connecting multiple layers. These axial plane traces are at shallow angles, ranging from  $25^{\circ}$  to  $45^{\circ}$  from the horizontal. In Figure 3.27a and b the folds exhibit exceptional asymmetry where the axial planes are vertical or close to vertical. The folded layers in Figure 3.27a and b display consistent layer thickness despite the highly asymmetric nature of the folds. The wide range in degree of symmetry is inconsistent with the classical model of parasitic folds, where it is predicted that all folds would be regionally axial planar.

***Bedding-cleavage relationships:***

Cleavage-bedding relationships at  $L_2$  are more complex than at other locations studied. The complications arise from symmetrical folds displayed on steep limbs. Figure 3.28 is a map of cleavage on photomicrographs. The photographs were taken in crossed nichols. The matrix material is silty slate and slate with variably developed cleavage. Cleavage along the left margin of the sample approximates regional axial planar cleavage. As at the other locations, cleavage forms divergent fan patterns around the outer-arc of minor folds. Cleavage tends to diverge significantly from the regional axial plane in the inner-arcs and around the outer-arcs of minor folds. Cleavage is always axial planar to minor folds whereas, cleavage diverges up to  $90^{\circ}$  to the regional cleavage, where this divergence is controlled by the symmetry of the folds. In other words, the more symmetric (axial plane at higher angle to regional limb dip) the fold is, the more cleavage diverges from the regional axial plane.



Figure 3.28. Thin section map of cleavage on photomicrographs. Foliation defining minerals are axial planar to the minor folds, but locally, foliation diverges up to  $90^\circ$  to the regional axial plane. Where folds exhibit good symmetry this divergence is best developed. These symmetric folds represent zones of low shear strain. Thin section from slab in Figure 3.30.

### ***Shortening recorded by minor folds:***

Values of shortening consist of measurements from two slabs (Figs. 3.29 and 3.30), one field photograph (Fig. 3.26), and a large field photo-collage (Fig. 3.24). A total of 45 values representing 23 cotichule layers were generated and are listed in Appendix 2 and illustrated in Figure 3.31. Shortening values range from 8 to 41% with an average of 22% and a standard deviation of 8.83%. The values generated from the slabs and single field photograph are higher than the values from the photo-collage. In the case of this location, the most representative values of shortening are those derived from the larger scale field photographs. Figure 3.41 illustrates that the majority of shortening values range from 10 - 30%, which is the most representative range based on the entire outcrop.

There are numerous examples of polyharmonic folding where the thinner layers are sympathetic to the thicker layers (e.g. Figs. 3.24 and 3.29). Layers 'a' and 'c' in panel 3 of Figure 3.24 demonstrate how thinner layers acquire the shape of thicker ones (i.e. 'b'). No significant difference is evident in shortening between these layers. In other cases, there are more pronounced differences in shortening in adjacent layers. Layer 'f' in panel 2 of Figure 3.24 is much less shortened than its direct neighbour, layer 'e'. The top of the straight segment of layer 'f' begins at the lower traceable axial plane. Layers 'a', 'b', and 'c' of panel 1 record little shortening whereas the sketched layers in the right side of panel 1 record greater amounts of shortening.

#### **3.2.4.3 Extensional features**

The folded cotichule layer in Figures 3.28 displays very well developed outer-arc and down-dip extension. Outer-arc extension (Fig. 3.32) is shown by of wedge-shaped fractures

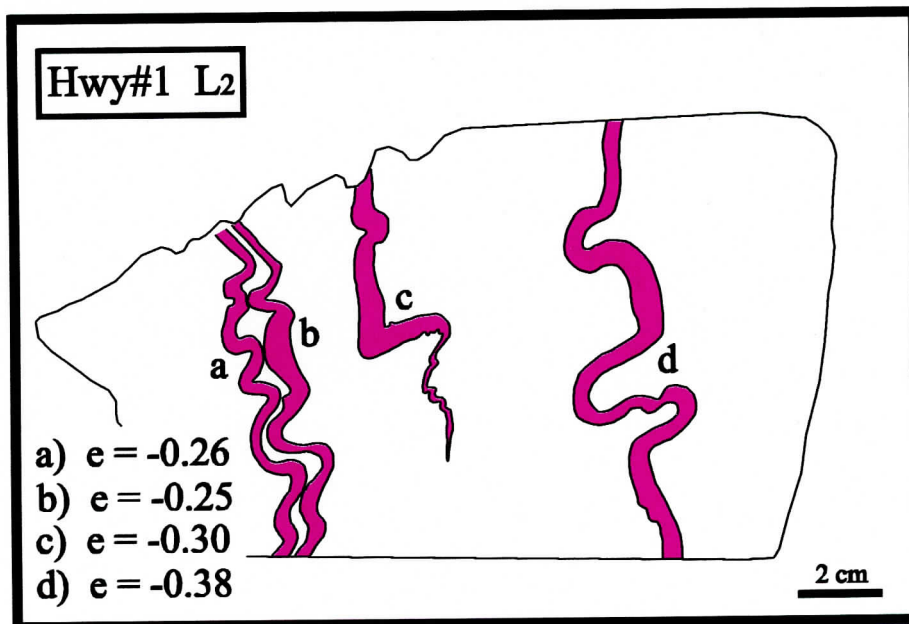
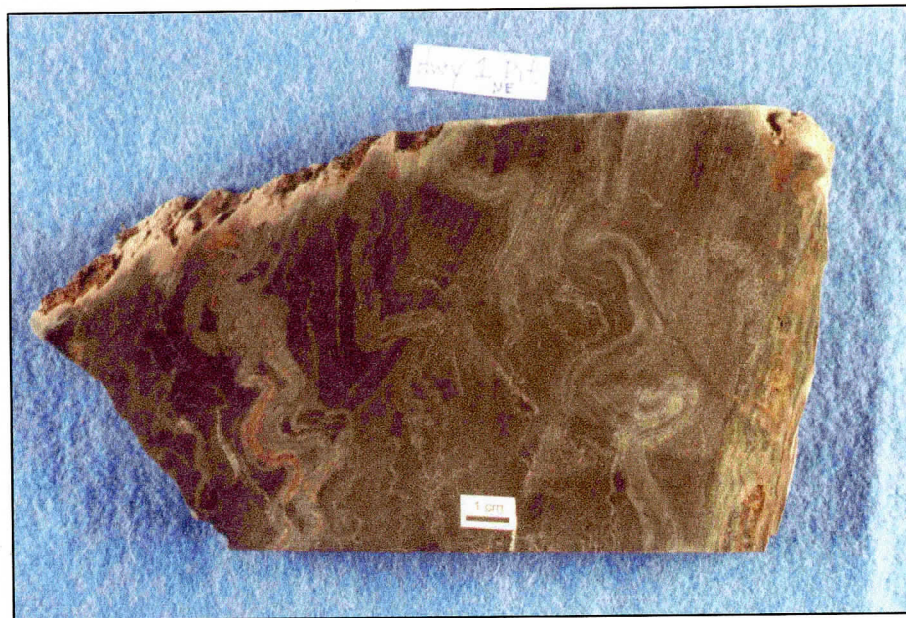


Figure 3.29. Slab photograph and sketch. Folds are symmetric to mildly asymmetric and display variable shortening values across the sample.

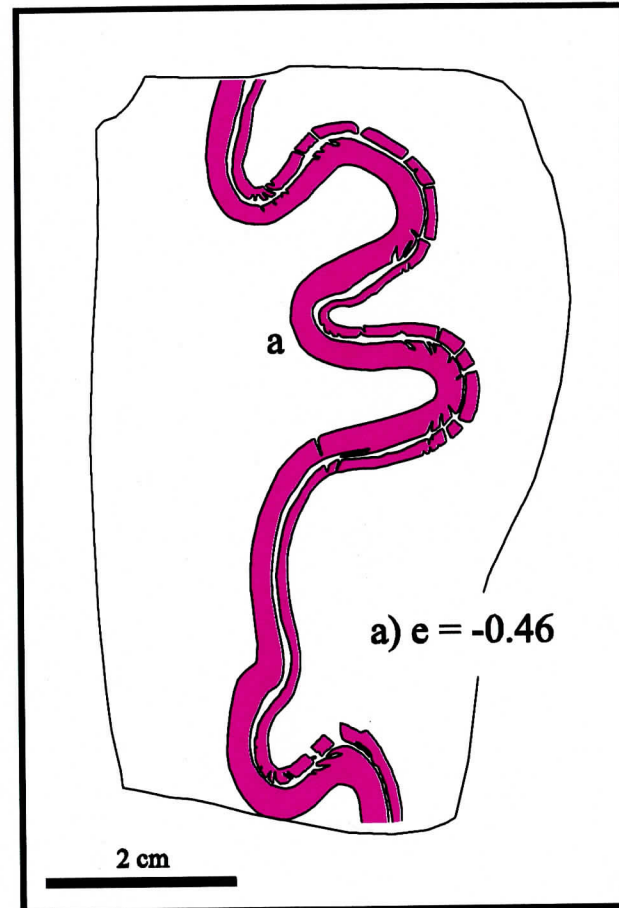


Figure 3.30. Slab photograph and sketch. Folds are symmetric to mildly asymmetric. Note that outer-arc extension is very well developed in the fold crests. Outer-arc extension indicates that the folds were formed when layers were stiff. The pattern of the outer-arc fractures indicates that these folds formed by tangential longitudinal strain during layer parallel shortening.

## L<sub>2</sub> (Highway #1)

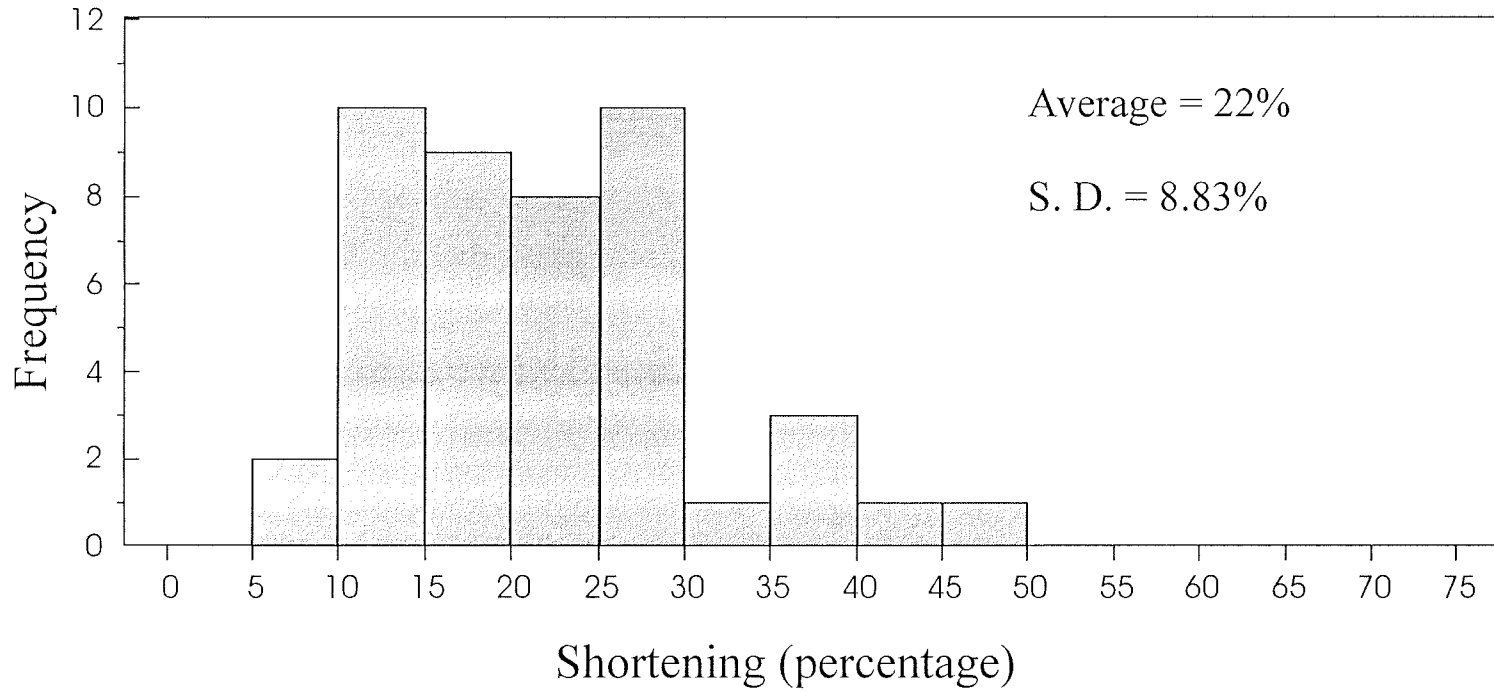


Figure 3.31. Histogram of shortening values. The average shortening value is 22% based on 45 data points (see Appendix 2).

that taper toward the inner arc, indicating that the neutral surface of the fold is very close to the inner arc. The fractures occur along garnet grain boundaries and the quartz that infills the wedges is euhedral to subhedral and displays moderate undulose extinction.

The dilation between the laminations in the cotecule layer in Figure 3.28 is greater on the limbs of the minor folds than in the hinges. This extension is oriented in the down-dip direction where the limbs of the folds are roughly horizontal. The voids between the extended laminations are infilled with subhedral quartz crystals. The quartz crystals of both the down-dip and outer-arc extension appear to be related (Fig. 3.32).

Figure 3.33 is a photomicrograph of a thin cotecule that is boudinaged. Fractures occur along garnet grain boundaries. Fractures are generally horizontal and are restricted to layer segments that are steeply dipping. Segments of the layer that are horizontal or very shallow are not boudinaged. The quartz grains are euhedral to subhedral with moderately undulose extinction and they display no apparent elongation. Boudinage represents 18% extension in the down-dip direction.

### **3.2.5 Location L<sub>3</sub> (Beaverbank Road)**

#### **3.2.5.1 General geology**

The L<sub>3</sub> outcrop is located along the Beaverbank Road (Figs. 2.3 and 3.34). The Beaverbank unit is exposed for 100 m across strike in the ditches of the road. There is also a small exposure ~600 m west of the Beaverbank Rd in the middle of a gravel road (Fig. 3.34). This location lies on the north limb of a subsidiary syncline of the Mt. Uniacke Synclinorium (Fig. 2.3). Bedding is consistent in the area at 055/68 and cleavage 050/75.





Figure 3.32. Photomicrographs of well-developed outer-arc extension. Inset image shows how the quartz between coticule interlamination appears to be the same as in the outer-arc extensional wedges.

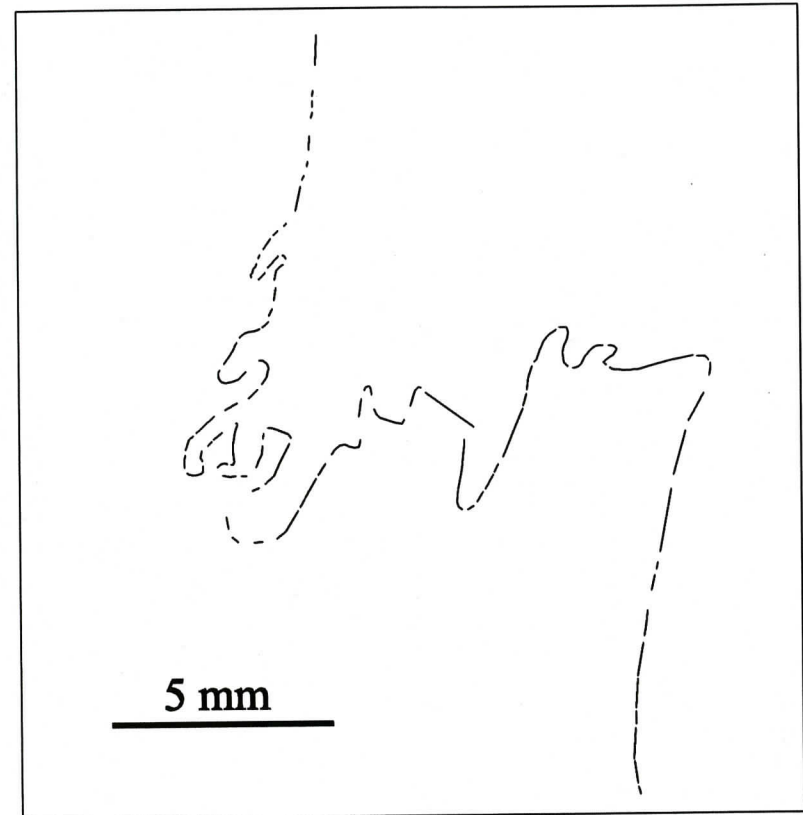


Figure 3.33. Photomicrograph and sketch showing a thin boudinaged coticule layer. The sketch shows only the coticule segments and the spaces between represent quartz-filled boudin necks. Note that boudinage only occurs in steeply dipping segments and not in subhorizontal segments.

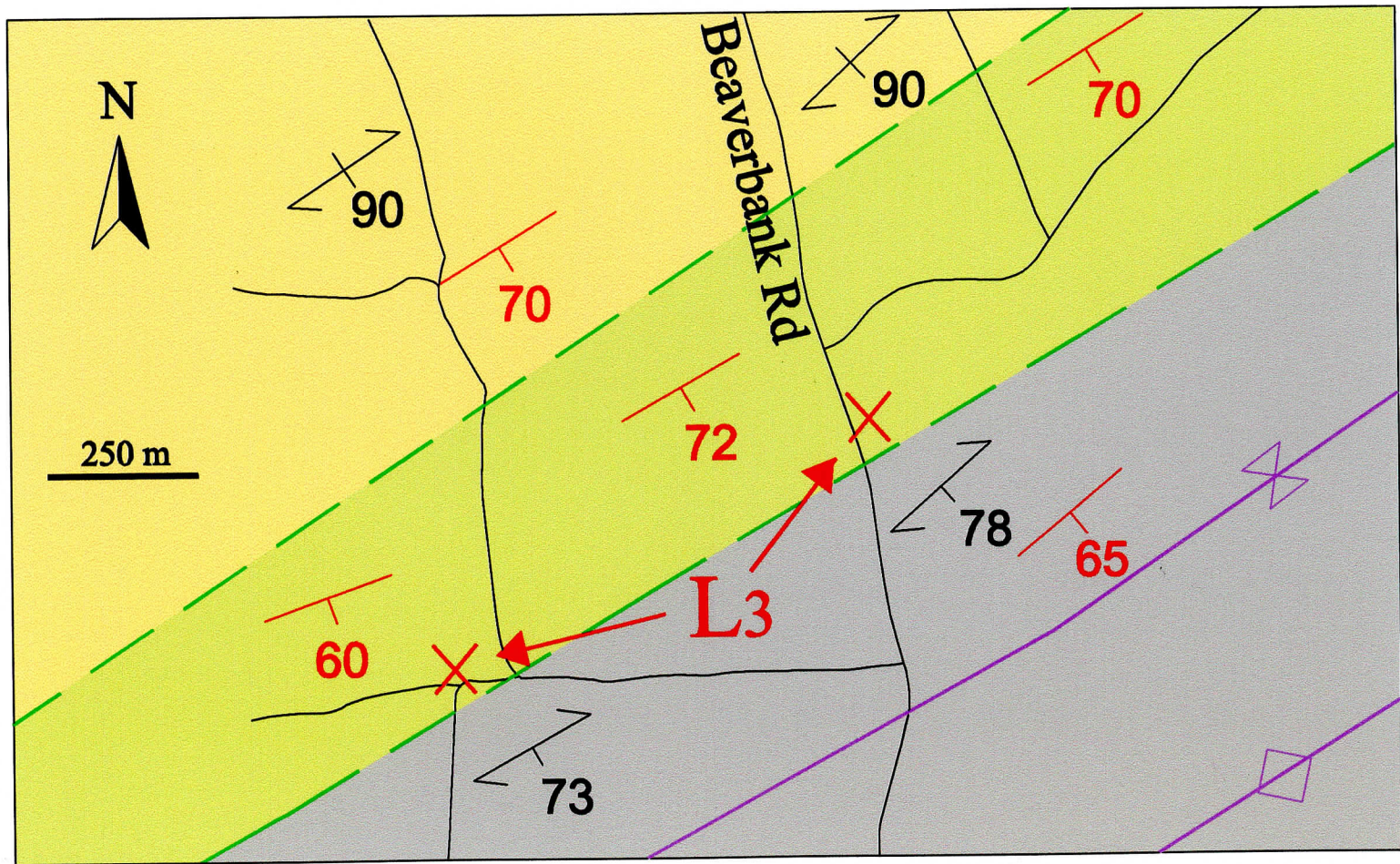


Figure 3.34. Outcrop location map of  $L_3$  (Beaverbank Road) including the small outcrop to the west of the road. Refer to Figure 2.3 for symbol definitions.

Coticule layers occur in a 50 m section across strike and are recognized by their distinctive purple colour. Layer thickness averages about 1.5 cm and spacing is variable, generally between 5 and 8 cm. Lithologically, coticule layers are similar to those at locations  $L_1$  and  $L_2$ , with 60-70% spessartine garnet, 20% carbonate, 15% quartz, and minor ferromagnesian minerals. The matrix material is consistently a silty slate with well-developed slaty cleavage. Minor spessartine occurs in the matrix material, especially adjacent to the coticule layers.

### **3.2.5.2 Minor folds**

#### ***Fold style:***

The shapes of minor folds at location  $L_3$  is quite variable. The lower section of the coticule rich sequence consists of generally planar layers with isolated isoclinally folded layers. The upper section, however, is characterized by variably tight to open folds (Figs. 3.35 and 3.36). Figure 3.35 shows the extent of the folded section on the east side of the Beaverbank Road whereas Figure 3.36 shows typical folds from the west side of the road, about 25 m directly on strike from Figure 3.35. On the east side of the road open box folds with isolated isoclinal folds characterize the folds. This two metre section is flanked on both sides by dominantly non-folded layers with isolated isoclinal folds. On the west side of the road folds are characterized by symmetric to highly asymmetric box and ptygmatic folds developed in steeply dipping layers (Figs. 3.36 and 3.37).

The noncylindricity displayed in the folds at this location is significant. As described above there is great fold shape variation between the east and west sides of the Beaverbank Road. The folds on the east side of the road occur in the hinge or on the limbs of a

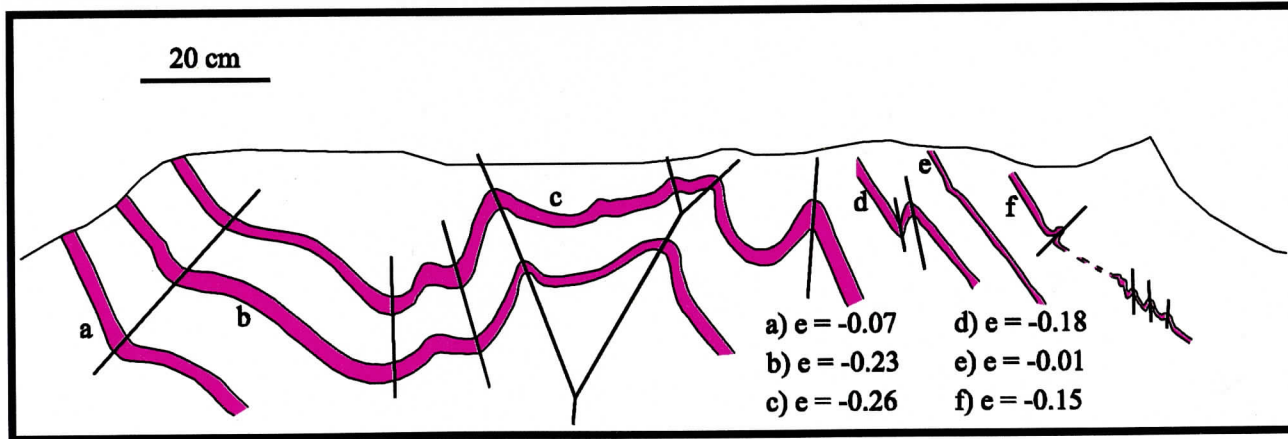


Figure 3.35. Field photograph and sketch of a profile section on the east side of the Beaverbank Road. The central fold in this section is an upright mesoscale modified box fold. Outside of this section coticule layers display only isolated folds and primarily planar layers.

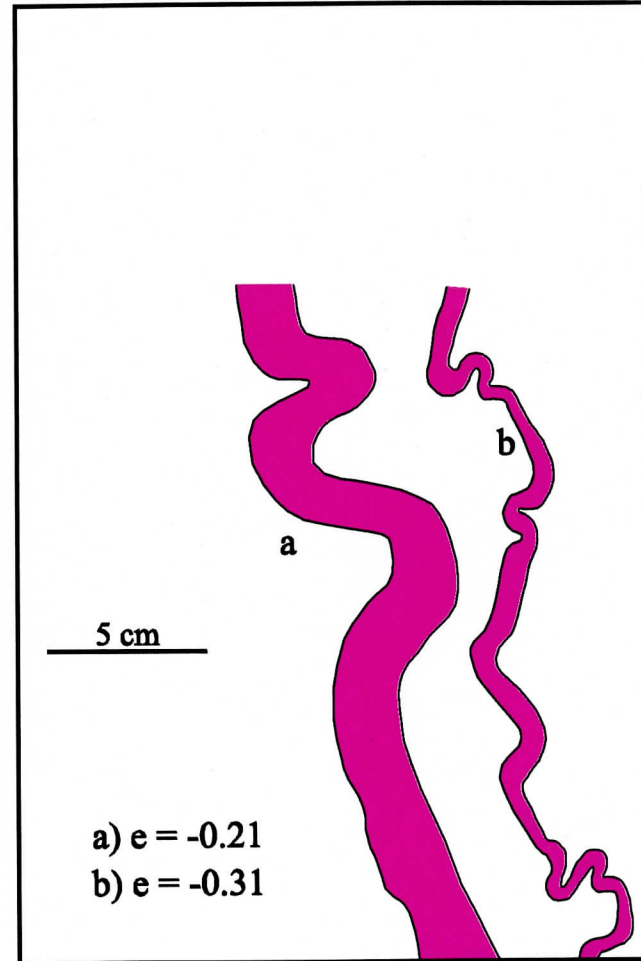
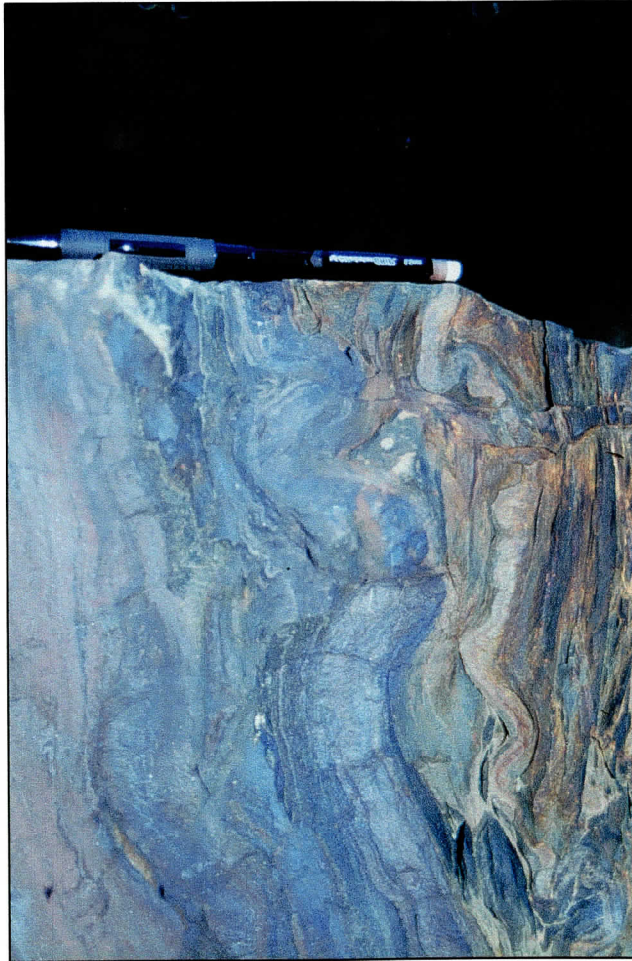


Figure 3.36. Field photograph and sketch of two steeply dipping folded coticule layers. The thinner layer is more shortened than the thicker layer. Polyharmony between the two layers is poorly developed.

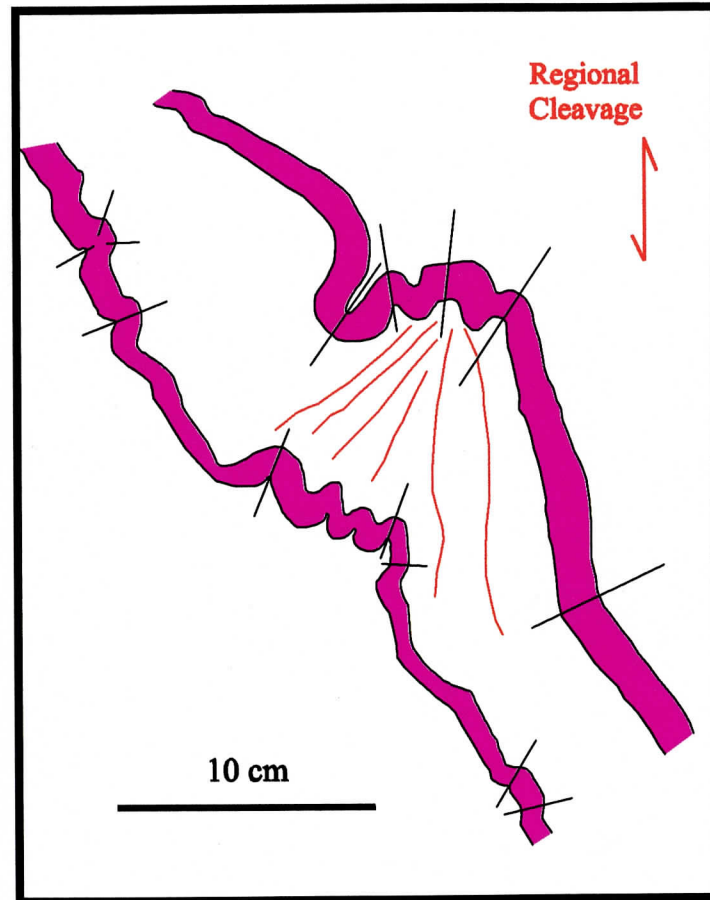


Figure 3.37. Field photograph and sketch of two folded coticule layers. Cleavage adjacent to folded coticule layers is generally regionally axial planar, but locally, cleavages diverges controlled by the symmetry of the folds. The two folded layers display moderately well developed polyharmony.

mesoscale upright box fold (Fig. 3.35), whereas the layers on the west side of the road are on a consistently steeply dipping limb and the folds display variable symmetry (Figs. 3.36 and 3.37).

Figure 3.38 shows line drawings of buckled coticule layers from six successive slabs, each 4 cm thick perpendicular to the hinge (see Figure A1.5 in Appendix 1). There is considerable variation in fold shape evident over just 20 cm along the hinge. The lower layer in slab 1 shows two well developed asymmetric ptygmatic folds that, by slab 6, are almost unrecognizable. In places, significant plunging terminations of these folds occur. Abrupt terminations of regional folds is also common in the Meguma Group (refer to section 2.2.2.1). Figure 3.39 shows a plan view of the small exposure on the gravel road 600 m west of the Beaverbank Road. The noncylindricity displayed in the doubly plunging layer is significant and characteristic of the majority of the minor folds at this location.

The minor folds display significant variation in symmetry. The lower layer in Figure 3.37 exhibits dominantly symmetric folds whereas the overlying layer consisting of a modified box fold that is asymmetric, close to being co-axial planar to regional folds. The folds in the slabs of Figure A1.5 in Appendix 1 display variable symmetry in the same layers along the hinge. Slab 1 displays folds that are rather asymmetric whereas in slab 6 the folds appear to be less asymmetric. Qualitatively, the folds at  $L_3$  are significantly more asymmetric than those at  $L_2$ .

***Shortening recorded by minor folds:***

Values of shortening consist of measurements from three field photographs and six successive slabs. A total of 44 values representing 22 coticule layers were generated and are



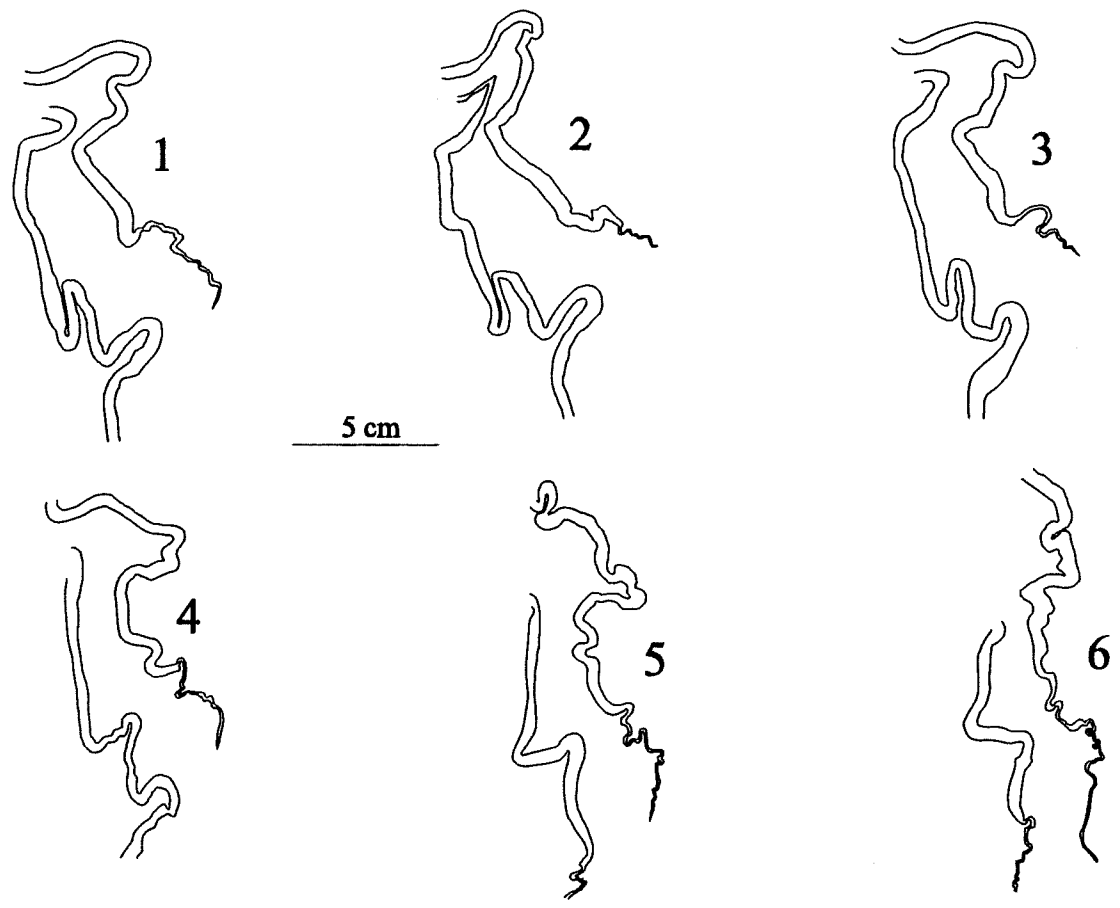


Figure 3.38. Line drawings of a two folded cuticle layer from six parallel, 4-cm thick slabs cut perpendicular to the hinge. The fold shapes change considerably along the hinge. Note also that the symmetry of the folds changes along the hinge. In slabs 1 - 3 the folds in the lower layer display moderate to high asymmetry, whereas in slabs 4 - 6 they display less asymmetry.

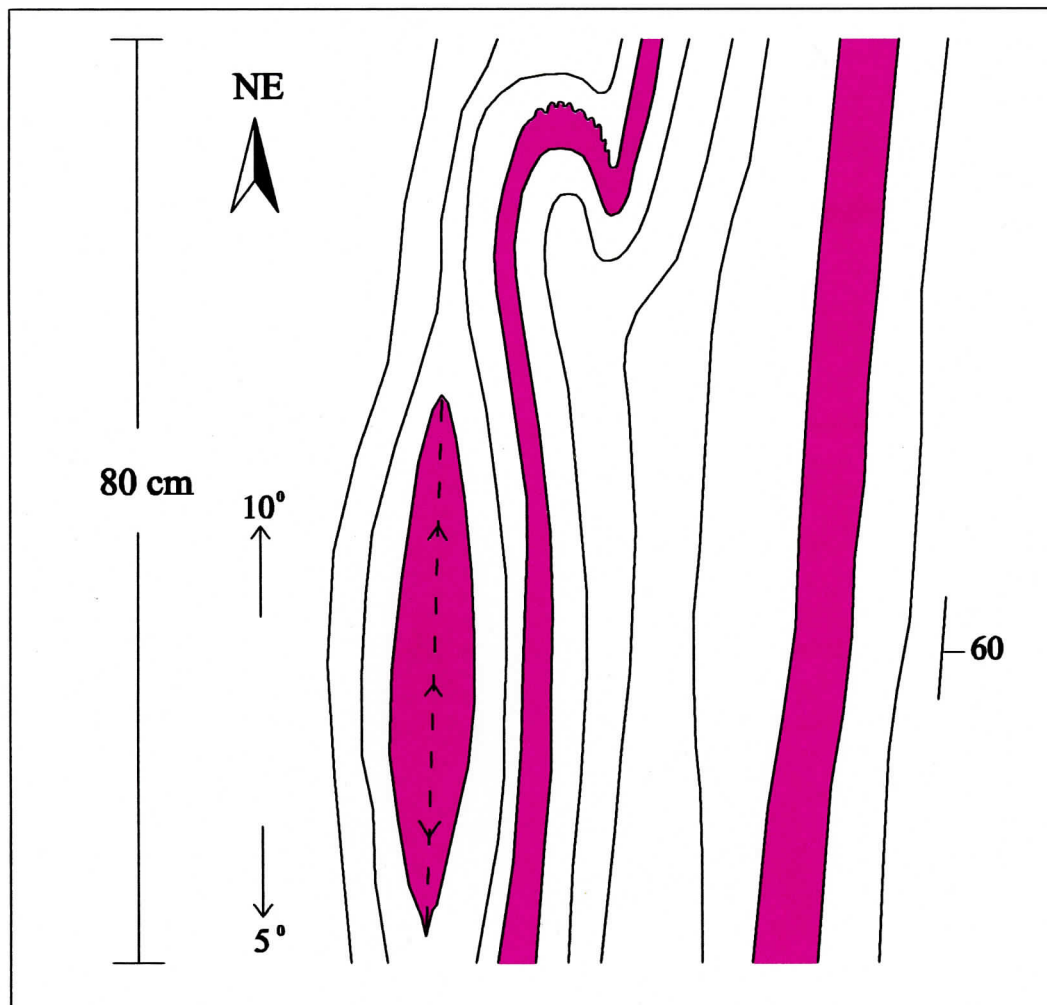


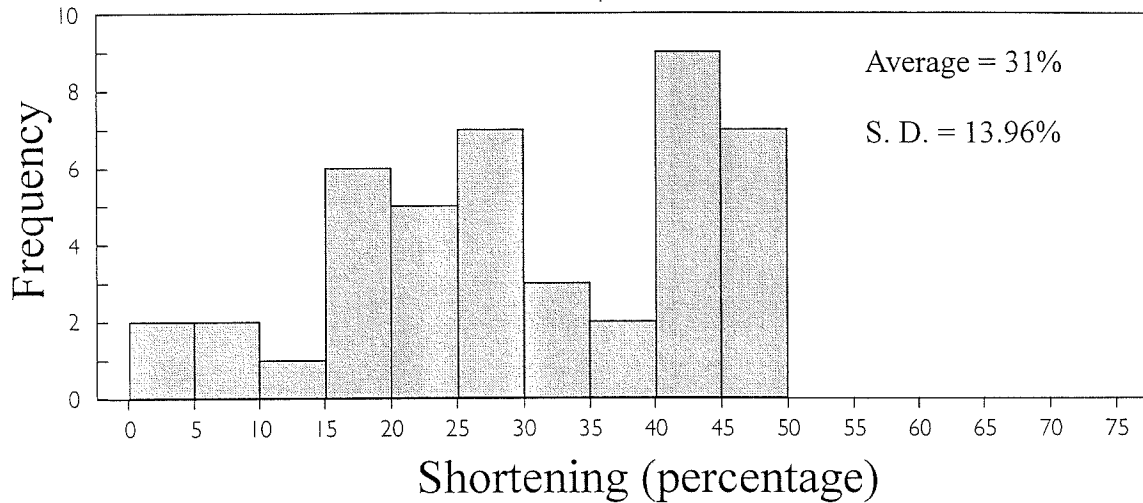
Figure 3.39. Plan view sketch of a doubly plunging folded cotiule layer. Arrows indicate direction and magnitude of plunge. Noncylindrical folds of this type are the major fold style in the study area. In fact, these types of folds mimic the regional fold style which is also noncylindrical.

listed in Appendix 2 and illustrated in Figure 3.40. Shortening values range from 1 to 48% with an average of 31% and a standard deviation of 13.96%. From Figure 3.40 two distinct data populations are apparent. The high values represent the six successive slabs, which have a range from 28 to 48%, an average of 41%, and a standard deviation of 7.0% (Figs. A1.5 in Appendix 1 and 3.40). The low values represent the field photographs which have a range from 1 to 32%, an average of 18%, and a standard deviation of 8.83% (Fig. 3.40). As the field photographs captured longer segments of the cotichule layers than the slabs they are considered more representative of the entire outcrop. The slab data are derived from a sample which was collected because of the locally well developed folding. Also, the shortening values do not represent the entire outcrop where numerous non-folded and isolated folds were observed in the field. Qualitatively then, this location appears to record less shortening than displayed at location  $L_2$ .

On the east side of Beaverbank Road most of the folded cotichule layers are restricted to the section shown in Figure 3.35. Outside of this section bedding is steep ( $60^\circ$ ) and folding is restricted to isolated layers and intermittently along the length of the layer. The folds developed in layer 'a' in Figure 3.35 are typical of the extent of folding to the north (to the left of the photo-section). On the west side of the road, similar isolated folds are developed in largely planar non-folded cotichule layers. Layer 'a' in Figure 3.36 illustrates how a planar layer is folded only in particular sections.

Layer 'b' in the slabs of Figure A1.5 in Appendix 1 shows a progressive decrease in shortening along the hinge in the northeast direction. The reduction in shortening is accompanied by a dramatic change in fold shape between slabs 4 and 5. Layer 'a' also

### L<sub>3</sub> (Beaverbank Road)



### L<sub>3</sub> (Beaverbank Road)

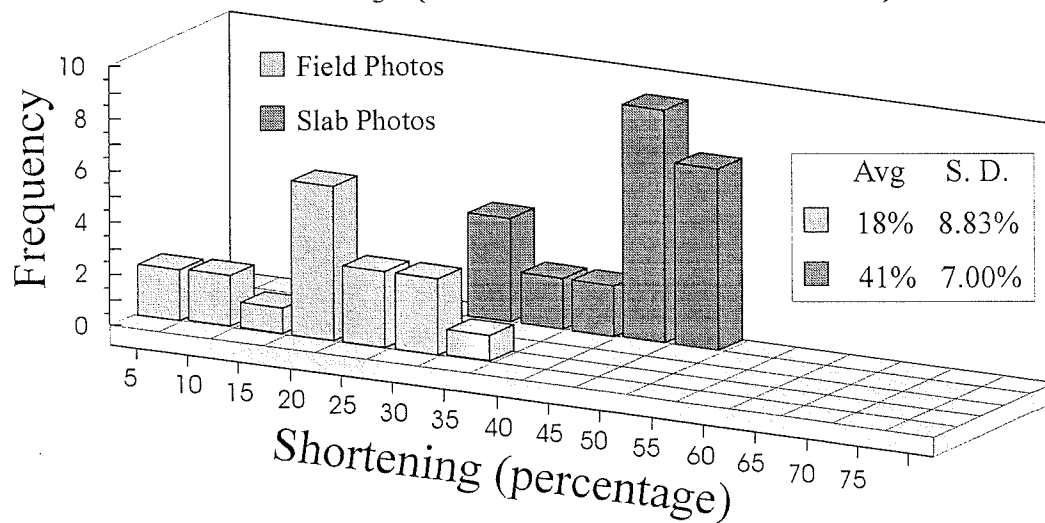


Figure 3.40. Histograms of shortening values. The upper histogram shows the entire population of data with an average of 31% based on 44 data points. The lower histogram separates the two data populations derived from (1) field photos and (2) slab photos. The slabs were cut from a sample taken specifically because it was folded and is anomalous in the magnitude of shortening. The data from the field photographs on the other hand, represent the range in shortening of minor folds through the outcrop. The average of shortening values from field photographs is 18% based on 20 data points.

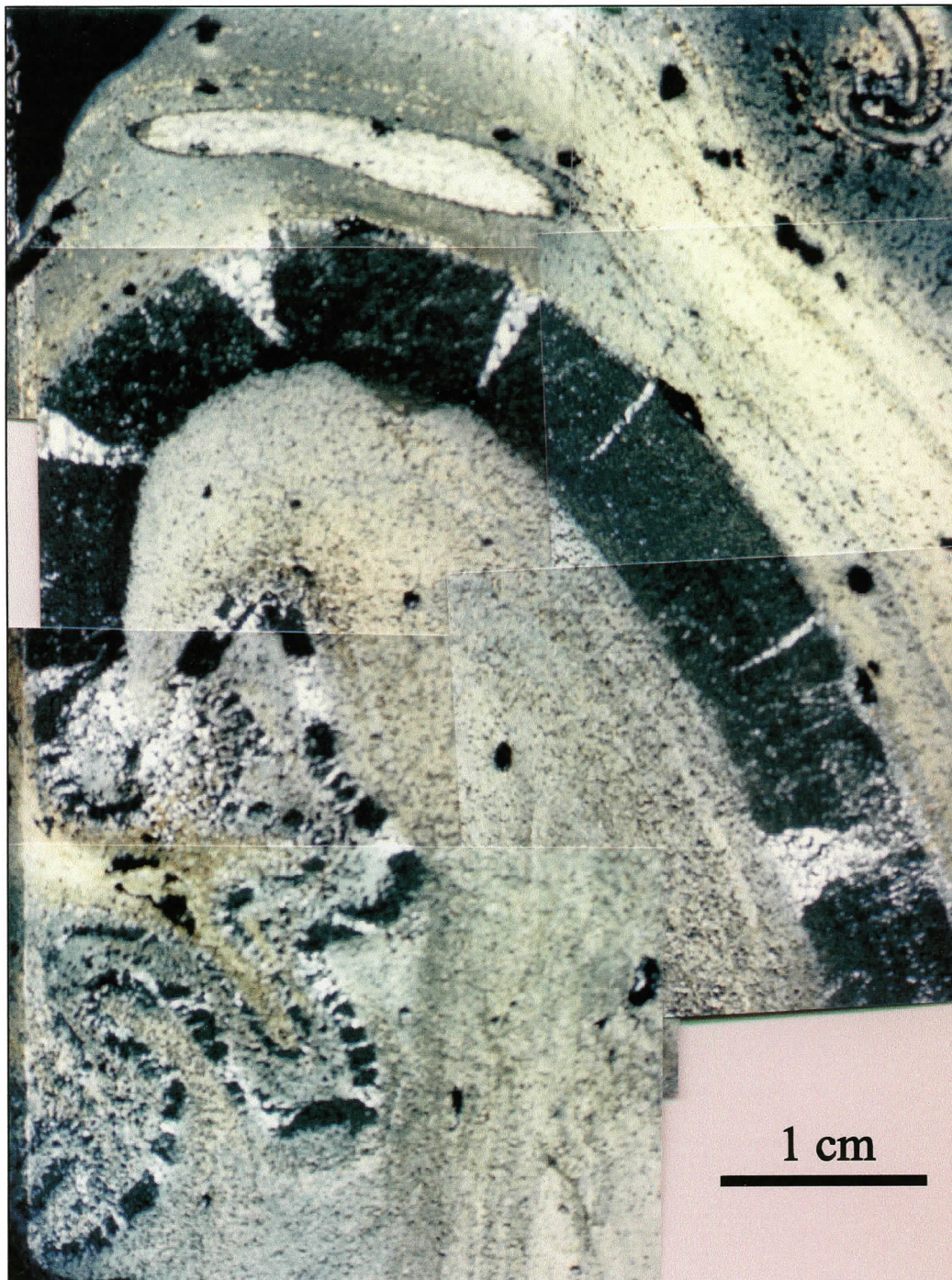


Figure 3.41. Photomicrographs showing a folded coticula layer of varying thickness. Well-developed outer-arc extension occurs as wedge-shaped fractures. These sedges taper almost to the inner-arc indicating that the neutral surface of the fold is very close to the inside edge of the layer. Horizontal to subhorizontal fractures are pervasive in the thin segment of the coticula layer. Note that the fractures do not necessarily occur perpendicular to the layer and do not occur in horizontal segments of the coticula layer. Extension in the thin segment represents 18% extension in the down-dip direction.

shows a decrease in shortening in the same direction but only over the interval from slab 5 to 6. Over the interval from slab 1 to 5 layer 'b' records similar values of shortening.

### **3.2.5.3 Extensional features**

Outer-arc extension is well developed in the coticule layer shown in the photomicrographs in Figure 3.41. The wedge shaped fractures taper from the edge of the outer arc to the inner arc indicating that the neutral surface is close to the inner-arc. The fractures occur along garnet grain boundaries and the infilled quartz is subhedral with moderately undulose extinction. In the thinned coticule layer to the left of the image numerous horizontal to subhorizontal fractures occur and quartz infills the boudin necks. This horizontal boudinage represents down-dip extension where all of the fractures are oriented approximately horizontal and therefore the boudinage is roughly vertical. Down-dip boudinage in the thin segment of the coticule layer represents 25% extension.

## **3.3 Minor fold comparison and discussion**

Similarities and differences in minor folds occur between each of the outcrop locations and will be compared in terms of fold style, bedding-cleavage relationships, and shortening. In general, the minor folds studied in the two regional fold hinge locations are similar, but quite different from those studied on the three limb locations. The principal similarities and differences in minor fold geometry between the hinge and limb are illustrated in Figure 3.43.

### **3.3.1 Fold styles**

*Fold shapes:* Minor fold shapes tend to be similar in both the hinge and limb with box folds, modified box folds and pygmatic folds occurring everywhere regardless of

structural location. The main difference in fold shape between the hinge and limb locations is in the tightness of the minor folds. Minor folds in the hinge tend to be tighter than on the limbs, reflected in the common occurrence of ptygmatic folds. Minor folds on the limbs tend to be more open, reflected in the common occurrence of open box folds, some without subsidiary folds developed in the median segment.

The fold shapes, especially box fold shapes, suggest that these folds were formed by buckling during layer-parallel shortening. Outer-arc extension of the minor folds indicates tangential longitudinal strain which occurs during buckling. The consistent relationship between layer thickness and fold wavelength also supports buckling during layer-parallel shortening.

*Cylindricity:* Minor folds in both the hinge and limb are similarly noncylindrical. Successive slabs from the hinge and limb display minor folds that vary in fold shape, symmetry, and shortening along the hinge and, in some cases, the variation is not systematic or consistent between adjacent layers. The noncylindrical nature of the minor folds is comparable to that of the regional folds. That is, at both scales, fold terminations are abrupt, fold amplitudes and wavelengths change along the hinge, and subsidiary folds occur in the median segments of the box folds. In one case of layers traced through four parallel slabs (Fig. 3.7) the rotation of the indicated median segment of a box fold in slab 1 onto a fold limb by slab 4 suggests variable hinge migration along the hinge. These observations indicate that hinge migration was active at the minor fold scale. Schematically, scenario d in Figure 1.8 shows a similar case where one hinge of a box fold is fixed and the other hinge migrates

toward the limb, fusing the median segment to the limb. Hinge migration along the hinge is expected in noncylindrical folds, which formed by lateral propagation.

*Symmetry:* Symmetry of minor folds is quite different between the hinge and limb of regional folds. Minor folds in the hinge, where bedding dips shallowly, are primarily symmetric. Locally however, parasitic fourth order folds on steep limbs of minor folds in the hinge display asymmetry, but their axial planes are invariably parallel to the regional axial plane (e.g. Figs. 3.3 and 3.5). Minor folds on regional fold limbs display a significant range in symmetry and, distinct differences are evident in the symmetry of the minor folds from locations  $L_2$  and  $L_3$ . At location  $L_3$  most of the minor folds are highly asymmetric (e.g. Figs. 3.35, 3.37, and A1.5 in Appendix 1) with their axial planes parallel, or closely parallel, to the regional axial plane. At location  $L_2$ , however, minor folds display the whole spectrum of asymmetry, from symmetric to mildly asymmetric (e.g. Fig. 3.24), to highly asymmetric (e.g. Fig. 3.27b). In general, the more asymmetry the fold displays, the closer the axial plane of that fold will be to the regional axial plane.

The variation in symmetry of minor folds between and within locations  $L_2$  and  $L_3$  is interpreted to reflect the amount of shear strain (flexural flow) accommodated by the rocks. Qualitatively, a simple deduction can be made that the more asymmetric a fold is, the more shear strain has been applied to the rock since the introduction of buckle folds. Comparing locations  $L_2$  and  $L_3$ , both have similar limb dips and therefore, both should display the same shear strain. However, the regularly asymmetric minor folds at  $L_3$  indicate more shear strain, whereas at  $L_2$  the variable symmetry of minor folds indicates variable shear strain, and



partitioning of shear strain between different intervals. The apparent partitioning may be a result of heterogeneous shear strain (compare Figs. 3.27b and 3.26).

### **3.3.2 Bedding-cleavage relationships**

Bedding-cleavage relationships in both the hinge and the limb of regional folds indicate that cleavage is axial planar to the minor folds regardless of the symmetry of the minor folds. Cleavage is locally deflected by the folded competent layers. Foliation-defining minerals are generally regionally axial planar in the hinge of regional folds and thick slate intervals on the limbs, whereas foliation adjacent to coticule layers is parallel to the axial plane of the minor folds. In the case of symmetric minor folds on regional folds limbs, the dip of cleavage can diverge up to  $90^{\circ}$  from the regional axial plane (Fig. 3.28).

That cleavage is axial planar to the minor folds suggests a relationship between formation of cleavage and minor folds. The axial planar relationship of cleavage to minor fold also supports heterogeneous shear strain at location  $L_2$ , where cleavage dips ranges from  $90^{\circ}$  to parallel to the regional axial plane.

At all locations foliation wraps around euhedral to subhedral spessartine grains and no inclusion trails are observed in the spessartine. All outer-arc fractures associated with buckle development occur along the spessartine grain boundaries. Spessartine growth must have occurred prior to the formation of cleavage and development of the buckle folds.

### **3.3.3 Shortening recorded by minor folds**

Shortening recorded by minor folds is the most significant data set for understanding the development of the minor folds with respect to regional fold development. Locations  $H_1$  and  $H_2$  record very similar values, around 50%, whereas the combined average of the folds

## Hinge and Limb Comparison

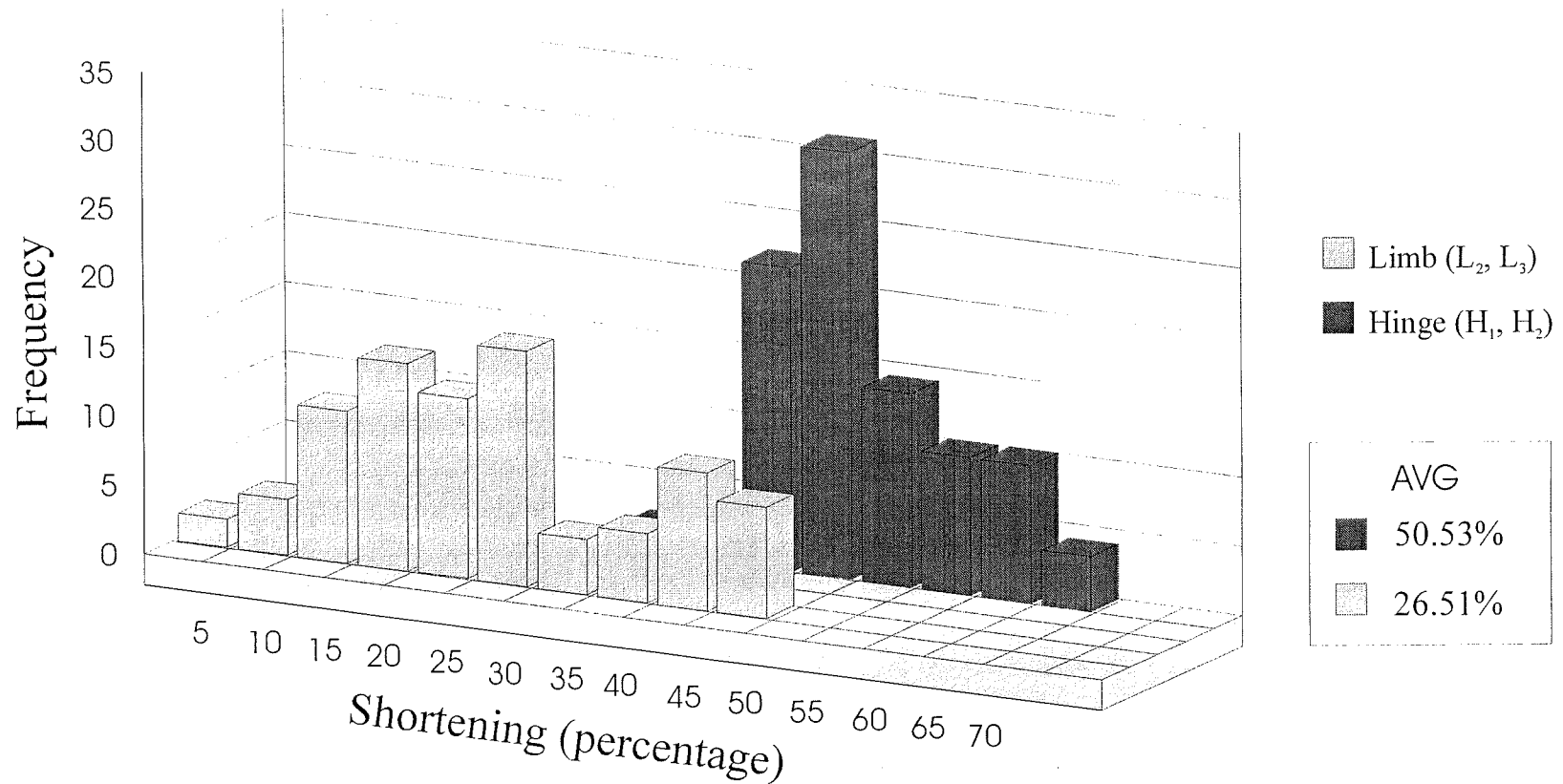


Figure 3.42. Histogram comparing the range of values of shortening from the regional fold hinge and limb. Data from the limbs include  $L_2$  and  $L_3$  and not the non-folded layers at  $L_1$ . There is a distinct difference between the two structural domains where the average value of the hinge is almost double that of the limb.

at locations  $L_2$  and  $L_3$  is almost half that amount at 27% (Fig. 3.42 and Table 3.2). This distinct difference in shortening values is supported by the differences in minor fold tightness, where ptygmatic minor folds characterize the hinges of regional folds and open to tight box folds characterize the folded layers on regional fold limbs.

Fold shapes suggest minor folds formed by layer-parallel shortening. The differences in shortening between the regional fold hinge and limb indicate that more layer-parallel shortening was applied to the layers in the hinge than on the limbs. Assuming similar strain rates throughout the study area, the layers in the hinge presumably spent more time parallel to the shortening direction than layers on the limbs.

Location	Range	Average	Standard Deviation	Data Points (N)
<b>Hinge</b>	34 – 68%	<b>50.53%</b>	7.67%	94
<b>Limb</b>	1 – 48%	<b>26.51%</b>	12.30%	89
$H_1$	34 – 68%	55.56%	9.70%	34
$H_2$	40 – 57%	47.73%	4.10%	60
$L_1$	<b>0%</b>	<b>0%</b>	N/A	N/A
$L_2$	8 – 41%	22.38%	8.83%	45
$L_3$	1-48%	30.93%	13.96%	44
$L_3$ (slabs)	28 – 48%	40.83%	7.0%	24
$L_3$ (field)	1 – 31%	17.72%	8.83%	20

Table 3.2. Comparison chart of shortening for each study location. The shortening recorded on the hinge is within a similar range, but significantly different from the shortening recorded at the locations on the limbs. The limbs show a wide range in shortening between locations.  $L_1$  records no shortening and  $L_2$  and  $L_3$  record shortening in ranges overlapping each other. The values recorded at  $L_3$  have been separated out to identify two distinct data populations based on data source (slabs or field photos).

Also important are the variations in shortening values at each location on the regional fold limbs (Table 3.2).  $L_1$ , for instance, records no shortening whereas the two other locations record substantial shortening. As mentioned earlier, the most representative values

of measured shortening at  $L_3$  were generated from field photographs, as opposed to the smaller area of slab photographs, and many planar and isolated folds were not measured. The average shortening from field photographs at  $L_3$  is around 18% whereas the average shortening at  $L_2$  is just over 22%. The outcrop location order of least to most shortening is therefore,  $L_1$ ,  $L_3$ , and  $L_2$ . Following the assumption of similar strain rates through the study area, the  $L_1$ ,  $L_3$ ,  $L_2$  sequence is also the order of least to most time spent in a favourable position for layer-parallel shortening. It should be emphasized that the folds at  $L_1$  represent no shortening and therefore, this segment of the limb was rotated early in the fold history prior to significant layer-parallel shortening.

The non-folded layers at  $L_1$  indicate that buckling did not occur until after initiation of regional folds. The interpretation that cleavage and minor folding are contemporaneous, based cleavage patterns around folded cotecule layers, suggests that cleavage did not form until after the initiation of regional folding.

## **Chapter 4: Discussion and Conclusions**

### **4.1 Introduction**

The minor fold data presented in this thesis require explanation in terms of regional fold development. It has long been recognized that the style and distribution of minor folds is related to regional fold development (i.e. parasitic folds; de Sitter, 1958; Ramsay and Huber, 1987). Traditionally, minor folds have been interpreted as developing by layer-parallel shortening prior to regional fold development where, during regional folding, they acquire an axial planar relationship with the regional folds. The minor fold data presented here suggest a different story for the Meguma Group where minor fold development occurred during progressive regional fold development.

This chapter evaluates previous work on minor fold development in light of the data presented here. A fold model for the study area is presented describing the fold evolution in the profile plane. The fold profile model is augmented by a description of the various possibilities of Meguma Group fold evolution in profile and in the plane parallel to the hinge.

### **4.2 Evaluation of previous work on minor folds**

This section reviews the previous work on minor folds for the Meguma Group with respect to the data presented here. The two principal and contrary theories that came out of previous work are described in section 2.2.3. The main differences between these two theories is in the predictions of where the minor folds occur on regional folds. One theory predicts the occurrence of minor folds everywhere (i.e. Henderson et al., 1986) and the other model predicts localization of minor folds in hinges of regional folds (i.e. Williams and Hy,

1990). Neither model sufficiently explains the data presented here.

#### **4.2.1 Pre-regional fold buckling theory**

The pre-regional fold buckling theory that buckling pre-dated regional folding suggests that minor folds and cleavage developed during homogenous layer-parallel shortening prior to regional folding (Henderson et al., 1986; Graves and Zentilli, 1982). In this theory, regional folds developed by flexural folding with no continued layer-parallel shortening and therefore, strain recorded everywhere is the same. This proposed sequence of folding cannot account for the variation in shortening between the regional fold hinge and limb reported here and, more importantly, it cannot account for a fold limb with non-folded cotecule layers.

#### **4.2.2 Syn-regional fold buckling theory**

Williams and Hy (1990) and Mawer (1987) report that minor folds in bedding-parallel quartz veins only occur in regional fold hinges, suggesting that they were formed by layer-parallel shortening during regional fold development. This theory predicts that bedding-parallel quartz veins on regional fold limbs will be non-folded. This theory does not account for the occurrence of folded quartz veins and cotecule layers on regional fold limbs.

#### **4.3 Fold model for central the Meguma fold belt**

The discussion of minor folds and other fold-related structures above (section 3.3) suggests a complex strain history. Without further constraints on the relative age of many of the features discussed it is difficult to completely understand the strain history of these rocks. However, several important points from the above discussion must be accounted for,

and therefore provide the basis for a possible sequence of fold development. These points include: (1) regional fold style in the Meguma Group and study area is mainly box fold and chevron; (2) spessartine in the coticule layers was formed prior to minor folds and cleavage development indicating that the coticules were stiff layers prior to folding. The competency contrast ratios determined by the *Biot-Ramberg* equation also support stiff layer deformation; (3) minor fold shapes suggest formation during layer-parallel shortening; (4) non-folded coticule layers on a regional fold limb suggests that buckling occurred after regional fold initiation; (5) bedding-cleavage relationships indicate that minor folds and cleavage formed contemporaneously; (6) the noncylindrical nature of minor folds indicate that development of minor folds occurred by migration of the hinge in the fold profile and propagation parallel to the hinge; (7) variation in shortening values between the regional fold hinge and limb.

#### **4.3.1 Fold model (profile plane)**

Figure 4.1 presents a possible sequence of fold development for the central Meguma fold belt based on the above constraints. The following is a discussion of the model.

##### **Stage A (Fig. 4.1):**

The earliest stage of folding consisted of the development of regional-scale conjugate kink bands and, therefore, box folds, during initial bulk shortening. This early formation of regional folds is consistent with a box fold environment where no to little layer-parallel shortening occurs prior to folding. This early development of regional box folds resulted in the early rotation of some segments onto limbs prior to layer-parallel shortening, where some coticule layers may not be folded (i.e.  $L_1$ ). Initiation of minor fold development may have occurred in flat segments of box folds, by layer-parallel shortening (i.e.  $L_2$ ,  $L_3$ ,  $H_1$ , and  $H_2$ ).

Cleavage development accompanied minor fold development, forming an axial planar relationship with the minor folds. Foliation-defining minerals wrap around spessartine indicating that spessartine was already formed.

**Stage B (Fig. 4.1):**

Continued shortening resulted in limb steepening, limb lengthening, and layer-parallel shortening in the median segment of the box folds. Rotation of the fold segments from the hinge to the limb was accomplished by hinge migration. Fold segments which rotated from a flat segment to a limb may record moderate shortening. Shortening is essentially turned off as the segment is rotated to steep limb dips (e.g.  $L_3$ ). Minor folds and cleavage on limbs were sheared by flexural-flow, acquiring a regional fold axial plane relationship (e.g.  $L_3$ ). Buckling of cotecule layers continued in flat segments (e.g.  $L_2$ ,  $H_1$ , and  $H_2$ ).

**Stage C (Fig. 4.1):**

Continued bulk shortening resulted in further limb lengthening, fold tightening, and buckling of cotecule layers by layer-parallel shortening in the median segments of box folds. Regional fold tightening and limb lengthening was accomplished by hinge migration where median segments, in part or whole, were rotated to the limb, probably at varying intervals during fold development. The more shortening recorded by minor folds on a regional fold limb may indicate that the segment spent a greater time in a regional hinge than another limb segments recording less shortening (e.g. comparing  $L_2$  and  $L_3$  where  $L_3$  is interpreted to have rotated to a limb prior to  $L_2$ ). Heterogeneous shear strain resulted in variable symmetry of folds and divergence of cleavage from the regional cleavage trend (e.g.  $L_2$ ). Regional fold



hinge zones remain in a favourable position for layer-parallel shortening where continued buckling results in the maximum values of shortening (e.g.  $H_1$  and  $H_2$ ).

**Stage D (Fig. 4.1):**

Stage D represents the present-day cross-section across the study area. The final stage of folding consisted of fold tightening, where minor folds in regional fold hinges continued to develop (e.g.  $H_1$  and  $H_2$ ). Final fold tightening may have also resulted in heterogeneous shear strain accommodated by a combination of flexural-flow and flexural-slip (i.e. the scalloped-shaped crenulation at  $L_2$ ). Overall, the magnitude of shortening values of folded coticule layers on regional fold limbs provide an estimate of the relative time a particular fold segment spent parallel to bulk shortening, assuming similar strain rates everywhere.

According to the previous theories of Meguma Group fold development minor folds were developed by layer-parallel shortening, and this study suggests the same. The difference between the other theories is in the relative timing of layer-parallel shortening. Here, it is suggested that layer-parallel shortening was active after the initiation of regional-scale box folds, in their median segments. Because of the scale of the box folds it may be difficult to distinguish between buckle folds developed in a median segment of a box fold and buckle folds developed in a flat-lying sequences of rocks prior to regional folding.

Based on the non-folded coticule layers (i.e.  $L_1$ ) on a regional fold limb, this study demonstrates that significant layer-parallel shortening was not active prior to regional folding. Therefore, minor folds occurring on regional fold limbs were most likely formed in a median segment of a box fold then rotated to a limb by hinge migration. In addition, the

range in values of shortening recorded by minor folds indicates that strain is variable across a fold and not homogeneous as predicted by pre-regional fold buckling. The variation in shortening magnitudes can be explained in terms of residency time (assuming similar strain rates everywhere) in a position favourable for layer-parallel shortening such as a hinge. In other words, less shortening recorded by a package of layers indicates that they were rotated from a hinge to a limb early in the fold history. The difference in shortening values between  $L_2$  and  $L_3$  is why they are interpreted to have rotated to limbs at different intervals (Fig. 4.1).

The analysis of Horne (1998) provides for the structural evolution of the Ovens Anticline in southern Nova Scotia is relevant to this study. He documented minor folds developed in metasandstone layers in thrust sheets. These thrust sheets are interpreted to have originated from a median segment of a box fold synclinorium. Similar interbedded metasandstone and slate sequences occur on the limbs of the Ovens Anticline, a chevron fold, but are not folded. This difference in minor fold distribution (folds in hinges and not on limbs) was interpreted as reflecting layer-parallel shortening in hinges syn-regional folding (Horne, 1998). The Ovens Anticline may represent a fixed hinge (i.e. no hinge migration) condition where the anticline, at its current level of exposure, was always an anticline and did not evolve from a box fold through the fold history. Overall, the evolution of the Meguma folds may have been affected by hinge migration in some cases (e.g. central Meguma) and hinge fixing in others (e.g. the Ovens).

#### **4.3.2 Fold evolution in plan view**

Hinge migration is an integral fold mechanism in the development of the regional and minor scale folds in the study area. It has been shown that hinge migration occurs by the

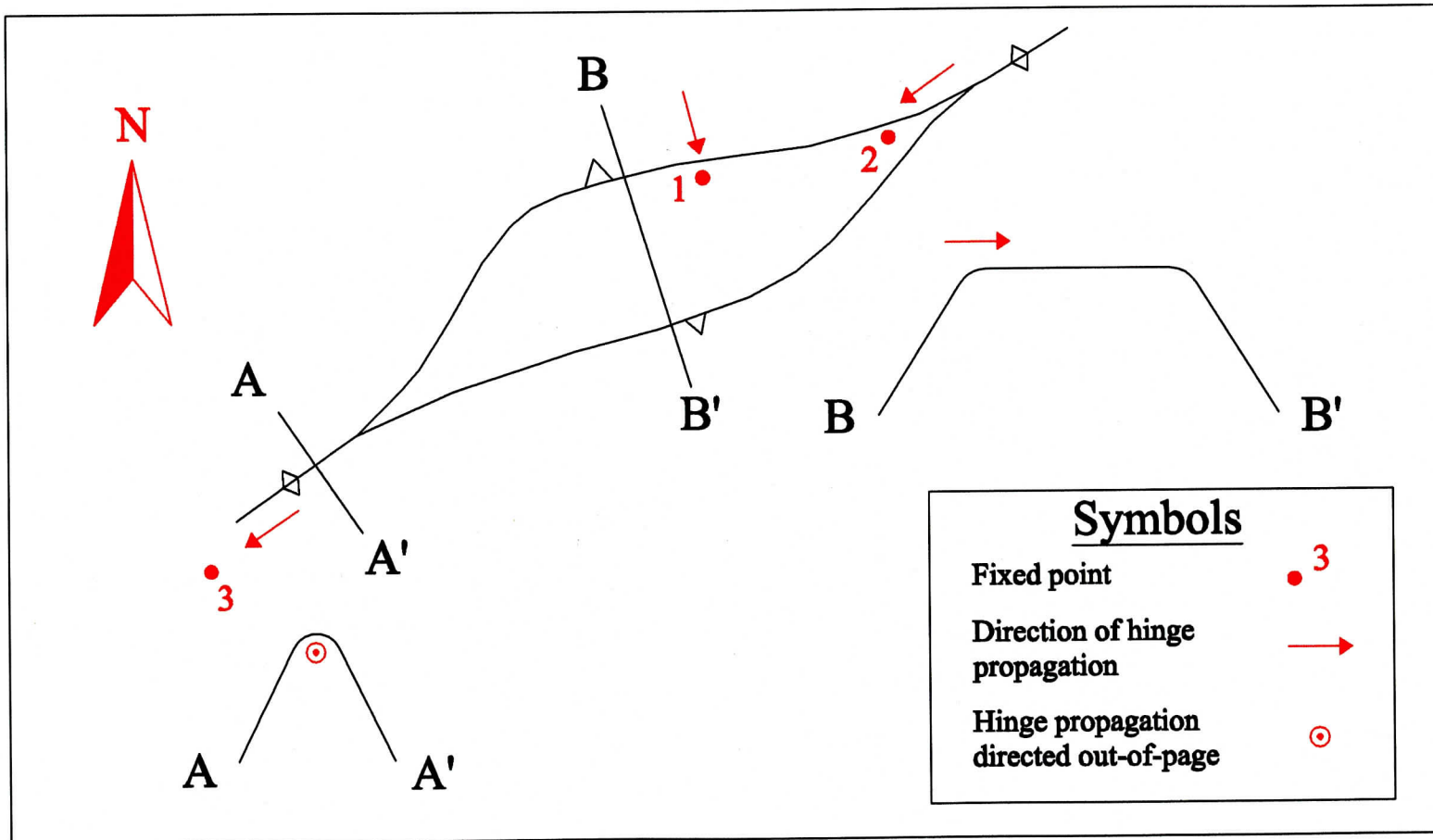


Figure 4.2. Plan view schematic of the possible processes of fold development. Propagation of the hinge occurs perpendicular (i.e. evident in the profile plane) and parallel to the hinge. A scale is intentionally omitted as folds of all scales develop in this manner. See text for discussion.

propagation of the hinge parallel to the hinge and in the profile plane. Figure 4.2 summarizes the various ways a fixed point in a flat segment of a fold is rotated to a fold limb by propagation of the hinge during fold development. Intentionally, no scale is identified on the schematic because these processes occur at the minor- and regional-fold scale. Point 1 on Figure 4.2 rotates from the median segment of the box fold to the limb as the hinge migrates perpendicular to the hinge line (i.e. in the profile plane) as the box fold tightens across B - B'. The red arrows indicate direction of hinge migration. Point 2 can move from the median segment of the box fold to the limb of a chevron fold when the box fold hinges fuse together by the southwestward migration of the chevron hinge parallel to the hinge line. Point 3 is in initially unfolded rocks, but as the chevron fold propagates southwestward, parallel to the hinge, point 3 is rotated to the limb of the fold.

#### **4.4 Conclusions**

This study has addressed the relationship of minor folds developed in coticule layers and regional folds in the central Meguma fold belt with respect to the style of regional fold evolution. In summary, identification of minor fold style, including shape, symmetry, and noncylindricity; bedding-cleavage relationships; and shortening recorded by minor folds led to a discussion of the importance of hinge migration (perpendicular and parallel to the hinge line) in the development of the folds at all scales. The following is a list of conclusions arrived at from the results of this study.

- 1) The garnet in coticule layers grew prior to cleavage and minor fold development.
- 2) Minor folds were formed by layer-parallel shortening in the flat segments of regional folds after the initiation of regional box and chevron folds.

3) Fold propagation at all scales occurred in the profile plane and parallel to the hinge line by hinge migration resulting in the variation of shortening recorded by minor folds.

These conclusions reflect a complex fold history previously unrecognized in the Meguma fold belt. It has long been understood that shortening of anisotropic rock sequences such as the turbidites of Meguma Group is accommodated by chevron- and box- style fold development (Price and Cosgrove, 1990; Ramsay and Huber, 1987; Fowler and Winsor, 1996). Theoretically, these folds are understood to develop by hinge migration (Dubey and Cobbold, 1977; Biot, 1965; Fowler and Winsor, 1996), but little field evidence has been documented in support of the theory. This study documents numerous examples suggesting that hinge migration must have been an important process in the development of the folds.

#### **4.5 Recommended further work**

This study has provided new data and new interpretations for the fold development for the central Meguma fold belt with implications for the entire Meguma fold belt. However, many questions outside of the scope of this study have arisen and require further work. The recommendation most related to this study is to document minor folds in the cotecule layers and related structures across the entire fold belt. Although implications can be posed for the entire fold belt the fold model developed in this study is particular to the study area and features in other areas may suggest a different fold development. It would also be interesting to document whether there are variations in shortening between regions of the fold belt which may indicate localization of strain in one area over another.

Another problem arising from this study relates to the apparent heterogeneous shear

strain on fold limbs. The variation in symmetry of minor folds on regional fold limbs indicates that shear strain is not simply accommodated by flexural-flow, but that there is a more complex fold history still yet to be resolved. Perhaps flexural-flow and flexural-slip were active at the same time. At L<sub>2</sub> (Highway #1 Pit) scalloped-shape crenulation cleavage was found along bedding planes and may represent discrete slip planes developed during flexural slip. A detailed study of crenulation cleavage including absolute dating is required in order to fully understand the development of the crenulation cleavage.

The timing of cleavage development is also a problem that requires more work and may be related to the heterogeneous shear strain problem. In this study, cleavage was found to have a genetic relationship with minor folds and minor folds are interpreted to have formed syn-regional folding, therefore cleavage must also have formed syn-regional folding. However, more documentation of cleavage is required to conclude the timing of formation for certain. Documentation of cleavage across a box fold in the profile and along the hinge may shed more light on this problem.

The last recommendation for further work is related to the extension documented in this study. Wright and Henderson (1992) suggest that cleavage formation was accompanied by significant volume loss (up to 60%) based on the lack of evidence for fold-related extension. The extension documented in this study is most likely fold-related (cleavage-parallel) and may account for some of the missing volume interpreted by Wright and Henderson (1992) as volume loss. However, further documentation of the magnitude and orientation of extension is required in order to conclude whether the boudinage documented here is fold-related extension. Intergrowths of moderate- to well-developed muscovite in the quartz of the boudin necks may lend themselves to <sup>40</sup>Ar/<sup>39</sup>Ar dating.

## Appendix 1:

## Photographs and sketches of slabs

Hand samples from selective locations were cut into 4-cm thick successive slabs. Photographs of the slabs were scanned and the cuticle layers were digitized in AutoCAD R14<sup>®</sup>. Both edges of each cuticle layer were digitized and the distance between endpoints ( $l$ ) and length of the line ( $l_0$ ) were measured. These values were used to calculate extension values for each line using the equation  $e = (l - l_0)/l_0$ . Negative values of  $e$  represent the percentage of shortening. The average of the two lines for each layer is representative of the shortening of that layer and is listed on each figure.

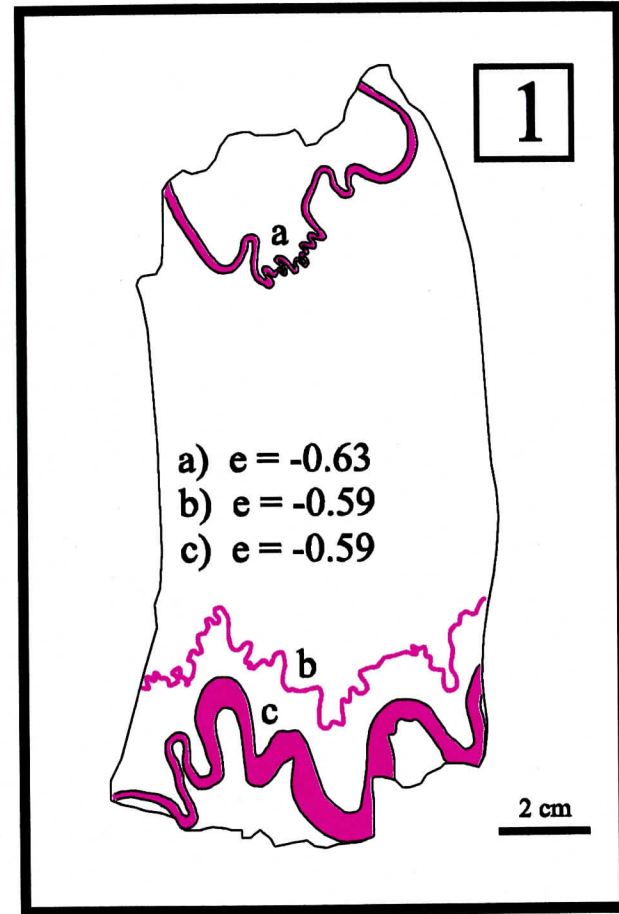


Figure A1.1. Photographs and sketches of four successive 4-cm thick slabs cut perpendicular to the hinge. Slabs are from  $H_1$  (Holland Road).



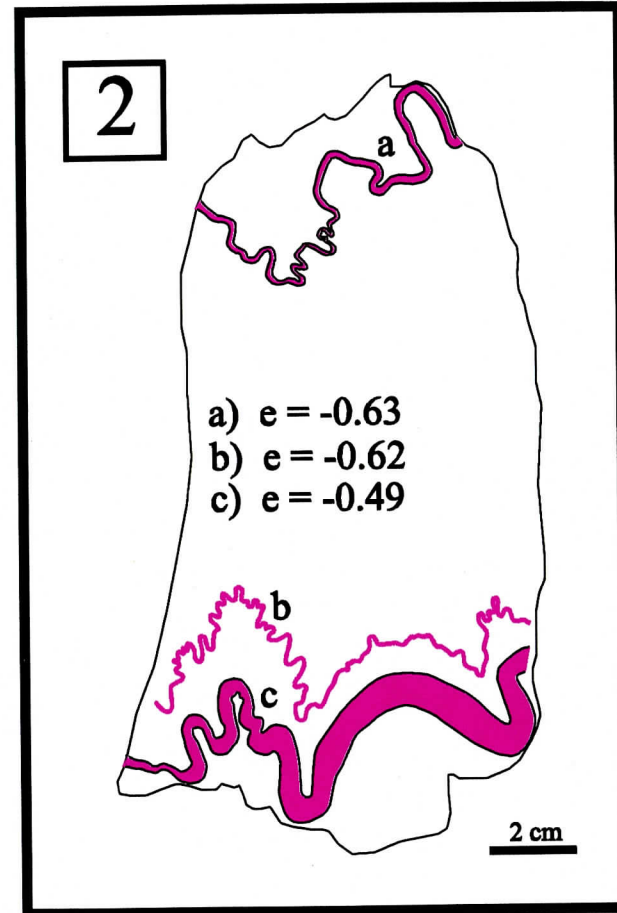


Figure A1.1 continued.

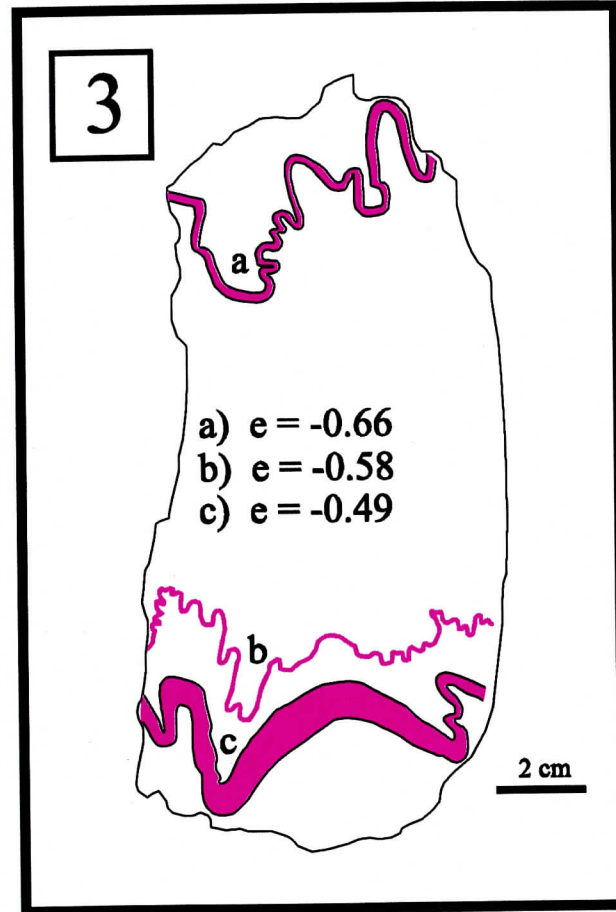


Figure A1.1 continued.

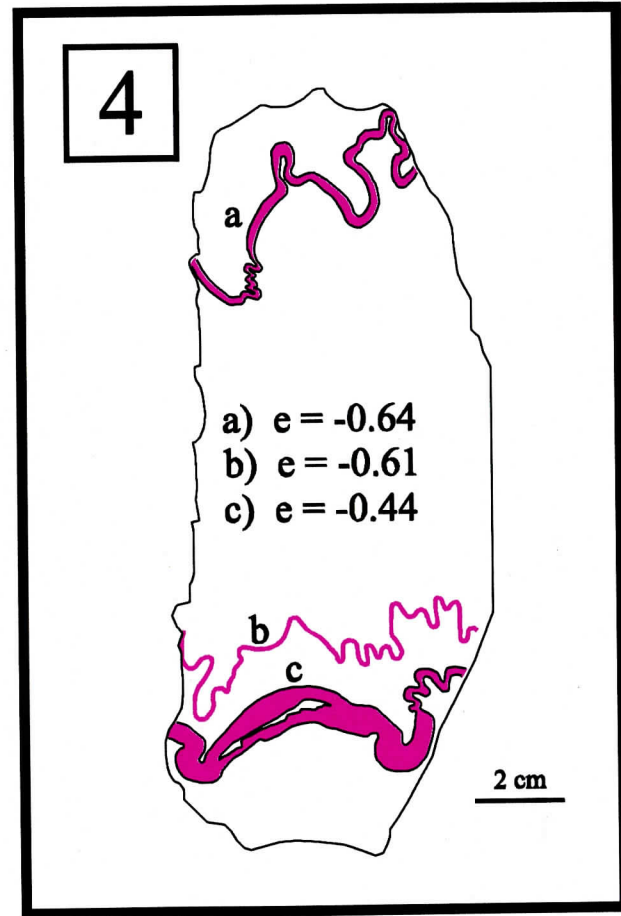


Figure A1.1 continued.

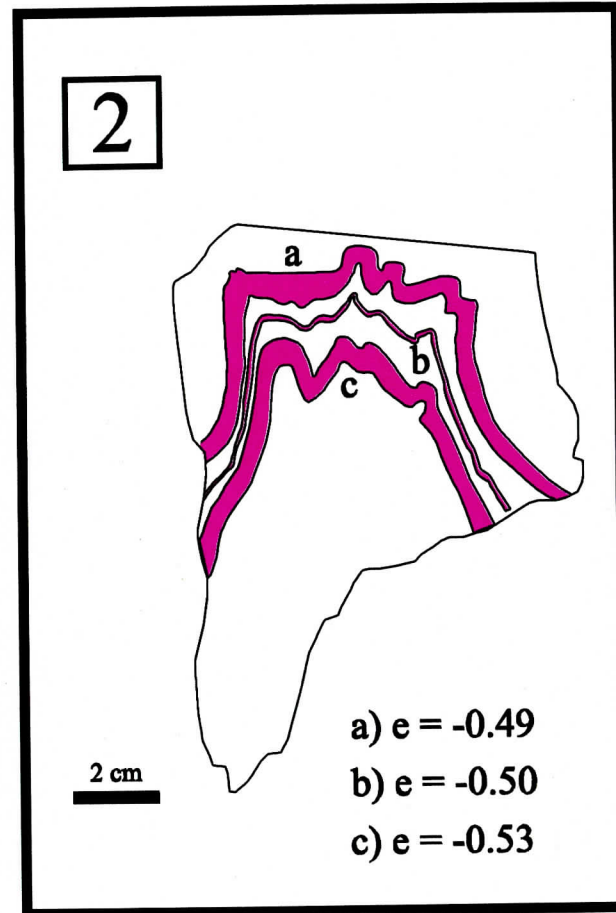


Figure A1.2. Photographs and sketches of four successive 4-cm thick slabs cut perpendicular to the hinge. Slabs are from H<sub>2</sub> (Bennery Lake).

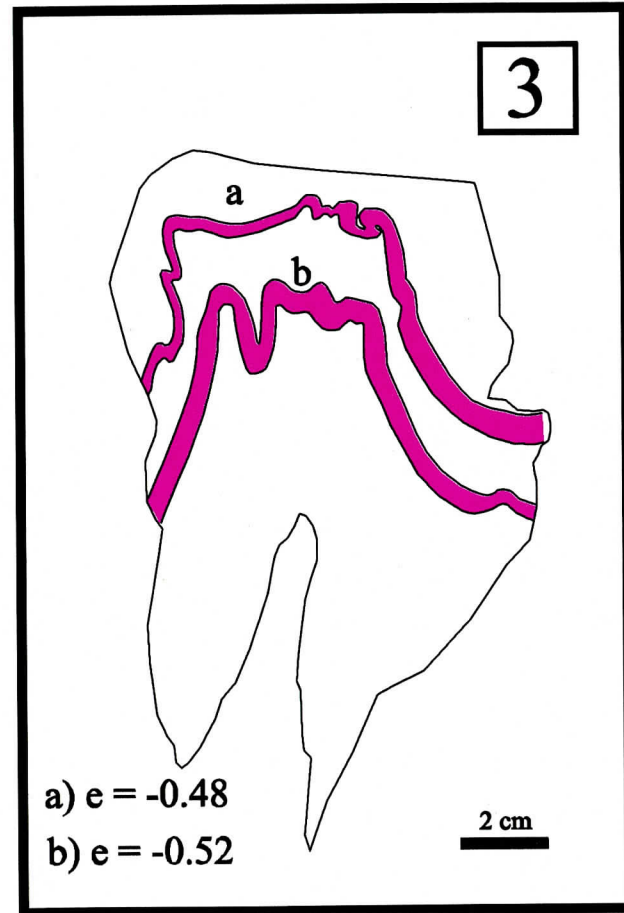
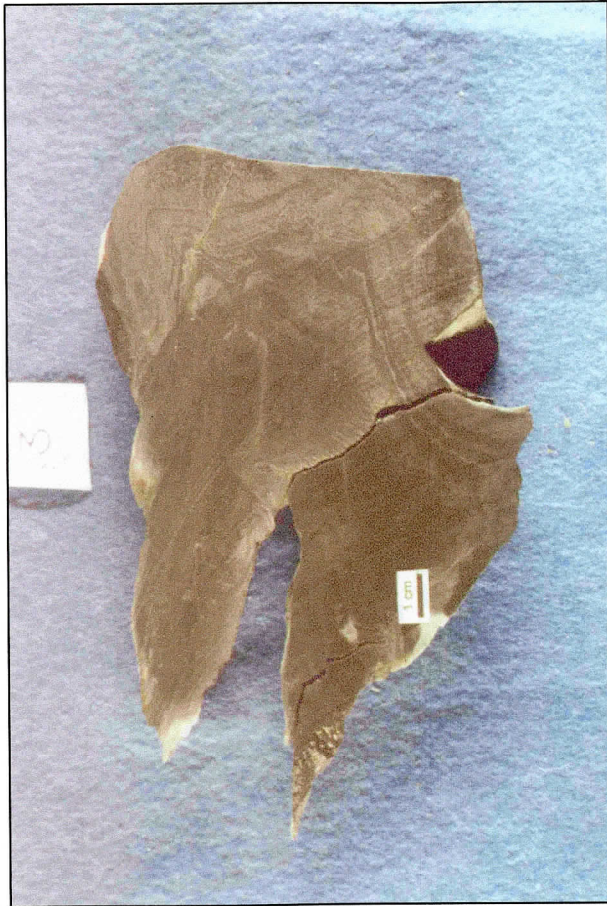


Figure A1.2 continued.

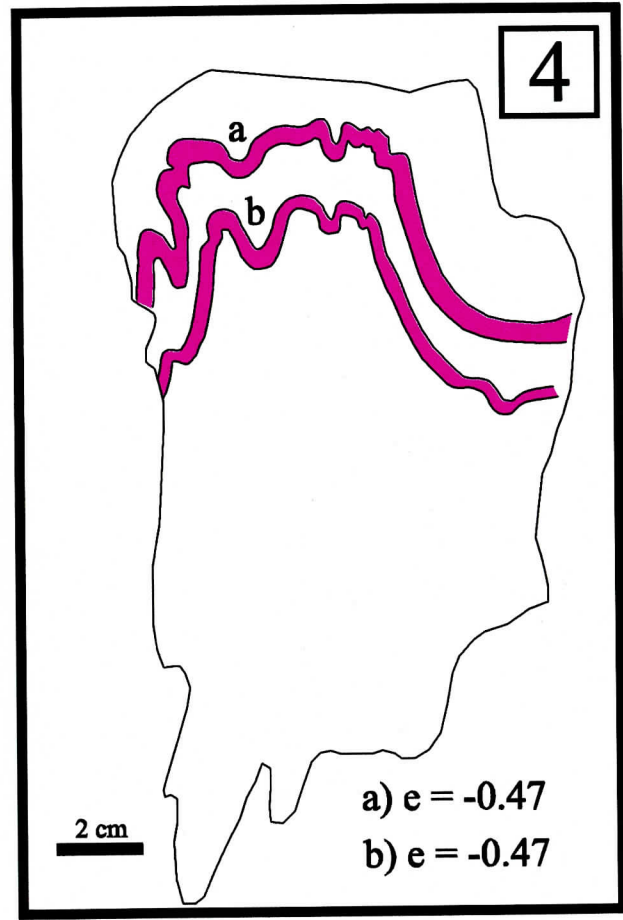


Figure A1.2 continued.

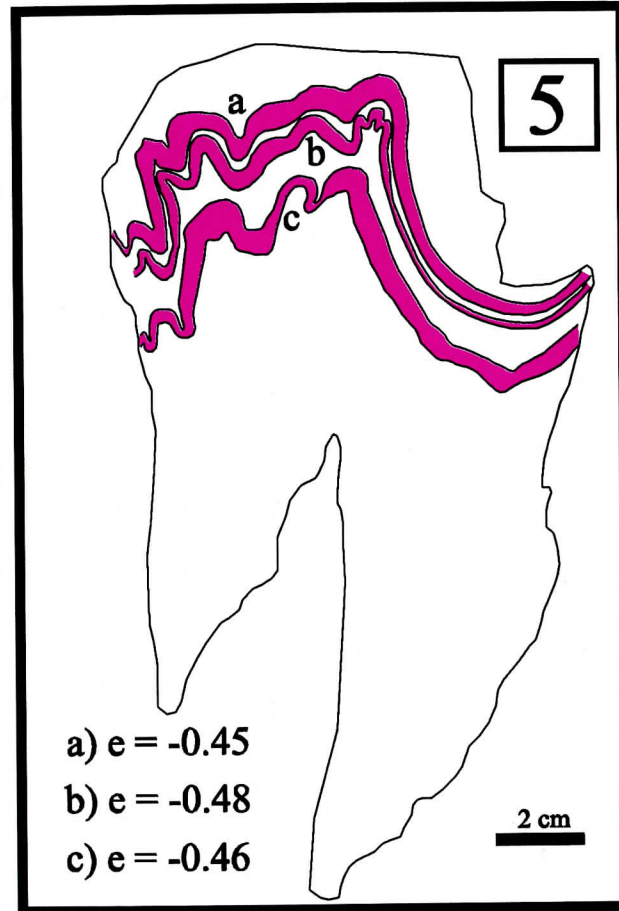


Figure A1.2 continued.

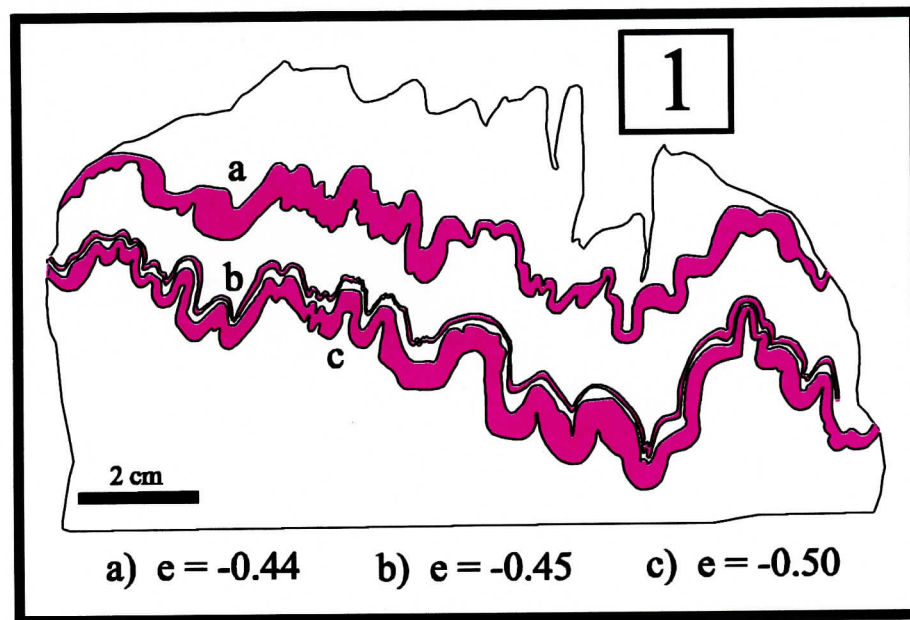
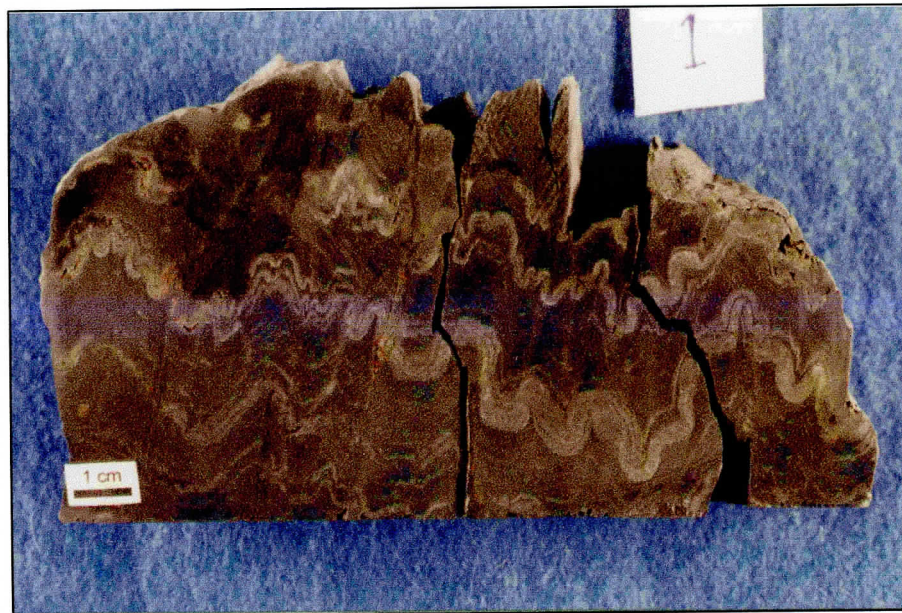


Figure A1.3. Photographs and sketches of five successive 4-cm thick slabs cut perpendicular to the hinge. Slabs are from H<sub>2</sub> (Bennery Lake).



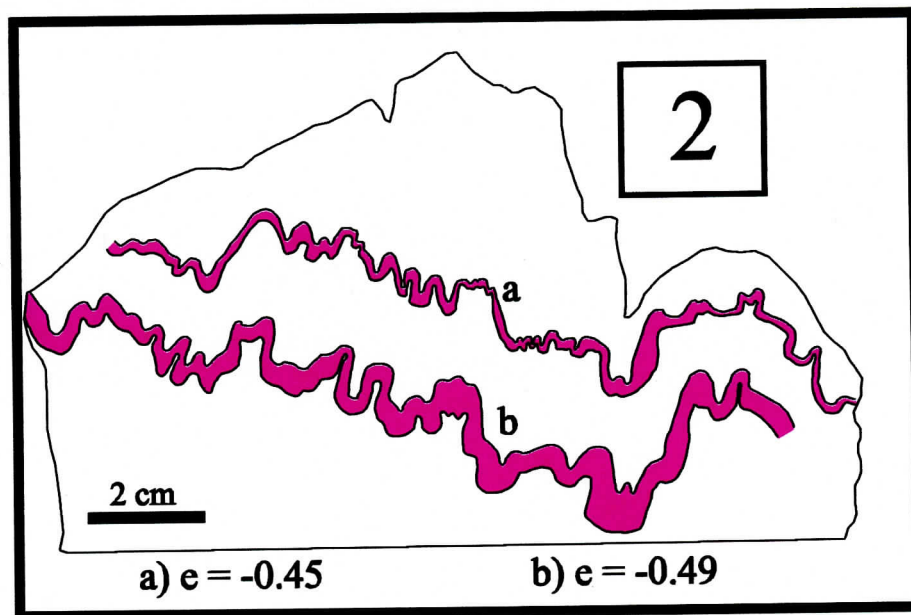


Figure A1.3 continued.

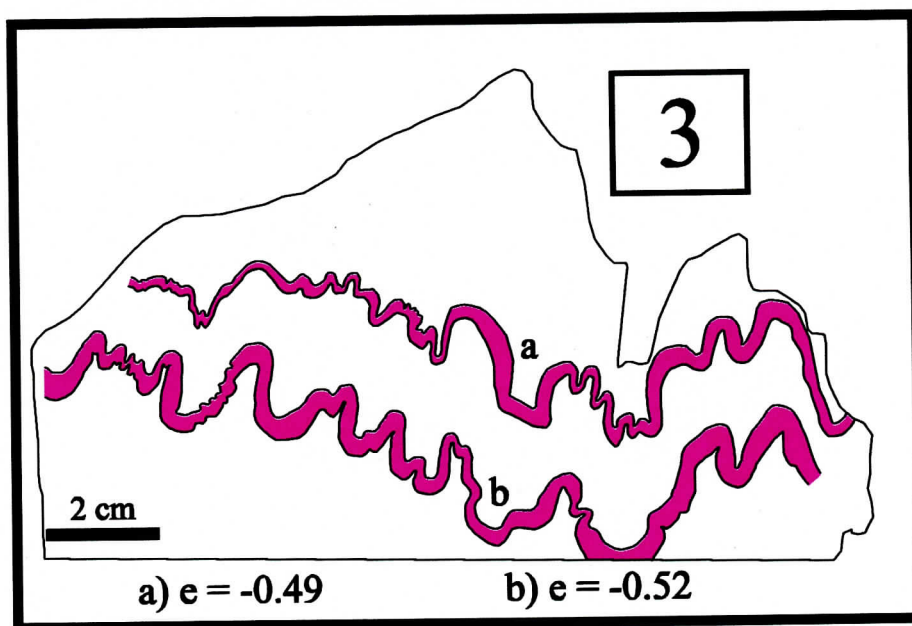
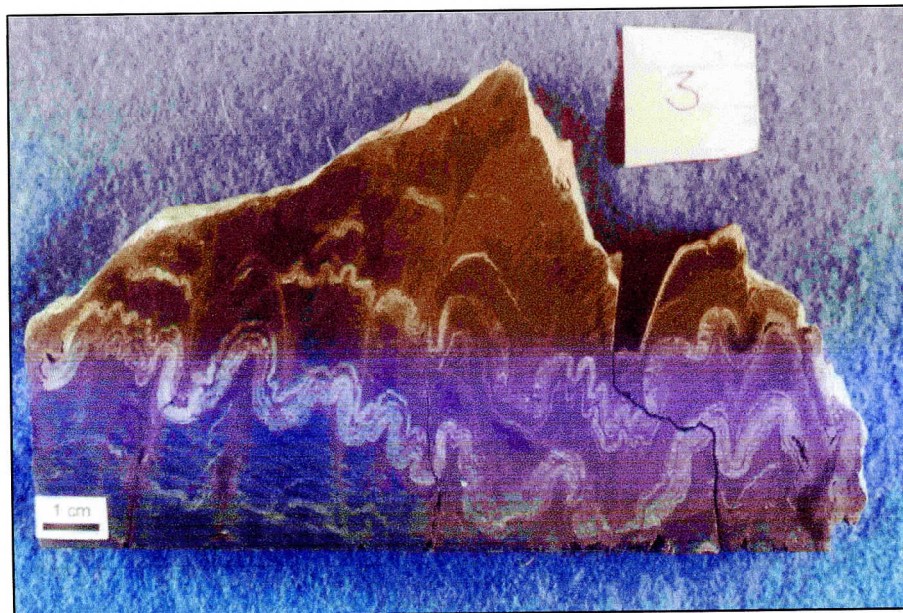


Figure A1.3 continued.

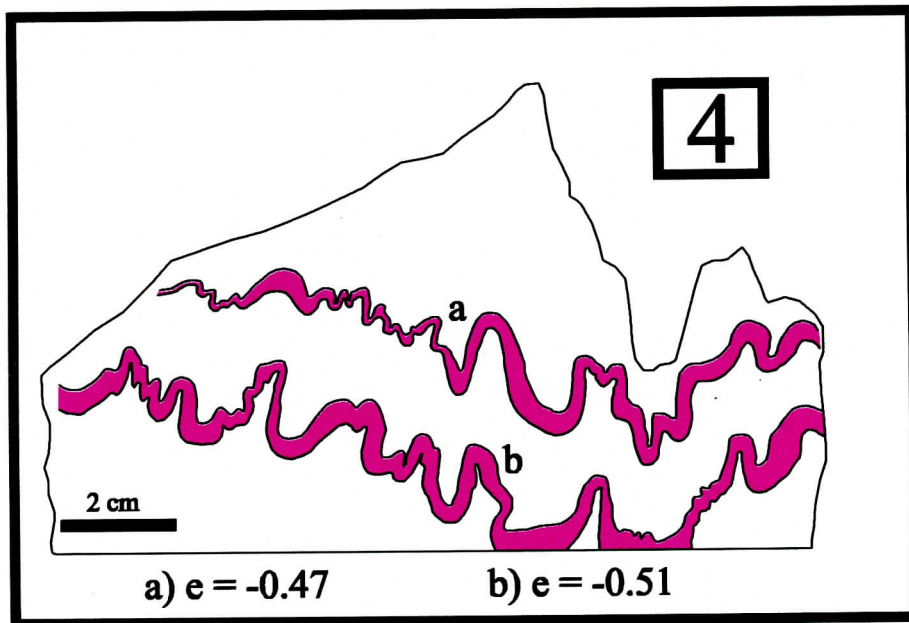
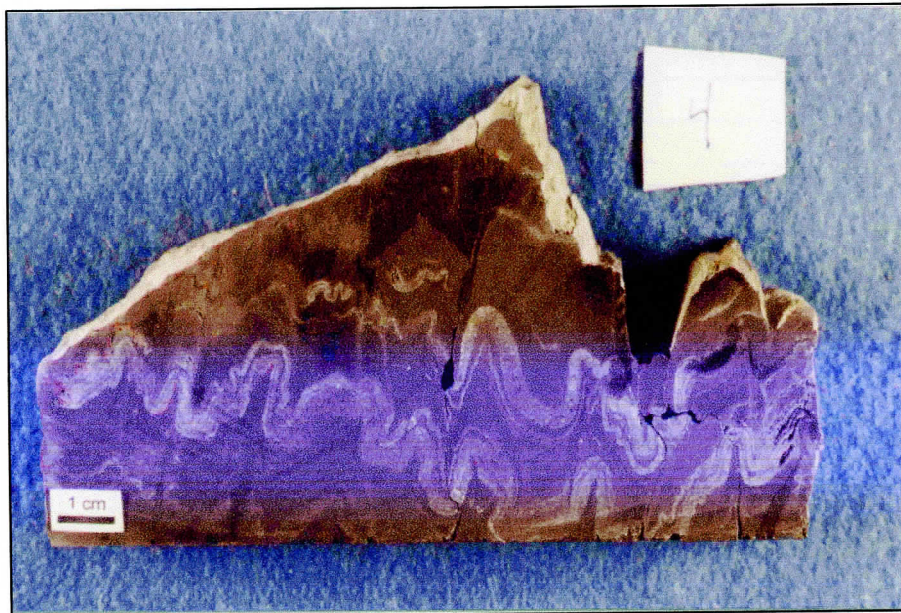


Figure A1.3 continued.

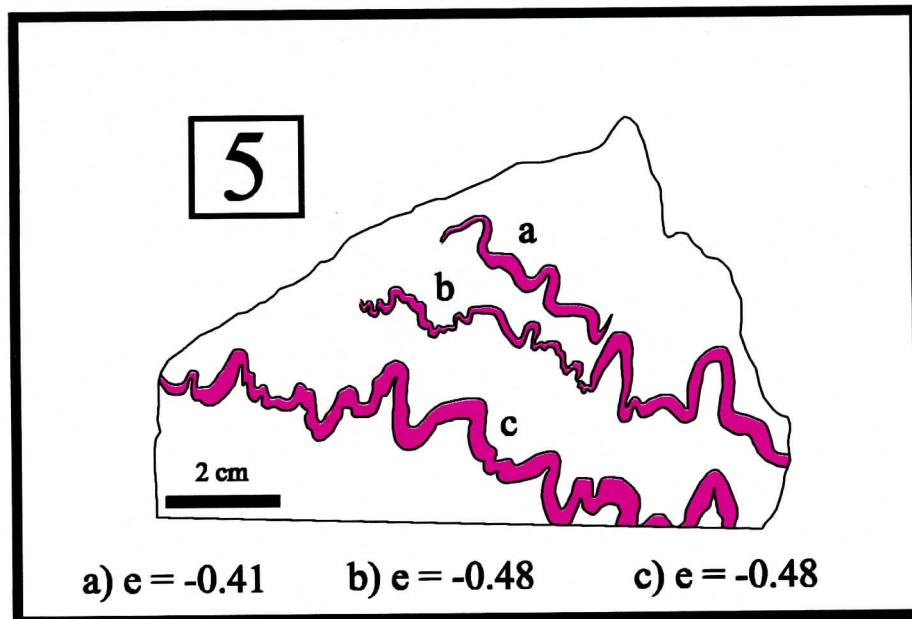
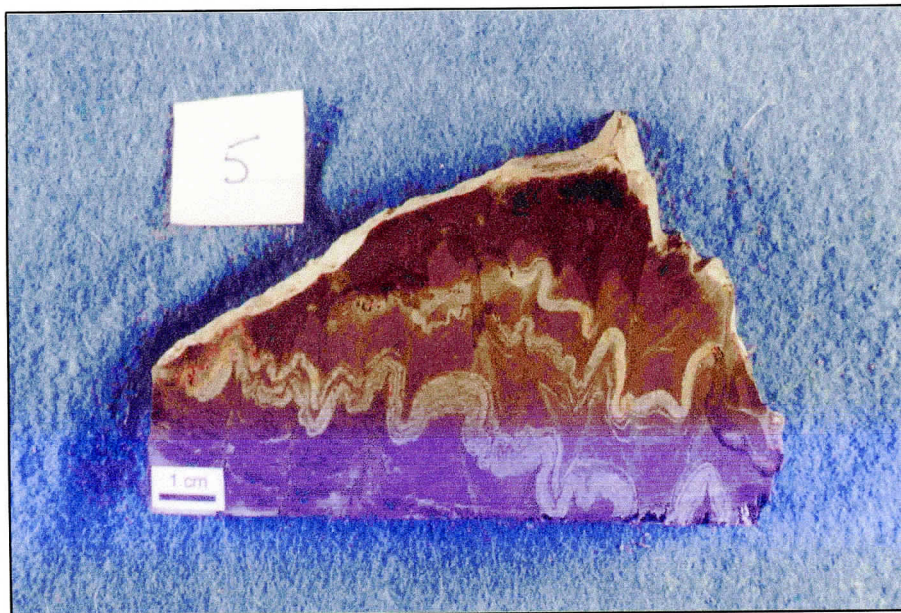


Figure A1.3 continued.



Figure A1.4. Photographs and sketches of three successive 4-cm thick slabs cut perpendicular to the hinge. Slabs are from H<sub>2</sub> (Bennery Lake).

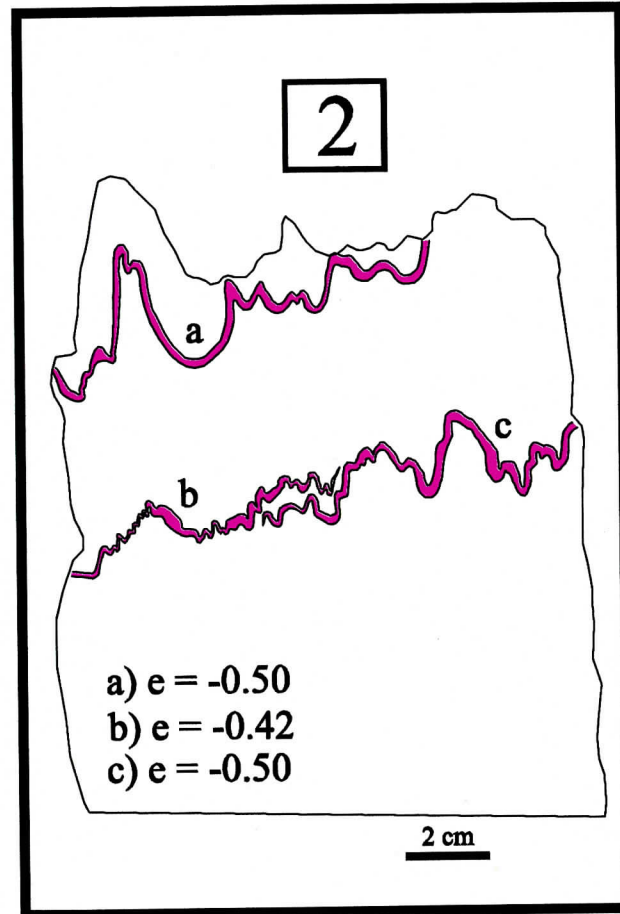


Figure A1.4 continued.

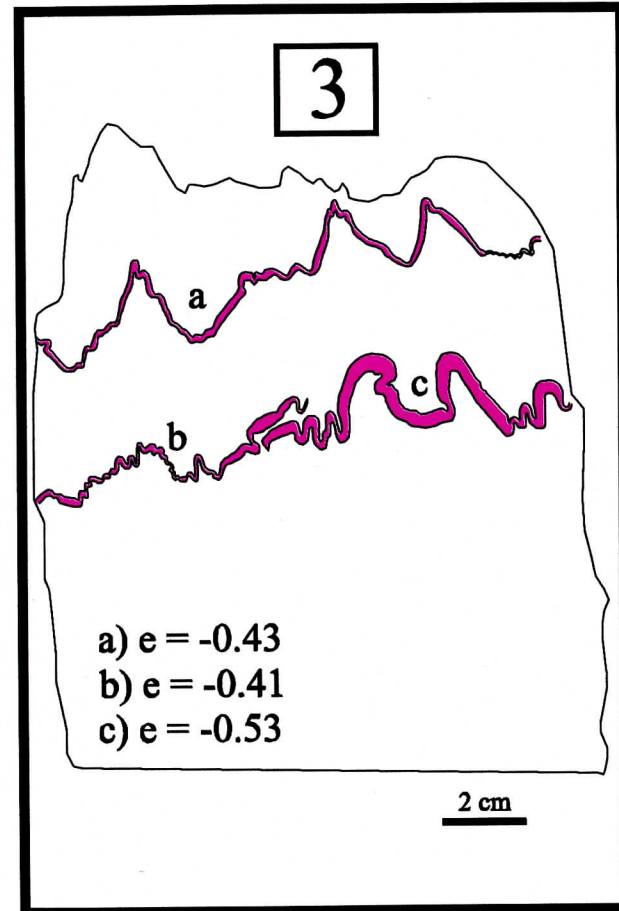


Figure A1.4 continued.

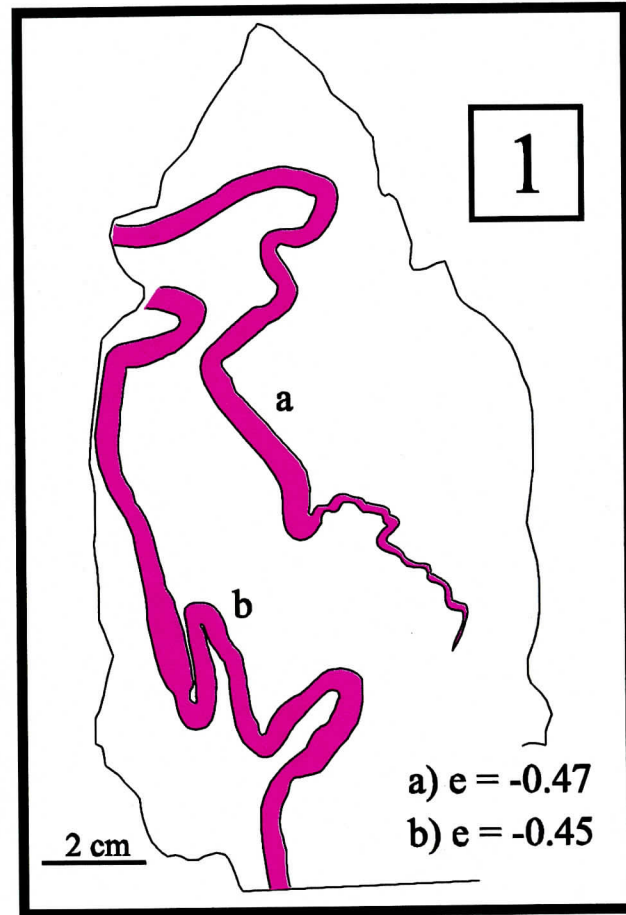


Figure A1.5. Photographs and sketches of six successive 4-cm thick slabs cut perpendicular to the hinge. Slabs are from  $L_3$  (Beaverbank Road).



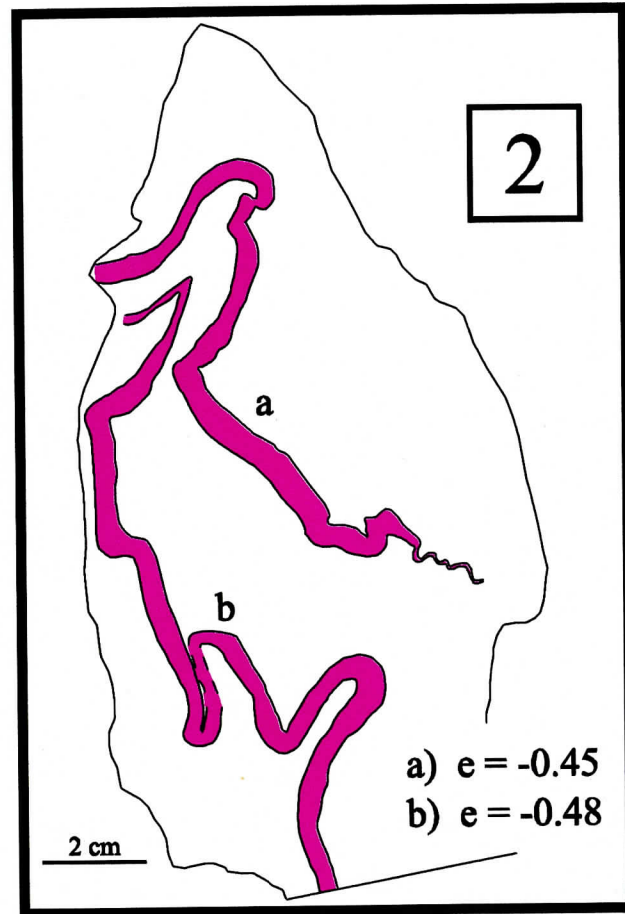


Figure A1.5 continued.

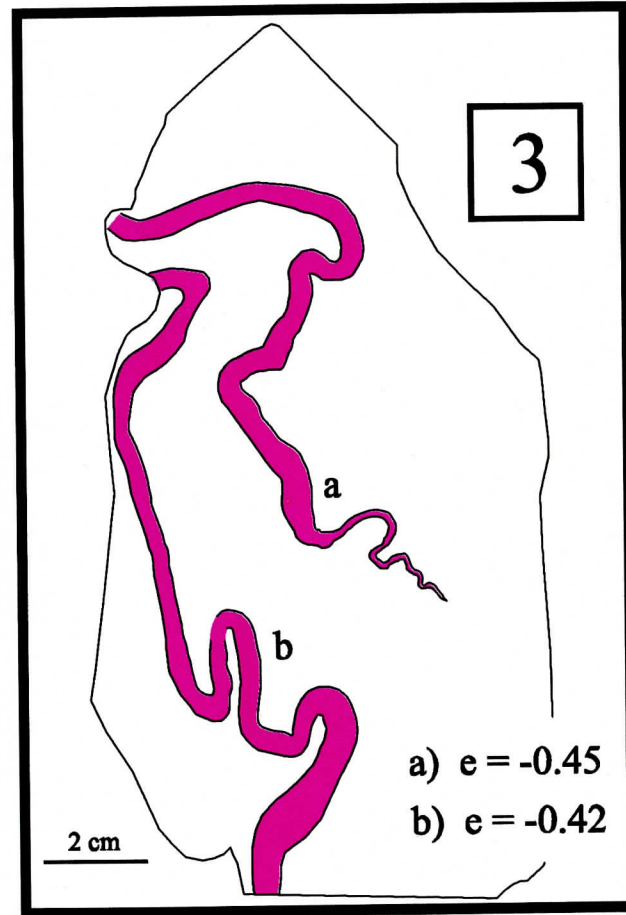


Figure A1.5 continued.

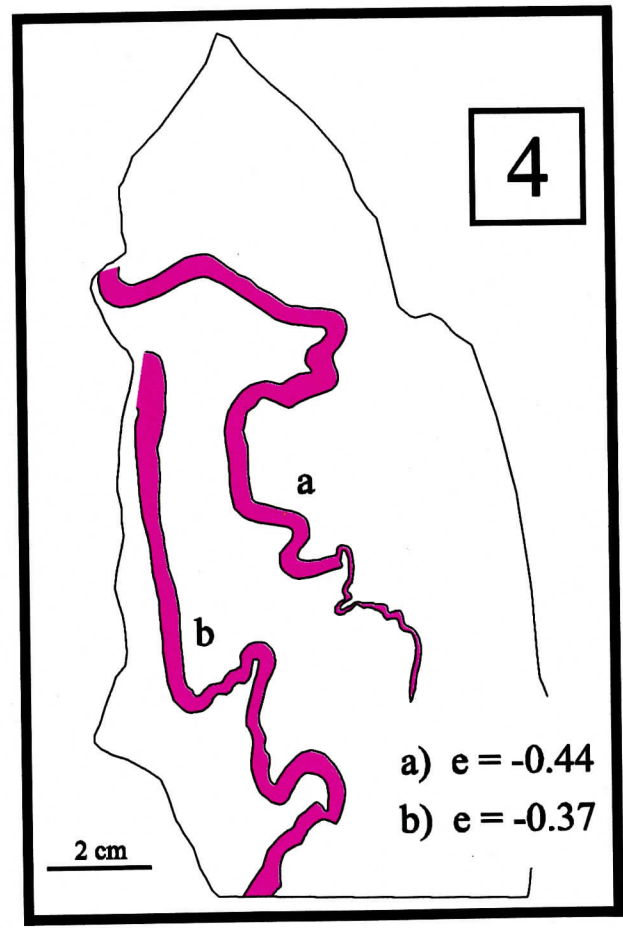


Figure A1.5 continued.

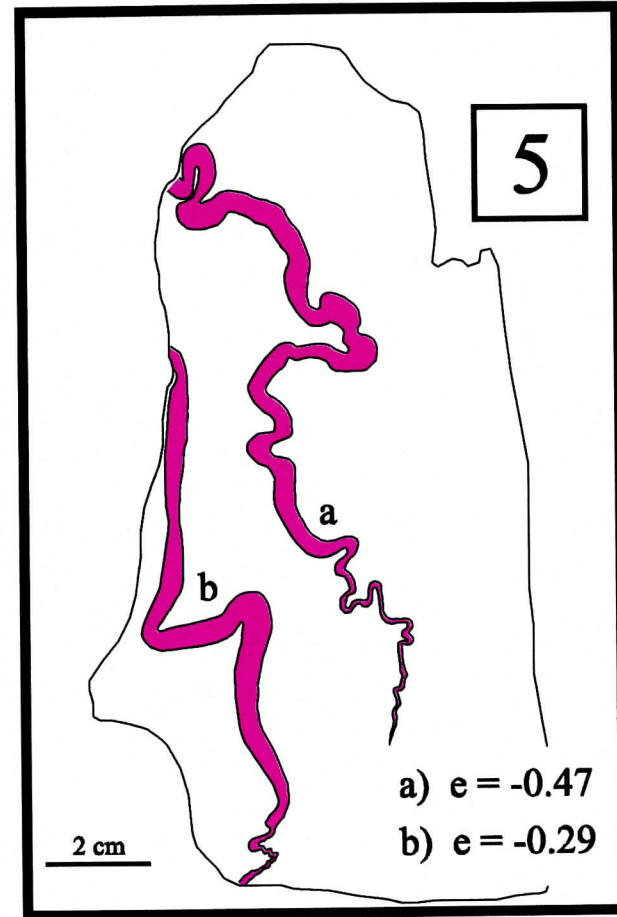


Figure A1.5 continued.

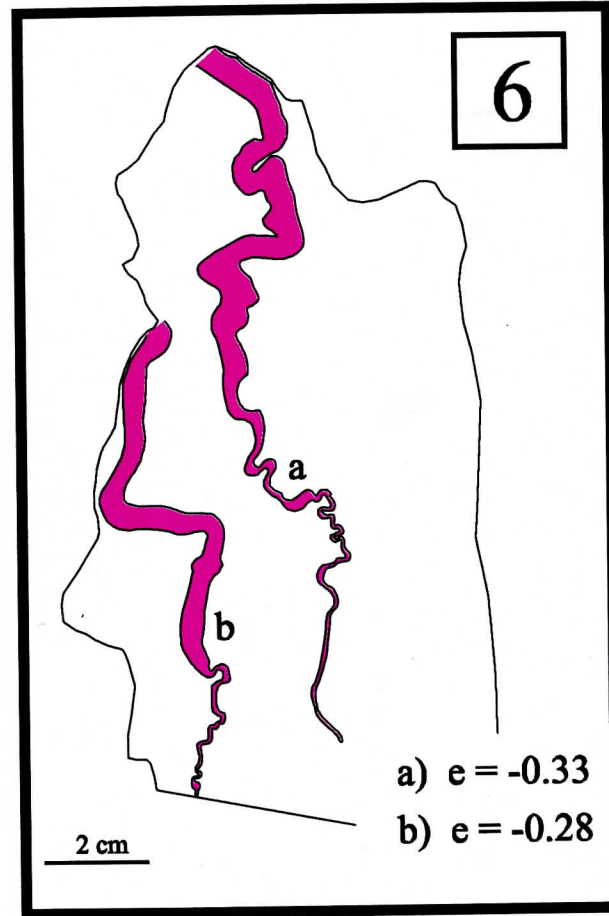


Figure A1.5 continued.

## Appendix 2:

## Table of shortening values

Values of shortening were generated from cuticle layers digitized from scanned field photographs (photo taken parallel to the fold hinge) and slab photographs (see Appendix 1). Both edges of each cuticle layer were digitized using AutoCAD R14<sup>®</sup> and the distance between the endpoints ( $l$ ) and the length of line ( $l_0$ ) were measured. Values of extension were generated for 183 lines representing 94 cuticle layers using the equation  $e = (l - l_0)/l_0$ . Negative values of  $e$  represent the ratio of shortening (i.e. multiply the value of  $e$  by -100 to obtain the percentage of shortening).

		$l$	$l_0$	$e = (l - l_0)/l_0$
<b>Holland Road (H1)</b>				
Slabs: Figure A1.1	1	27.28	75.36	-0.64
		28.57	78.50	-0.64
		39.39	97.07	-0.59
		43.14	102.67	-0.58
		42.35	105.21	-0.60
	2	29.26	79.21	-0.63
		30.31	80.32	-0.62
		42.42	113.00	-0.62
		46.33	89.48	-0.48
		45.71	92.25	-0.50
	3	29.07	86.35	-0.66
		30.06	86.24	-0.65
		38.58	92.59	-0.58
		38.14	74.98	-0.49
		38.00	72.34	-0.47
	4	26.25	72.75	-0.64
		27.11	73.76	-0.63
		32.51	83.47	-0.61
		32.89	58.36	-0.44
		33.43	59.40	-0.44
Field photo: Fig. 3.4		2.06	4.64	-0.56
		2.03	4.99	-0.59
		3.82	8.66	-0.56
		3.72	9.16	-0.59
Field photo: Fig. 3.3		68.93	116.32	-0.41
		68.32	118.05	-0.42
		29.87	45.26	-0.34
		29.44	43.11	-0.32
		30.54	57.30	-0.47
		29.50	56.14	-0.47
Field photo: Fig. 3.5		47.85	148.56	-0.68

		47.95	142.84	-0.66
		42.24	122.48	-0.66
		42.91	122.83	-0.65
Average				-0.56
Standard Deviation				9.70%
<b>Bennery Lake (Hz)</b>				
Slabs: Figure A1.3	1	81.63	146.41	-0.44
		86.26	157.06	-0.45
		89.11	162.88	-0.45
		88.96	163.50	-0.46
		93.56	184.45	-0.49
		94.11	191.97	-0.51
	2	83.87	151.58	-0.45
		84.68	152.23	-0.44
		86.13	161.48	-0.47
		84.59	170.90	-0.51
	3	80.69	161.71	-0.50
		81.92	159.05	-0.48
		86.70	177.31	-0.51
		85.05	181.32	-0.53
	4	73.33	139.50	-0.47
		73.76	140.21	-0.47
		84.87	171.21	-0.50
		85.01	181.03	-0.53
Slabs: Figure A1.2	2	41.44	81.66	-0.49
		39.08	77.97	-0.50
		34.01	67.34	-0.49
		33.49	67.32	-0.50
		32.86	67.41	-0.51
		29.92	64.80	-0.54
	3	44.56	84.87	-0.47
		44.14	84.57	-0.48
		43.12	87.31	-0.51
		41.33	87.79	-0.53



4	48.25	91.27	-0.47	
	46.87	87.46	-0.46	
	43.86	80.94	-0.46	
	43.73	82.52	-0.47	
5	52.02	94.07	-0.45	
	53.29	94.82	-0.44	
	50.15	96.99	-0.48	
	50.49	95.70	-0.47	
	48.47	91.39	-0.47	
	48.60	87.06	-0.44	
Slabs: Figure A1.4	1	41.97	70.14	-0.40
		41.95	71.33	-0.41
		21.51	37.12	-0.42
		21.74	38.23	-0.43
		32.00	57.24	-0.44
		32.12	59.44	-0.46
	2	42.99	89.36	-0.52
		44.27	86.16	-0.49
		31.82	54.95	-0.42
		32.03	54.95	-0.42
		36.19	72.27	-0.50
		36.53	73.53	-0.50
	3	56.97	99.55	-0.43
		57.07	97.74	-0.42
		32.18	54.50	-0.41
		31.95	54.54	-0.41
		33.90	73.15	-0.54
		34.11	72.78	-0.53
Field photo: Fig. 3.14		89.96	204.32	-0.56
		91.78	213.33	-0.57
Field photo: Fig. 3.13		100.10	214.34	-0.53
		100.16	218.68	-0.54
Average				-0.48
Standard Deviation				4.10%

Highway #1 Pit (L2)			
Field photos: Fig. 3.24 a	50.57	59.75	-0.15
	50.08	59.02	-0.15
b	18.87	21.74	-0.13
	19.43	22.19	-0.12
c	74.05	83.25	-0.11
	74.98	81.70	-0.08
d	43.36	59.46	-0.27
	43.02	57.92	-0.26
e	40.98	53.42	-0.23
	39.12	50.39	-0.22
f	95.23	118.23	-0.19
	95.31	118.24	-0.19
g	99.53	119.24	-0.17
	100.40	119.06	-0.16
2a	25.90	32.29	-0.20
	25.41	31.68	-0.20
b	102.76	140.46	-0.27
	102.84	142.17	-0.28
c	30.26	37.19	-0.19
	30.13	38.36	-0.21
d	27.22	31.15	-0.13
	26.78	30.56	-0.12
e	78.42	103.84	-0.24
	77.96	105.48	-0.26
f	57.01	63.68	-0.10
	58.09	65.04	-0.11
3a	95.98	126.95	-0.24
	95.24	120.83	-0.21
b	117.69	136.69	-0.14
	119.29	137.03	-0.13
c	68.13	83.82	-0.19
	66.38	83.26	-0.20
d	76.70	109.13	-0.30

		76.41	103.38	-0.26
Field photo: Fig. 3.26		103.07	171.38	-0.40
		104.52	176.01	-0.41
Slab: Fig. 3.29		36.14	49.82	-0.27
		36.90	49.47	-0.25
		37.27	50.73	-0.27
		37.77	48.87	-0.23
		32.10	47.77	-0.33
		33.15	45.63	-0.27
		49.00	79.00	-0.38
		49.03	79.77	-0.39
Slab: Fig. 3.30		83.61	155.62	-0.46
Average				-0.22
Standard Deviation				8.83%
<b>Beaverbank Rd (L3)</b>				
Slabs: Figure A1.5	1	60.26	108.57	-0.44
		58.47	108.80	-0.46
		68.12	129.52	-0.47
		66.71	125.36	-0.47
	2	55.85	101.82	-0.45
		54.53	99.33	-0.45
		67.82	129.99	-0.48
		66.71	128.44	-0.48
	3	56.28	102.83	-0.45
		56.86	103.31	-0.45
		69.89	119.79	-0.42
		67.56	114.57	-0.41
	4	58.10	103.39	-0.44
		58.91	105.62	-0.44
		62.08	97.22	-0.36
		55.35	89.91	-0.38
	5	66.81	129.20	-0.48
		65.91	124.68	-0.47
		59.95	84.40	-0.29

	57.08	80.17	-0.29
6	78.27	120.27	-0.35
	78.86	116.35	-0.32
	52.73	72.03	-0.27
	51.17	71.24	-0.28
Field photo: Fig. 3.36	111.22	140.35	-0.21
	112.20	140.83	-0.20
	108.82	158.94	-0.32
	108.43	155.87	-0.30
Field photo: Fig. 3.35	19.36	20.85	-0.07
	19.25	20.46	-0.06
	48.11	62.80	-0.23
	48.81	62.99	-0.23
	53.65	72.15	-0.26
	53.85	74.11	-0.27
	12.39	15.09	-0.18
	13.42	16.24	-0.17
	14.43	14.58	-0.01
	14.64	14.78	-0.01
	19.09	22.57	-0.15
	18.89	22.42	-0.16
Field photo: Fig. 3.37	4194.72	5114.21	-0.18
	4121.93	5054.41	-0.18
	4017.78	5118.35	-0.22
	4016.77	5113.40	-0.21
Average			-0.31
Standard Deviation			13.96%

## References

- Baker, D.E., Horne, R.J., and Feetham, M. 1998. Geological map of Airport. Nova Scotia Department of Natural Resources, Minerals and Energy Branch, Open File Map 1998-004, scale 1:10 000.
- Binney, W.P., Jenner, K.A., Sangster, A.L., and Zentilli, M. 1986. A stratabound zinc-lead deposit in Meguma Group metasediments at Eastville, Nova Scotia. *Maritime Sediments and Atlantic Geology*, **22**, p. 65-68.
- Biot, M.A. 1965. *Mechanic of incremental deformation*. Wiley, New York, N.Y. 505 p.
- Boulter, C.A. 1989. *Four dimensional analysis of geological maps; Techniques of Interpretation*. John Wiley and Sons. 296 p.
- Cobbold, P.R., Cosgrove, J.W. and Summers, J.M. 1971. Development of internal structures in deformed anisotropic rocks. *Tectonophysics*, **12**, p. 23-53.
- de Sitter, L.U. 1958. Boudins and parasitic folds in relation to cleavage and folding. *Geologie en Mijnbouw*, **20**, p.272-286.
- Dubey, A.K. and Cobbold, P.R. 1977. Noncylindrical flexural-slip folding in nature and experiment. *Tectonophysics*, **38**, p. 223-239.
- Erslev, E.A. and Ward, D.J. 1994. Non-volatile element and volume flux in coalesced slaty cleavage. *Journal of Structural Geology*, **16**, no. 4, p. 531-553.
- Faribault, E.R. 1899. On the gold measures of Nova Scotia and deep mining. *The Canadian Mining Review*, **18**, no.3, p. 78-82.
- Faribault, E.R. 1909. Waverley Sheet. Canada Department of Mines, Geological Survey Branch, Map 1025, scale 1:63,360.
- Faribault, E.R. 1913. The gold deposits of Nova Scotia. *The Canadian Mining Journal*, **34**, no. 22, p. 108-109 and no. 24, p. 780-781.
- Feetham, M., Ryan, R.J., Pe-Piper, G., and O'Beirne-Ryan, A.M. 1997. Lithological characterization of the Beaverbank unit of the Halifax Formation, Meguma Group, and acid rock drainage implications. *Atlantic Geology*, **33**, p. 133-141.

- Feetham, M., Horne, R.J., Baker, D.E., and Ham, L.J. 1998. Geological map of Soldier Lake. Nova Scotia Department of Natural Resources, Minerals and Energy Branch, Open File Map 1998-005. scale 1:10 000.
- Fletcher, H. and Faribault, E.R. 1911. Southeast Nova Scotia. Canada Department of Mines, Geological Survey, Map 53A, scale 1:250,000.
- Fowler, T.J. and Winsor, C.N. 1996. Evolution of chevron folds by profile shape changes: comparison between multilayer deformation experiments and folds of the Bendigo-Castlemaine goldfields, Australia. *Tectonophysics*, **258**, p. 125-150.
- Fuerten, F. 1984. Spaced cleavage formation in the metagreywackes of the Goldenville Formation, Meguma Group, Nova Scotia. Unpublished M.Sc. thesis, McMaster University, Hamilton, Ontario, Canada.
- Ghosh, S.K., Deb, S.K., and Sengupta, Sudipta. 1996. Hinge migration and hinge replacement. *Tectonophysics*, **263**, p. 319-337.
- Graves, M.C. 1976. The formation of gold-bearing quartz veins in Nova Scotia: Hydraulic fracturing under conditions of greenschist regional metamorphism during early stages of deformation. Unpublished M.Sc. thesis, Dalhousie University, Halifax, Nova Scotia, Canada.
- Graves, M.C. and Zentilli, M. 1982. A review of the geology of gold in Nova Scotia: In *Geology of Canadian Gold Deposits*, ed R.W. Hodder and K.W. Petruk. Canadian Institute of Mining and Metallurgy, Special Volume **24**, p. 233-242.
- Graves, M.C. and Zentilli, M. 1988. The lithochemistry of metal-enriched coticules in the Goldenville-Halifax transition zone of the Meguma Group, Nova Scotia. In *Current Research, Part 3*, Geological Survey of Canada, Paper 88-1B, p. 251-261.
- Haysom, S.J., Horne, R.J. and Pe-Piper, G. 1997. The opaque mineralogy of metasedimentary rocks of the Meguma Group, Beaverbank - Rawdon area, Nova Scotia. *Atlantic Geology*, **33**, p. 105-120.
- Henderson, J.R., Wright, T.O. and Henderson, M.N. 1986. A history of cleavage and folding: and example from the Goldenville Formation, Nova Scotia. *Geological Society of America*, **97**, p. 1354-1366.
- Henderson, J.R. and Henderson, M.N. 1986. Constraints on the origin of gold in the Meguma Zone, Ecum Secum area, Nova Scotia. *Maritime Sediments and Atlantic Geology*, **22**, p. 1-13.

- Henderson, J.R. and Henderson, M.N. 1987. Meguma Gold Deposits; nested saddle reefs or early hydraulic extension veins. In Mines and Mineral Branch Report of Activities 1987, Part A, eds. J.L. Bates and D.R. MacDonald. Nova Scotia Department of Mines and Energy Report 87-5, p. 213-215.
- Henderson, J., Wright, T. and Henderson, M.N., 1992. Strain history of the Meguma Group, Lunenburg and Ecum Secum areas, Nova Scotia. Geological Association of Canada, Mineralogical Association of Canada Joint Annual Meeting, Wolfville, Nova Scotia; Field Excursion C-11: Guidebook.
- Hicks, R., Jamieson, R.A., and Reynolds, P.H. 1999. Detrital and metamorphic  $^{40}\text{Ar}/^{39}\text{Ar}$  ages from muscovite and whole-rock samples, Meguma Supergroup, southern Nova Scotia. Canadian Journal of Earth Sciences, **36**, p. 23-32.
- Horne, R.J. 1995. Update on bedrock mapping of the Rawdon Syncline. In Minerals and Energy Branch Report of Activities 1994; Nova Scotia Department of Natural Resources, Minerals and Energy Branch Report 95-1, p. 57-61.
- Horne, R.J., Baker, D., Feetham, M. and MacDonald L. 1997. Preliminary geology of the Waverley-Halifax Airport area, central Meguma Project area: with some insights on the timing of deformation and veining in the Meguma Group. In Minerals and Energy Branch, Report of Activities, 1996, eds. D.R. MacDonald and K.A. Mills. Nova Scotia Department of Natural Resources, Report 97-1, p. 55-72.
- Horne, R.J., MacDonald, L.A., Bhatnagar, P. And Ténrière, P. 1998. Preliminary bedrock geology of the Lucasville-Lake Major area, central Meguma Mapping Project, central Nova Scotia. In Minerals and Energy Branch, Report of Activities, 1997, eds. D.R. MacDonald and K.A. Mills. Nova Scotia Department of Natural Resources, Report 1998-1, p. 15-25.
- Horne, R.J. and Baker, D.E. 1998. Geological map of Fall River. Nova Scotia Department of Natural Resources, Minerals and Energy Branch, Open File Map 1998-006, scale 1:10 000.
- Horne, Richard, J. 1998. An evaluation of flexural-slip folding in the Meguma Group, Halifax and Ovens areas, Southern Nova Scotia. Unpublished MSc thesis, Dalhousie University, Halifax, Nova Scotia, 247 p.
- Horne, R., White, C., Muir, C., Young, M, and King, M.S. in press. Geology of the Weymouth - Church Point area, southwest Nova Scotia, NTS sheets 21A/05 and 21B/08. In Minerals and Energy Branch, Report of Activities, 1999, eds. D.R. MacDonald and K.A. Mills. Nova Scotia Department of Natural Resources.

- Keenan, P.S. and Kennedy, M.J. 1983. Coticules - a key to correlation along the Appalachian-Caledonian orogeny? *In* Regional Trends in the Geology of the Appalachian-Caledonian-Hercynian-Mauretanide Orogeny. Reidel Publishing Company, Dordrecht, p. 355-361.
- Keppie, J.D. 1976. Structural model for the saddle reef and associated gold veins in the Meguma Group, Nova Scotia. Nova Scotia Department of Mines, Paper 76-1, 34 p.
- Keppie, J.D. 1993. Synthesis of Palaeozoic deformational events and terrane accretion in the Canadian Appalachians. *Geol Rundsch*, **82**, p. 381-431.
- Keppie, J.D. and Dallmeyer 1987. Dating transcurrent terrane accretion: an example from the Meguma and Avalon composite terranes in the northern Appalachians. *Tectonics*, **6**, p. 831-847.
- King, M.S. and Horne, R.J. 2000. Application of combined enhanced aeromagnetic and digital elevation data in the geological interpretation of the eastern Meguma Terrane of Nova Scotia. *In* Program and Abstracts, Atlantic Geoscience Society Colloquium and Annual General Meeting, Fredericton 2000.
- Kontak, D.J., Horne, R.J., Sandeman, H., Archibault, D. and Lee, J.K.W. 1998.  $^{40}\text{Ar}/^{39}\text{Ar}$  dating of ribbon-textured veins and wall-rock material from Meguma lode gold deposits, Nova Scotia: implications for timing and duration of vein formation in slate-belt hosted vein gold deposits. *Canadian Journal of Earth Sciences*, **35**, p. 746-761.
- MacInnis, I.N. 1986. Lithogeochemistry of the Goldenville-Halifax Transition (GHT) of the Meguma Group in the manganese-zinc-lead deposit at Eastville, Nova Scotia. Unpublished BSc thesis, Dalhousie University, Halifax, Nova Scotia. 138 p.
- Malcolm, W. 1929. Gold Fields of Nova Scotia. Geological Survey of Canada, Memoir 385, 253 p.
- Mawer, C.K. and White, J.C. 1987. Sense of displacement on the Cobequid-Chedabucto fault system, Nova Scotia, Canada. *Canadian Journal of Earth Sciences*, **24**, p. 217-223.
- Mawer, C.K. 1987. Mechanics of formation of gold-bearing quartz veins, Nova Scotia, Canada. *Tectonophysics*, **135**, p. 99-119.



- Mawer, C. K. and Williams, P. F. 1991. Progressive folding and foliation development in a sheared, coticule-bearing phyllite. *Journal of Structural Geology*, **13**, no. 5, p. 539-555.
- Muecke, G.K., Elias, P. and Reynolds, P.H. 1988. Hercynian/Alleghanian overprinting of an Acadian Terrane:  $^{40}\text{Ar}/^{39}\text{Ar}$  studies in the Meguma Zone, Nova Scotia. *Chemical Geology*, **73**, p. 153-167.
- O'Beirne-Ryan, A.M. Petrography of coticules from the Meguma Group: a report on selected samples from the central Meguma area. Unpublished report Nova Scotia Department of Natural Resources.
- O'Brien, B.H. 1988. A study of the Meguma Terrane in Lunenburg County, Nova Scotia. Geological Survey of Canada Open File Report 1823, 80 p.
- Price, N.J. and Cosgrove, J.W. 1990. *Analysis of Geological Structures*. Cambridge University Press, Cambridge.
- Ramsay, J.G. and Huber, M.I. 1983. *The techniques of Modern Structural geology, Volume 1: Strain Analysis*. Academic Press, London. 307 p.
- Ramsay, J.G. and Huber, M.I. 1987. *The techniques of Modern Structural geology, Volume 2: Folding and Fracturing*. Academic Press, London. 393 p.
- Ryan R.J., Fox, D., Horne R.J., Corey, M.C. and Smith, P.K. 1996. Preliminary stratigraphy of the Meguma Group in central Nova Scotia. In *Mines and Minerals Branch Report of Activities, 1995*, eds D.R. MacDonald and K.A. Mills. Nova Scotia Department of Natural Resources, Report 96-1, p. 27-34.
- Schenk, P.E. 1991. Events and sea-level changes on Gondwana's margin: The Meguma Zone (Cambrian to Devonian) of Nova Scotia. *Geological Society of America Bulletin*, **103**, p. 512-521.
- Schenk, P.E. 1995. Meguma Zone. In *Geology of the Appalachian-Caledonian Orogen in Canada and Greenland*, ed H. Williams. Geological Survey of Canada, *Geology of Canada*, No. 6, p. 261-277.
- Treagus, J.E. and Treagus, S. H. Folds and strain ellipsoid. *Journal of Structural Geology*, **3**, p. 1-17.
- Waldron, J.W.F. 1992. The Goldenville-Halifax transition, Mahone Bay, Nova Scotia: relative sea-level rise in the Meguma source terrane. *Canadian Journal of Science*, **29**, p. 1091-1105.

- Weiss, L. E. 1980. Nucleation and growth of kink bands. *Tectonophysics*, **65**, p. 1-38.
- Wright, T.O. and Henderson, J.R. 1992. Volume loss during cleavage formation in the Meguma Group, Nova Scotia, Canada. *Journal of Structural Geology*, **4**, no. 3, p. 281-290.
- Williams, P.F. and Hy, C. 1990. Origin and deformational and metamorphic history of gold-bearing quartz veins on the Eastern Shore of Nova Scotia. In *Mineral Deposits of Nova Scotia, Volume 1*, ed A.L. Sangster. Geological Survey of Canada, Paper 90-8, p. 169-194.

# L2 (HWY #1)

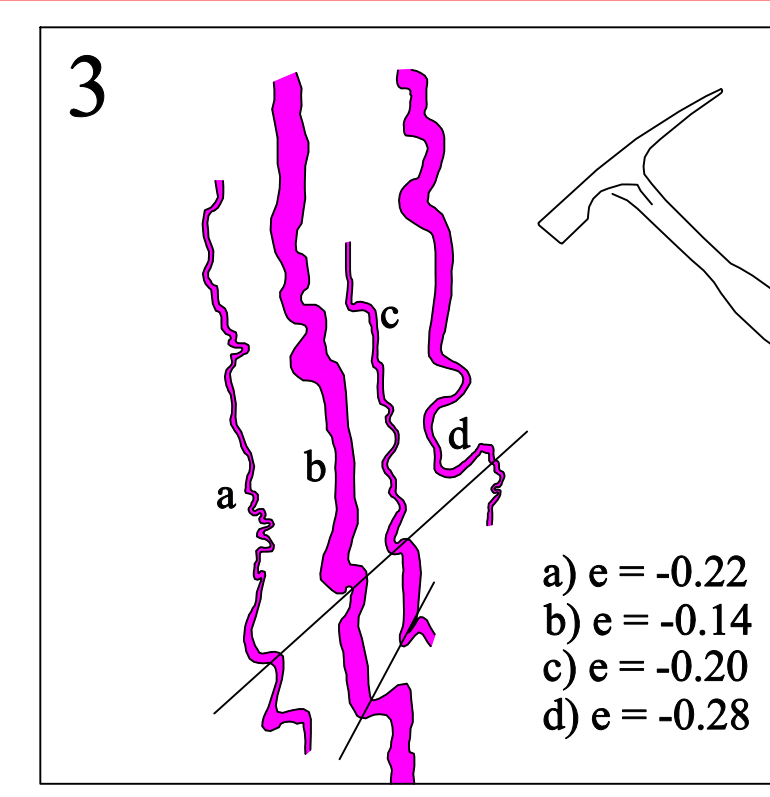
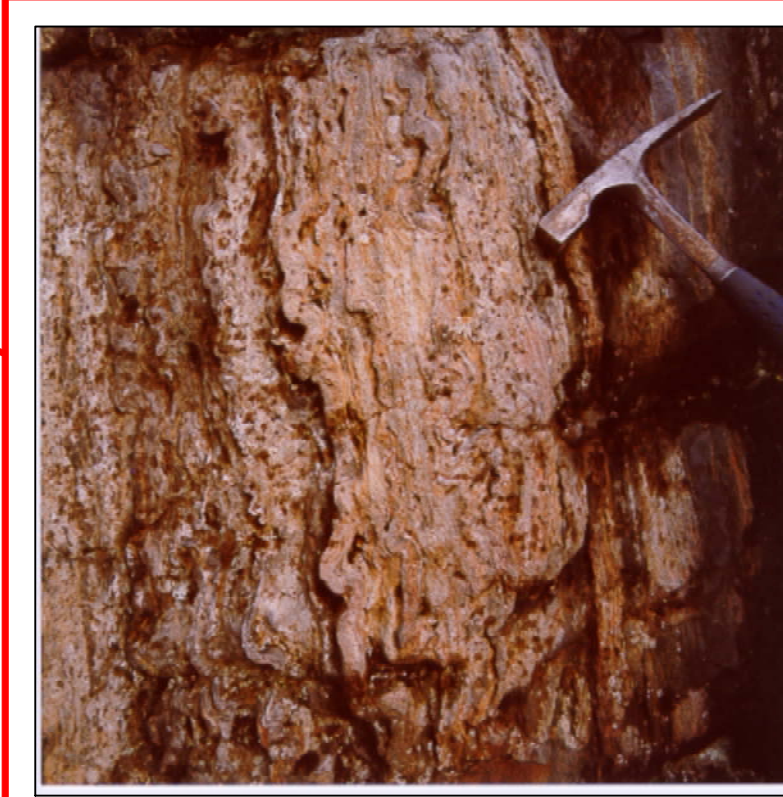
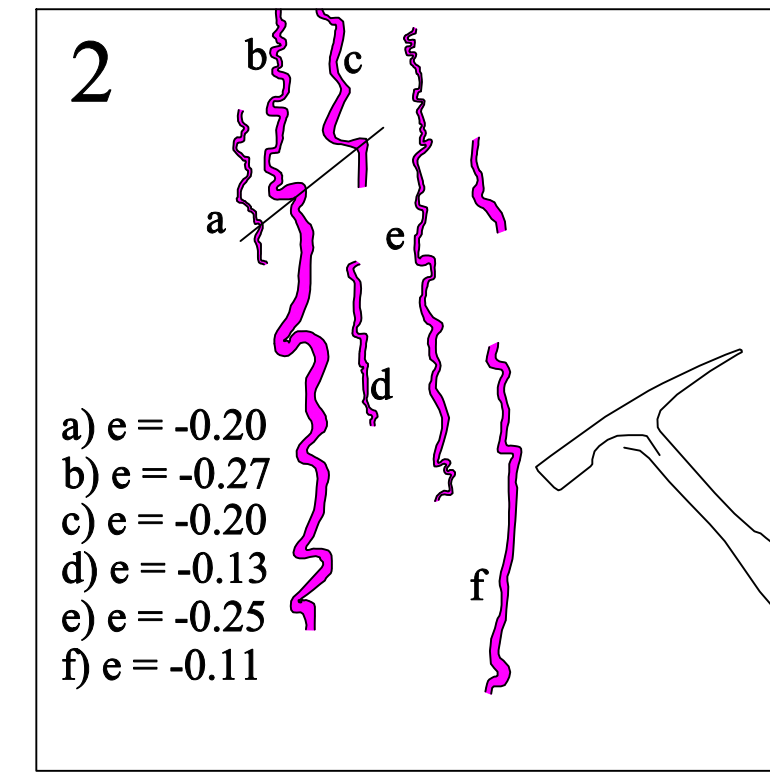
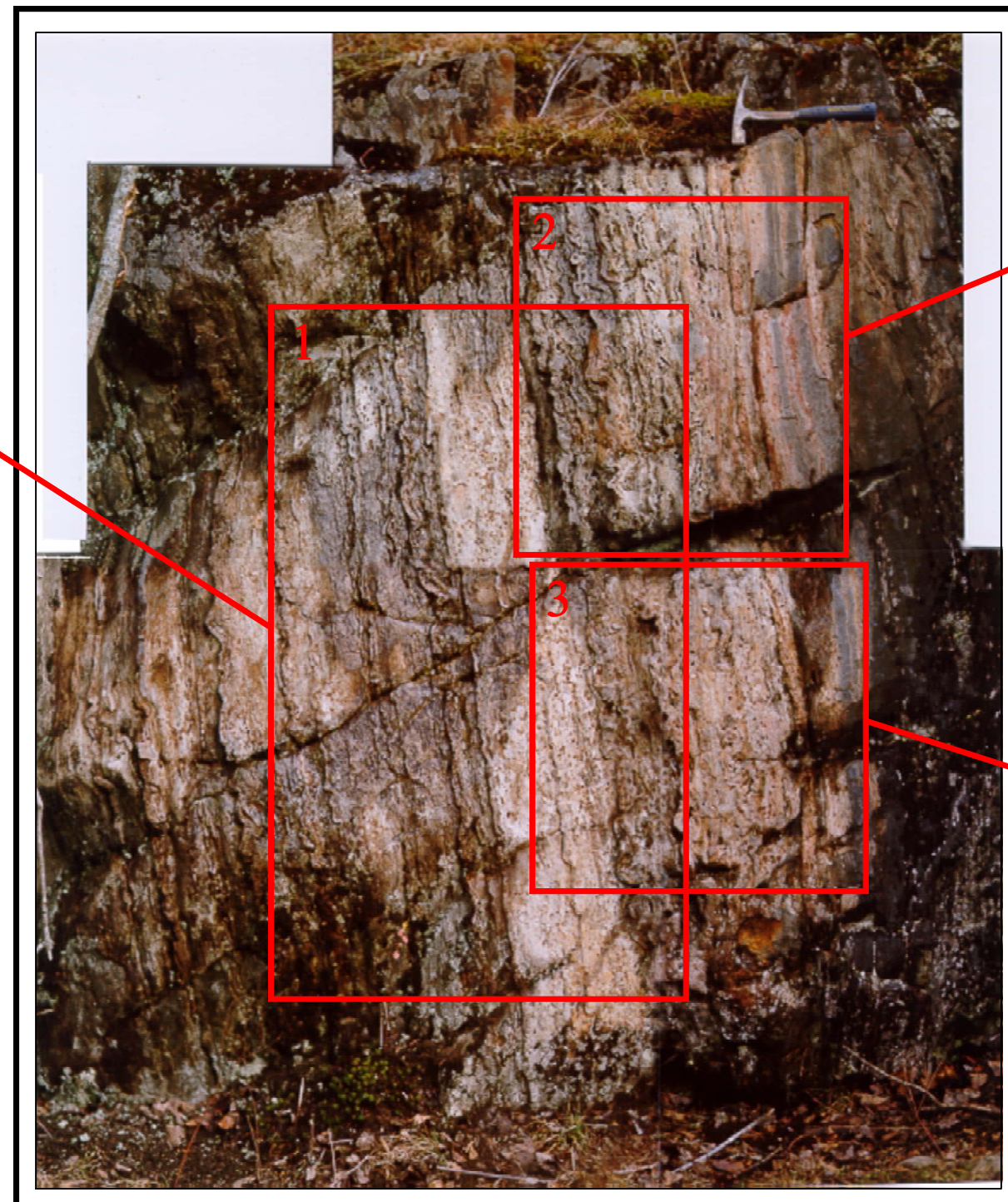
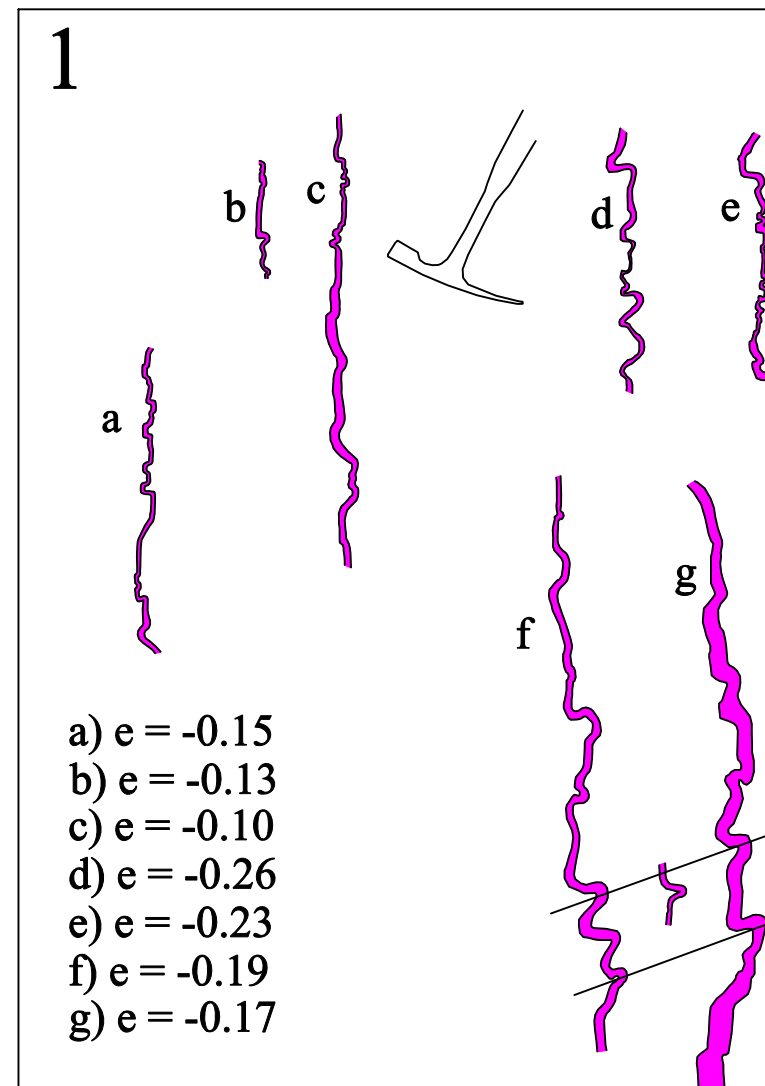
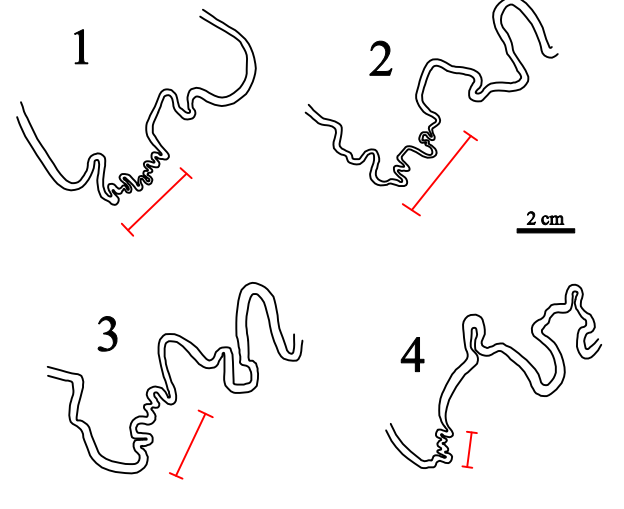
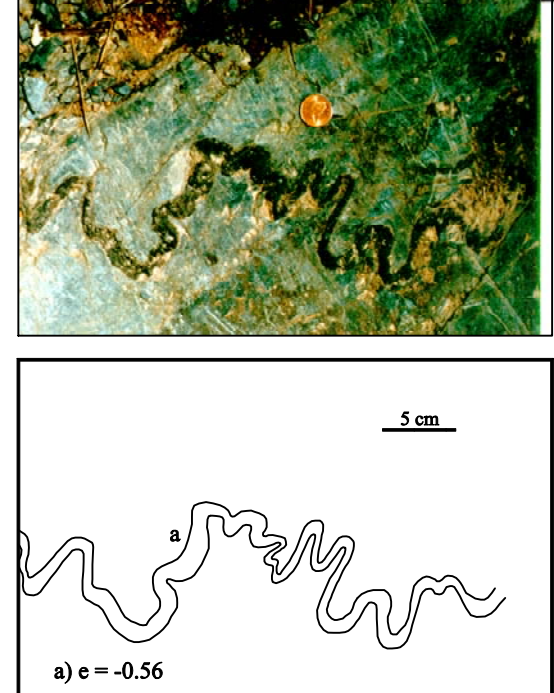
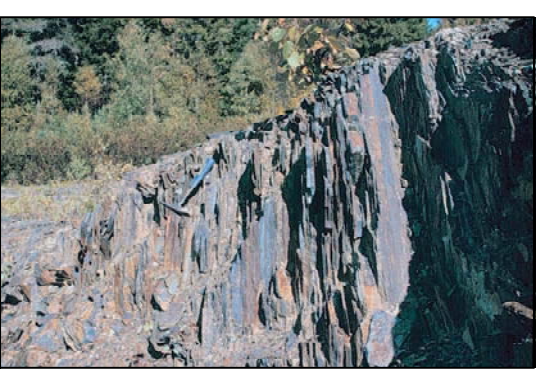
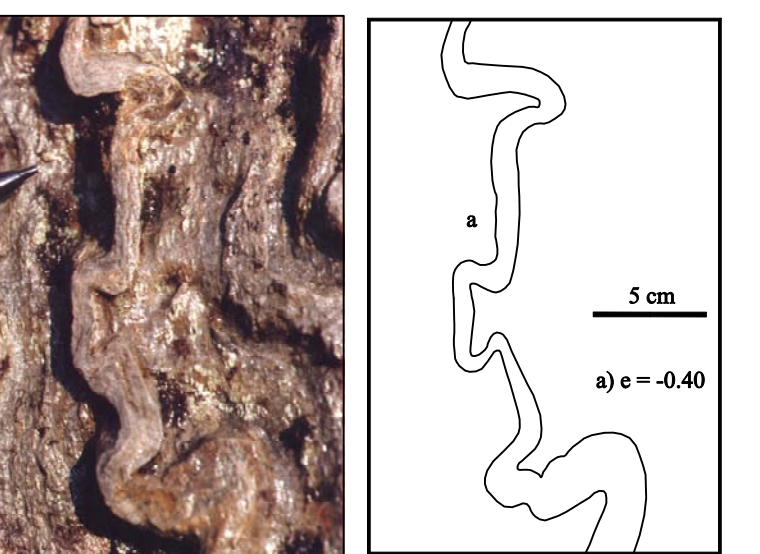
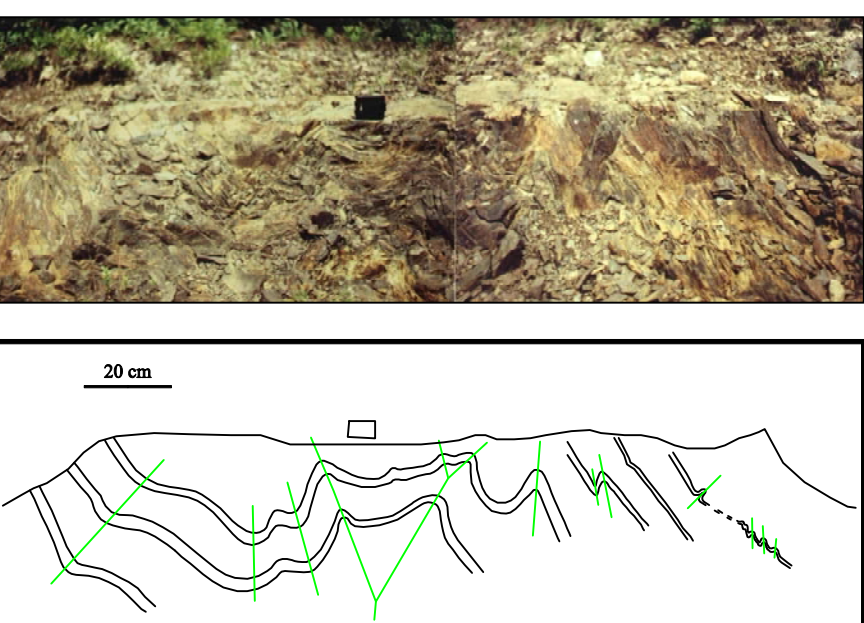

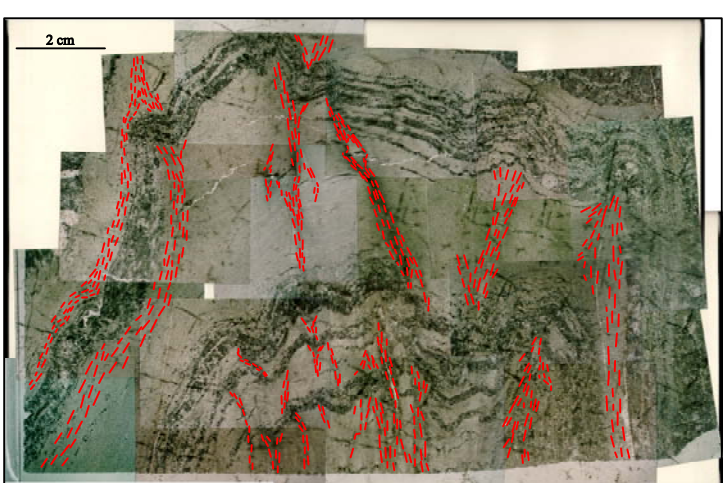

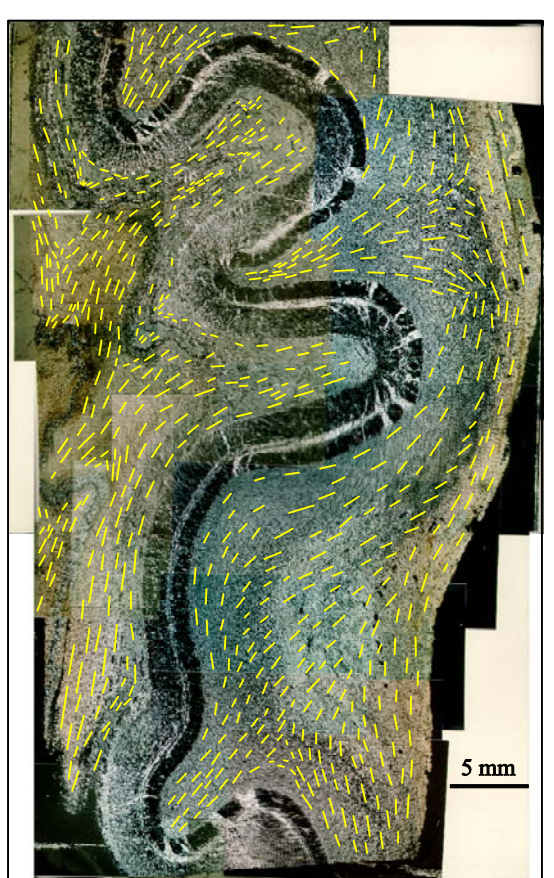
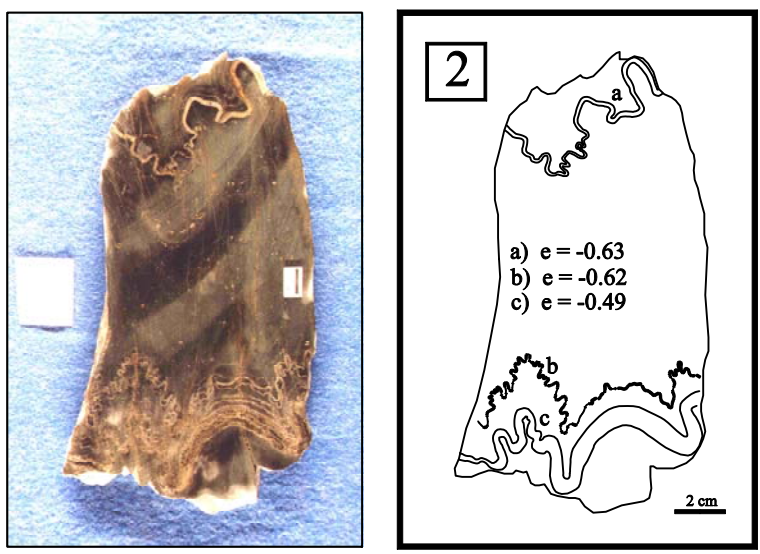
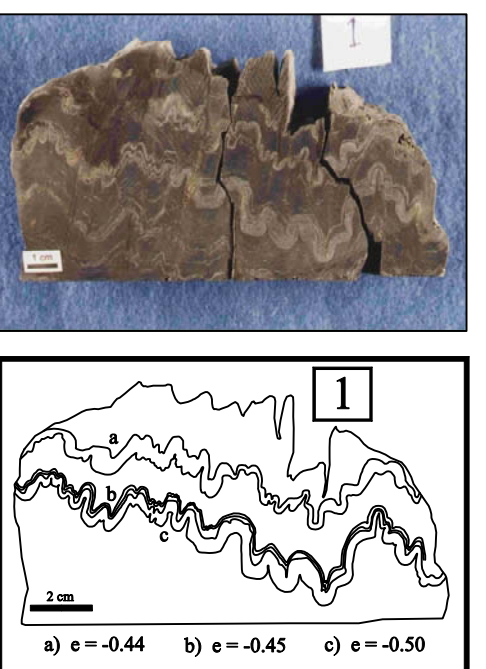
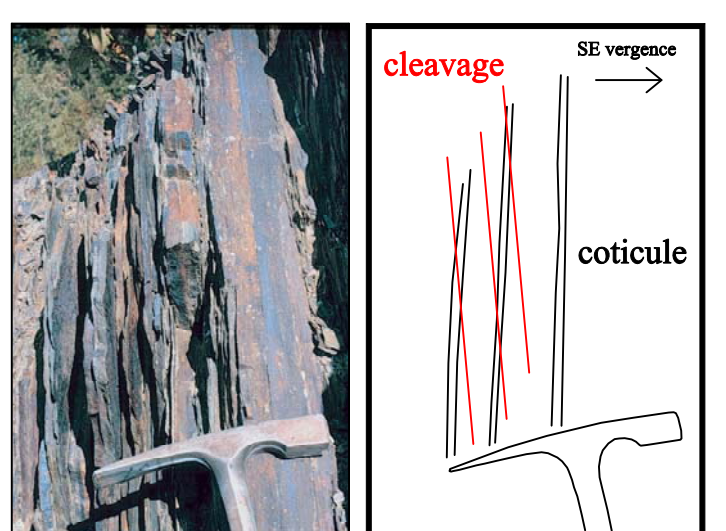
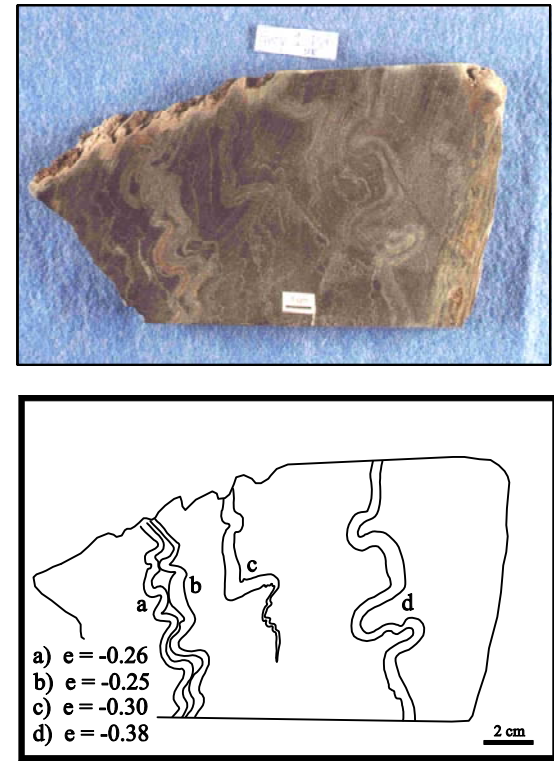
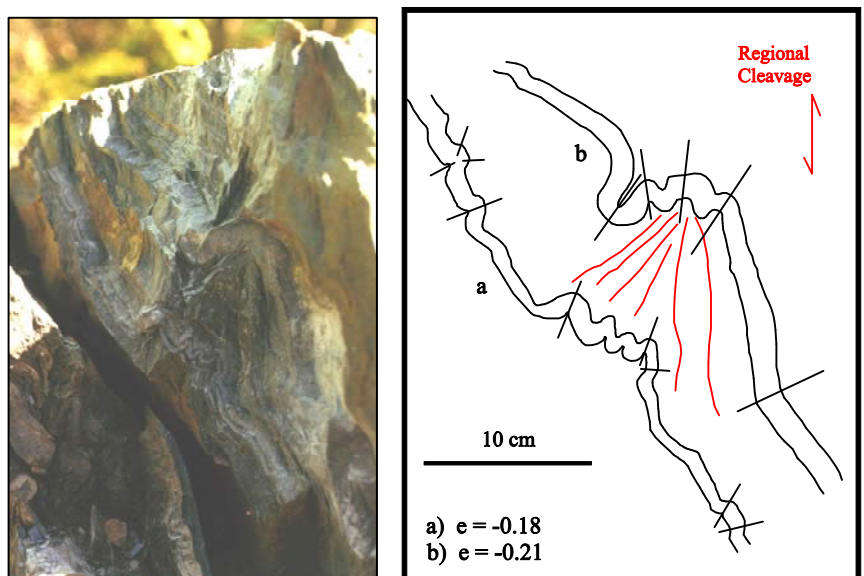


Figure 3.24. Field photographs and sketches of a vertical face exposure. Coticule layers protrude from the matrix material making recognition of the fold style very easy. Fold styles range from symmetric box folds to highly asymmetric ptygmatic folds. The sketched-in axial planes show a relationship between adjacent layers. As evident by the orientation of the axial planes there is a large range in the symmetry of the folds. There is also a large range in shortening values through the exposure, and even between directly adjacent layers. See text for discussion.

**Figure 3.43. Comparison of minor folds from the regional fold hinge and limb**

	HINGE		LIMB		
Physical Properties	H <sub>1</sub> (Holland Road)	H <sub>2</sub> (Bennery Lake)	L <sub>1</sub> (South Uniacke Pit)	L <sub>2</sub> (Highway #1 Pit)	L <sub>3</sub> (Beaverbank Road)
<p><b>Minor Fold Style</b></p> <p>Noncylindrical folds are common at all locations. Refer to Figure 3.7 for description.</p>	 <p>Noncylindrical folds are common at all locations. Refer to Figure 3.7 for description.</p>	 <p>Ptygmatic folds developed in the median segment of modified box folds are common in the regional fold hinge. Refer to Figure 3.14 for description.</p>	 <p>Non-folded coticle layers characterize this location. Refer to Figure 3.21 for description.</p>	 <p>Modified box and isoclinal folds of varying symmetry characterize this location. The symmetry of the folds ranges from perfectly symmetric to moderately asymmetric to highly asymmetric. Refer to Figure 3.26 for a description.</p>	 <p>Modified box and isoclinal folds characterize this location. The majority of minor folds are highly asymmetric where their axial planes are parallel to the regional fold axial plane. Refer to Figure 3.35 for description.</p>
<p><b>Bedding-cleavage relationships</b></p> <p>Cleavage and bedding are closely related indicating formation at the same time. Divergent cleavage shadows are common around the hinges of minor folds. Refer to Figure 3.9 for description.</p>	 <p>Cleavage and bedding are closely related indicating formation at the same time. Divergent cleavage shadows are common around the hinges of minor folds. Refer to Figure 3.9 for description.</p>	 <p>Cleavage is axial planar to minor folds and the regional fold. Cleavage tends to be controlled by the fold patterns in the coticle layers. Refer to Figure 3.16 for description.</p>	 <p>Foliation-defining minerals wrap around metamorphic spessartine grains indicating that spessartine formed prior to cleavage. Refer to Figure 3.23 for description.</p>	 <p>Cleavage is axial planar to the minor folds regardless of the symmetry displayed by the fold. Cleavage can diverge up to 90 degrees from the regional axial plane. Refer to Figure 3.28 for description.</p>	
<p><b>Shortening recorded by minor folds</b></p> <p><math>e = (1 - l_o)/l_o</math></p> <p>Shortening values are consistent at around 50% and all coticle layers are folded. Refer to Figure A1.1 in Appendix 1 and Table 3.2 for discussion.</p>	 <p>Shortening values are consistent at around 50% and all coticle layers are folded. Refer to Figure A1.1 in Appendix 1 and Table 3.2 for discussion.</p>	 <p>Shortening values are consistent at around 50% and all coticle layers are folded. Refer to Figure A1.3 in Appendix 1 and Table 3.2 for discussion.</p>	 <p>Non-folded coticle layers characterize this location. Cleavage is close to bedding and indicates SE vergence. Refer to Figure 3.22 for description.</p>	 <p>Shortening values range considerably and are generally less than 30%. Refer to Figures 3.29 and 3.24 and Table 3.2 for discussion.</p>	 <p>Shortening values range from zero to more than forty percent, but generally indicate shortening less than 25%. Refer to Figure 3.37 and Table 3.2 for discussion.</p>

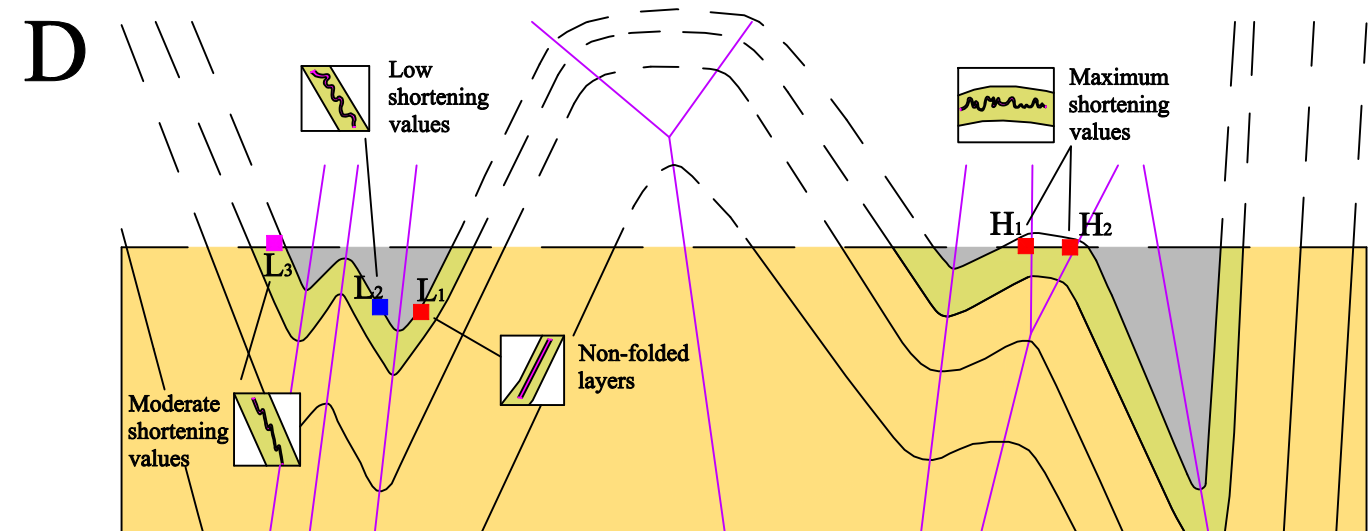
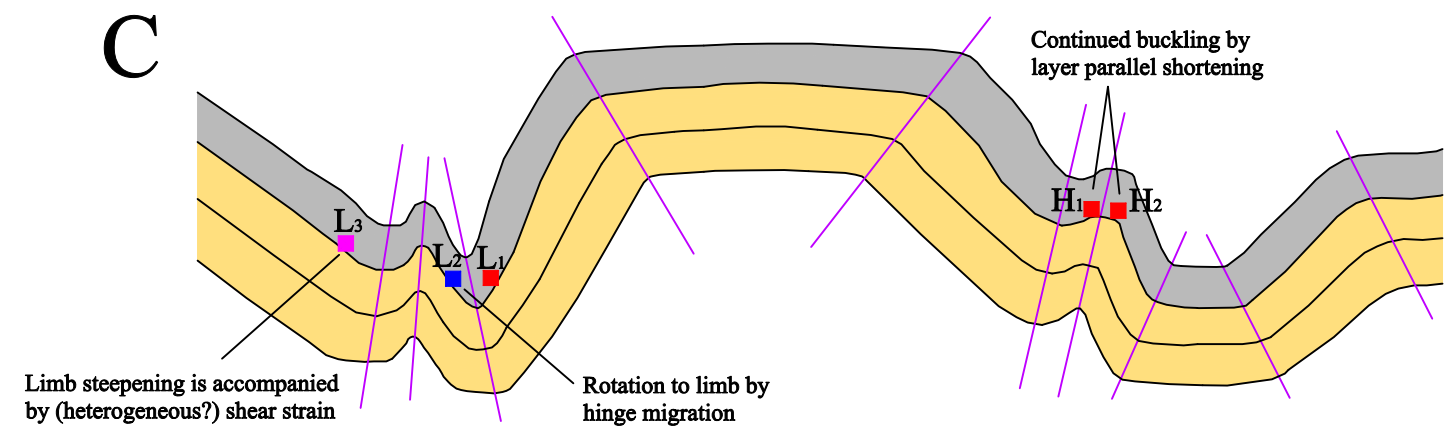
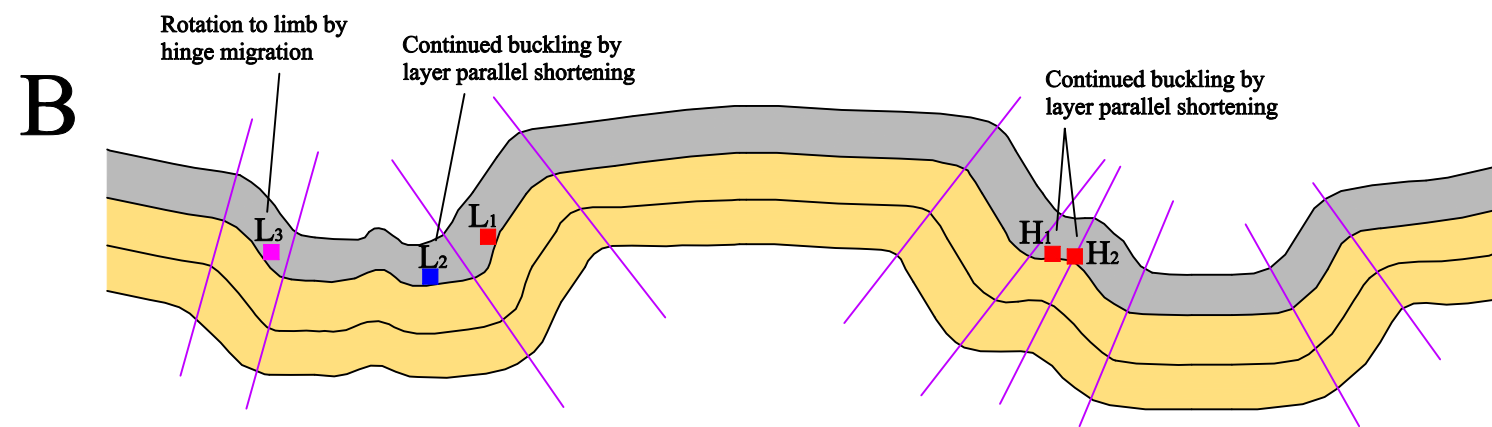
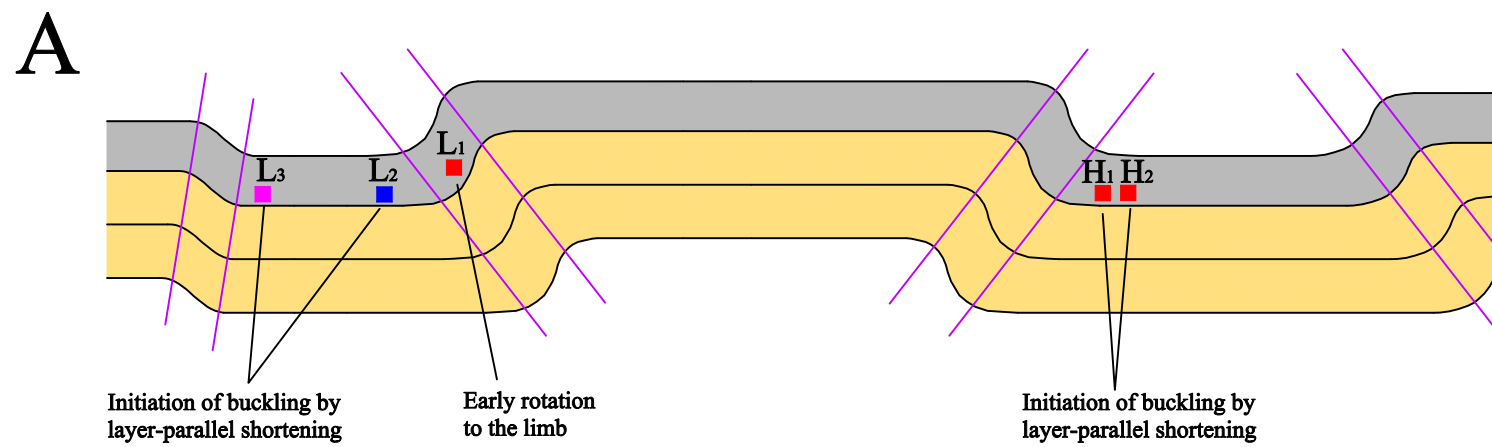


Figure 4.1. Possible sequence of fold development in the profile plane for the central Meguma. Stage D represents the present-day cross-section. See text for discussion.